NIVA
Norsk institutt for vannforskning

ICP Waters Report 156/2024

Trends and patterns in surface water chemistry in Europe and North America between 1990 and 2020, with a focus on calcium

International Cooperative Programme on Assessment and Monitoring Effects of Air Pollution on Rivers and Lakes

Convention on Long-Range Transboundary Air Pollution

UNECE
Convention on Long-range Transboundary Air Pollution

Report

Norwegian Institute for Water Research

This report has been quality assured according to NIVA's quality system and has been approved by:

Rolf D. Vogt
Lead Author

Øyvind Kaste
Quality Assurer

Hans Fredrik V. Braaten
Research Manager

www.niva.no

Title
Trends and patterns in surface water chemistry in Europe and North America between 1990 and 2020, with a focus on calcium

Trender og mønstre i overflatevannskjemi i Europa og Nord-Amerika mellom 1990 og 2020, med særlig søkelys på kalsium

Pages
54 + Appendix

Date
29.01.2024

Authors
Rolf David Vogt (NIVA), Jens Arle (UBA), Kari Austnes (NIVA), Herman van Dam (Waternatuur), Martyn Futter (SLU), Jens Fölster (SLU), Cathrine Brecke Gundersen (NIVA), Scott Higgins (ILSD-ELA), Daniel Houle (ECCC), Jakub Hruška (CGS), Agnieszka Kolada (IOS), Don Monteith (UKCEH), Andrew Paterson (MOECC), Michela Rogora (CNR IRSA), James E. Sample (NIVA), John Stoddard (USEPA), Sandra Steingruber (DT-UACER), Rafał Ulańczyk (IOS), Jussi Vuorenmaa (Ymparisto), and Heleen de Wit (NIVA)

Topic group
Monitoring

Distribution
Open

Clients
Norwegian Ministry of Climate and Environment,
United Nations Economic Commission for Europe (UNECE)

Client's contact person
Eli Marie Åsen

Published by NIVA
10300

Abstract
The report presents trends in major anions and cations, pH, TOC and bicarbonate in surface waters in Europe and North America from 1990 to 2020. Special attention is given to trends in calcium, which showed some unexpected increases. The trends in calcium are analysed in relation to changes in bicarbonates, organic anions, and deposition loads. The surface waters show strong signs of chemical recovery.

Keywords: Air pollution, Surface water acidification, Trends, ICP Waters
Emneord: Luftforurensing, Forsuring, Trender, ICP Waters

CONVENTION ON LONG-RANGE TRANSBOUNDARY AIR POLLUTION

INTERNATIONAL COOPERATIVE PROGRAMME ON ASSESSMENT AND MONITORING OF THE EFFECTS OF AIR POLLUTION ON RIVERS AND LAKES

Trends and patterns in surface water chemistry in Europe and North America between 1990 and 2020, with a focus on calcium

Prepared at the ICP Waters Programme Centre
Norwegian Institute for Water Research
Oslo, January 2024

Table of contents

Preface

The International Cooperative Programme on Assessment and Monitoring of the Effects of Air Pollution on Rivers and Lakes (ICP Waters) was established under the Executive Body of the UNECE Convention on Long-range Transboundary Air Pollution (CLRTAP) in July 1985. Since then, ICP Waters has been an important contributor to documenting the effects of implementing the Protocols under the Convention. ICP Waters has prepared numerous assessments, reports and publications that address the effects of long-range transported air pollution.

ICP Waters and its Programme Centre are chaired and hosted by the Norwegian Institute for Water Research (NIVA), respectively. A programme subcentre is established at NORCE in Bergen. ICP Waters is supported financially by the Norwegian Ministry of Climate and Environment and the Trust Fund of the UNECE LRTAP Convention.

The main aim of the ICP Waters programme is to assess, on a regional basis, the degree and geographical extent of the impact of atmospheric pollution, particularly acidification, on surface waters. More than 20 countries in Europe and North America participate in the programme on a regular basis.

An important basis of the work of the ICP Waters programme is the data from existing surface water monitoring programmes in the participating countries, collected through voluntary contributions. The ICP Waters site network is geographically extensive and includes long-term data series (over 25 years) for over 500 sites in Europe and North America. The programme conducts annual chemical intercomparison and biological intercalibration exercises.

This report presents long-term trends (1990-2020) in surface water acidification and concentrations of major anions and cations in Europe and North America, with a focus on calcium (Ca^{2+}) concentration and its governing factors (deposition, land cover, climate). Calcium is a key component in the buffering of surface waters from acidification, and changes in calcium over time are linked to changes in strong acid anions, organic acidity, and bicarbonate. The variabilities of these controls are investigated in a statistical analysis.

Rolf D. Vogt has been the lead author of the report. Cathrine B. Gundersen was the main responsible for the latest data call. James E. Sample has been responsible for trend calculations. A reference group consisting of Martyn Futter, Jens Fölster, Sandra Steingruber, Daniel Houle, Don Monteith and Michela Rogora contributed with comments during the writing of the report. The remaining authors have contributed with data, as well as input to the final draft of the report.

We wish to thank the National Focal Centres and their national funder organisations for their timely deliveries of high-quality monitoring data to ICP Waters databases.

Oslo, 17 January 2024

Heleen de Wit

ICP Waters Programme Centre

Summary

Trends in water chemistry in acid-sensitive regions present evidence for the effects of changing air pollution on surface waters. Recent evidence suggests that calcium, an important component of the capacity to buffer acidity, shows smaller changes than expected given the changes in strong acid anions in surface waters. Here, we present 1) a trend analysis of water chemistry in acid-sensitive regions from 1990 to 2020, and 2) a more detailed analysis of changes in calcium and its controlling factors, in terms of trends in strong acid anions, organic acidity, and bicarbonate.

Sulphate concentrations have declined significantly at 427 of the 430 selected sites from 1990 to 2020, and 4 of the 10 regions show more than a 40% decline for the period between 1990 – 2004 and 2006 – 2020. Nitrate declined in 8 of the regions, although 192 of the individual sites show no trend or an increase. Notably, chloride declined in 7 of 10 regions, and in Great Britain/Ireland/Netherlands (UK-IE-NL) the negative slopes were steeper than for sulphate and nitrate. Chloride levels are affected by the deposition of sea salts as well as air pollution. Changes in levels of sulphate and nitrate were more prevalent in the first period (1990 – 2004) than during the last (2006 – 2020), indicating air pollutants levelling off in recent years. On a regional scale, base cation concentrations have declined by approximately half the equivalent change in concentration of sulphate. All regions show increasing ANC between 1990 and 2020, reflecting a widespread recovery. Water pH has increased only slightly in all the regions, despite the large reduction in strong acid deposition. This is partially due to the replacement of the strong acids by weak acids (i.e., organic humic acids and carbonic acid), manifested as an increase in positive ANC. Trajectories of sulphate, ANC and pH indicate that recovery has slowed in Europe while accelerating in North America since the early 2000s. This is related to slower emission declines in Europe and faster declines in North America after 2000.

Based on the principle of electroneutrality, changes in cation and anion equivalent concentrations in runoff should balance. The large decline in strong acid anions would therefore be expected to be accompanied by downward trends in base cations, including calcium (Ca^{2+}). However, recent evidence suggests that in some regions, Ca^{2+} has increased despite the decline in sulphate (SO_4^{2-}). The sites included in this report show mostly declining trends in Ca^{2+}, with some exceptions. Increases in Ca^{2+} concentrations occurred in catchments that have a pH above 5.5 and have only been slightly anthropogenically acidified. At these sites, the temporal increase in especially bicarbonate (HCO_3^-), but also partly weak organic acid anions ($Org.^-$), is larger than the decrease in SO_4^{2-} concentrations. Consequently, the resulting negative charge (sum of strong acid anions, organic acidity, and bicarbonate) is increasing, leading to an associated increase in Ca^{2+}, which is the dominating cation at most sites. The increase in $Org.^-$ is driven by the increase in organic matter solubility, related to the decline in acid deposition, as previously established in ICP Waters data analyses. We hypothesize that the increase in HCO_3^- could be due to an increase in weathering rates. Longer growing seasons, higher forest biomass (both climate-related) and increased concentrations of dissolved organic matter (driven by reduced acid deposition) could all lead to more dissolved CO_2, root exudates and organic acidity in soil solution that might promote higher mineral weathering. To what extent these processes also affect recovery in more acidic and severely acidified sites is beyond the scope of this study.

We conclude that surface waters in Europe and North America show strong chemical recovery. In the past decade, chemical recovery in Europe is levelling off while it is accelerating in North America, in agreement with air pollution trends. In less acidic sites, observed increases in calcium are better explained by changes in bicarbonate than changes in strong acid anions. This might be the result of a climate-induced increase in weathering rates, and if this is correct, we should consider incorporating this in the process description of the models used to predict future chemical recovery.

Sammendrag

Trender innen vannkjemi i forsuringsfølsomme områder dokumenterer effektene av endret luftforurensning på overflatevann. Nyere data tyder på at kalsium, en viktig komponent i forhold til å bufre surheten i vann, viser mindre endringer enn forventet i forhold til nedgangen i sterke syres anioner i overflatevann. Her presenterer vi 1) trendanalyser av vannkjemi i forsuringsfølsomme regioner fra 1990 til 2020, og 2) en mer detaljert analyse av endringer i kalsium og dets kontrollerende faktorer, i form av trender i sterke syre anioner, organisk surhet og bikarbonat.

Konsentrasjonene av sulfat har gått betydelig ned fra 1990 til 2020 i 427 av de 430 studerte lokalitetene, og 4 av de 10 regionene viser mer enn 40 % nedgang for perioden mellom 1990 – 2004 og 2006 – 2020. Nitrat avtok i 8 av regionene, selv om 192 av overvåkningsstasjonene enten ikke viser noen trend, eller viser en økning. Klorid avtok i 7 av 10 regioner, og i Storbritannia/Irland/Nederland (UK-IE-NL) var nedgangen større enn for sulfat og nitrat. Kloridnivået påvirkes av avsetning av havsalt samt luftforurensning. Endringer i nivåene av sulfat og nitrat var større under den første perioden (1990 – 2004) enn i den siste (2006 – 2020), noe som tyder på at nedgangen i luftforurensningene har flatet ut de siste årene. På regional skala har konsentrasjonene av basekationer avtatt omtrent halvparten av tilsvarende endring i sulfatkonsentrasjon. Alle regioner viser økende syrenøytraliserende kapasitet (ANC) mellom 1990 og 2020, noe som gjenspeiler en utbredt gjenhenting fra forsuring. pH i vann har bare økt litt i alle regionene, til tross for den store nedgangen i avsetningen av sterke syrer. Dette er delvis på grunn av at de sterke syrene er erstattet med svake syrer (dvs. organiske humussyrer og karbonsyre). Dette ser vi som en økning i positiv ANC. Utviklingen for sulfat, ANC og pH indikerer at takten i gjenhentingen fra forsuring har avtatt i Europa mens den har akselerert i Nord-Amerika siden tidlig på 2000-tallet. Dette har sammenheng med mindre reduksjoner i utslipp i Europa og raskere reduksjoner i Nord-Amerika etter 2000.

Basert på prinsippet om ladningsbalanse må endringer i ekvivalente konsentrasjoner av kationer og anioner i vannprøvene balansere. Den store nedgangen i sterke syrers anioner vil derfor forventes å være ledsaget av tilsvarende trender i basekationer, inkludert kalsium (Ca^{2+}). Stasjonene som er studert i denne rapporten viser stort sett fallende trender i Ca^{2+}, med noen unntak. Ferske data tyder på at Ca^{2+} i noen regioner har økt til tross for nedgangen i sulfat (SO_4^{2-}). Økninger i Ca^{2+}-konsentrasjoner finner vi i nedbørfelt som har en pH over 5,5 og som kun er mindre antropogent forsuret. På disse stedene er det en økning over tid i spesielt bikarbonat (HCO_3^-), men også til dels svake organiske syreanioner (Org.$^-$) , som er større enn nedgangen i SO_4^{2-} konsentrasjoner. Følgelig øker den resulterende negative ladningen (summen av sterke sure anioner, organisk surhet og bikarbonat), noe som fører til økningen i Ca^{2+}, som i de fleste steder er det dominerende kationet. Økningen i Org.$^-$ er drevet av økningen i løseligheten av organisk materiale, relatert til nedgangen i sur nedbør, som tidligere rapportert fra ICP Waters dataanalyser. Vi antar at økningen i HCO_3^- kan skyldes økt forvitringshastighet. Lengre vekstsesong, større skogbiomasse (begge klimarelatert) og økte konsentrasjoner av løst organisk materiale (drevet av redusert syreavsetning) kan alle føre til økt forvitring gjennom at surheten i jordvannet øker på grunn av mer oppløst CO_2 og økt tilførsel av organiske syrer fra røtter. I hvilken grad disse prosessene også påvirker gjenhentingen fra forsuring i sterkt forsurede områder ligger utenfor målsetningen for denne studien.

Vi konkluderer med at overflatevann i Europa og Nord-Amerika viser stor grad av gjenhenting fra forsuring. Det siste tiåret har denne trenden i Europa flatet ut mens den har akselerert i Nord-Amerika, i samsvar med luftforurensningstrendene. I mindre sure vannforekomster er det observert økninger i kalsium som er bedre forklart av endringer i bikarbonat enn endringer i sterke syrers anioner. Dette kan være et resultat av en klimaindusert økning i forvitringshastigheten, og hvis dette er riktig, bør vi vurdere å inkludere dette i prosessbeskrivelsen for modellene som brukes for å forutsi fremtidig gjenhenting fra forsuring.

1 Introduction

1.1 The ICP Waters programme

Over the past five decades, there has been significant global attention focused on the issue of acid atmospheric deposition, commonly known as "acid rain," particularly in Europe and North America. Polluted air masses containing sulphur and nitrogen compounds traverse long distances, crossing international borders. Consequently, these acidifying substances have far-reaching effects on surface waters, groundwater, and forest soils, extending well beyond the countries where they originate. To address this environmental concern, the Convention on Long-range Transboundary Air Pollution (CLRTAP) was adopted in 1979 and became effective in 1983. This marked the initial step in implementing measures to reduce emissions of air pollutants on an international scale, with a primary focus on Europe and North America.

The Working Group on Effects (WGE) has aided the Convention by advancing scientific knowledge to support its Protocols. The WGE's sixth International Cooperative Programme (Modelling and Mapping, Waters, Vegetation, Forests, Materials, Integrated Monitoring) and a Joint Task Force with the World Health Organisation (WHO) on Human Health are dedicated to quantifying the effects of air pollution on the environment through monitoring, modelling, and scientific review.

The International Cooperative Programme on Assessment and Monitoring of the Effects of Air Pollution on Rivers and Lakes (ICP Waters) was established under the Executive Body of the Convention on LRTAP at its third session in Helsinki in July 1985. Norway has led ICP Waters since 1987.

One of the responsibilities of ICP Waters, as listed in the mandate[1], is to plan and conduct technical work to assess the extent, spatial patterns, temporal trends, and impact of air pollution, as well as its confounding factors, using monitoring data and other sources of scientific evidence. The monitoring programme is therefore designed to assess, on a regional scale, the degree and geographical extent of surface water acidification. The collected data serve to relate trends in acidic deposition with the changes in the physical, chemical, and biological status of lakes and streams. Additionally, they provide information on dose/response relationships under different environmental conditions. The ICP Waters Programme is based on existing monitoring programmes in participating countries, and it is implemented through voluntary national contributions.

1.2 The ICP Waters database

The ICP Waters database encompasses surface water data sourced from 19 countries spanning Europe and North America (Table 1). The dataset presently comprises 577 sites with long-term monitoring records, predominantly located in "acid-sensitive" regions. These areas exhibit low ANC and a history of acid deposition (Skjelkvåle et al., 2011). In 2023, much effort has been dedicated to completing the records available for all sites, with particular emphasis on the period from 2016 to 2020. Data used in this report are available on GitHub[2].

---

[1] https://www.unece.org/fileadmin/DAM/env/documents/2019/AIR/EB/ECE_EB.AIR_2019_9-1916525E.pdf

[2] https://github.com/JamesSample/icpw2/tree/master/thematic_report_2023

Table 1. ICP Waters sites by country.

Country	Number of sites
Armenia	10
Canada	115
Czech Republic	8
Estonia	1
Finland	26
Germany	33
Ireland	20
Italy	12
Latvia	8
Moldova	2
Netherlands	11
Norway	83
Poland	14
Slovakia	12
Spain	3
Sweden	92
Switzerland	10
United Kingdom	22
United States	95
Total	577

1.3 Objectives

As outlined above, a major aim of ICP Waters is to assess the long-term trends in aquatic chemistry that can be attributed to atmospheric pollution. The indicators most amenable to such analysis are those that respond to changes in the deposition of sulphur and nitrogen compounds, and their analysis has therefore featured as a recurring theme in the scientific reports issued by the Task Force, with a periodicity of about 4 years. As time series have grown longer, and as deposition levels have decreased, it has become evident that adding an extra three to five years of data does not result in significant alterations to regional and temporal trends. Readers of past ICP Waters reports might therefore recognize recurring elements and phrases. In the most recent reports, we have instead directed the attention to specific aspects of temporal development. In 2007 the specialist topic was "confounding factors", in which we explored how factors other than acid deposition could affect chemical and biological recovery (Skjelkvåle and de Wit, 2007). In 2011 and 2015 the emphasis shifted to biological recovery, or the lack thereof, along with attempts to compare trends from two different periods in water and precipitation. Additionally, efforts were made to predict future trends (Skjelkvåle and de Wit, 2011; Garmo et al., 2015). In the last report, published in 2020 (Garmo et al., 2020), we analysed shifts in long-term trends in average chemistry spanning 26 years (1990-2016). This analysis identified the specific points in time when significant changes had occurred. Furthermore, the last report featured a chapter dedicated to a review of how changes in land use impact the recovery of acidified waters.

In the current report, we follow up on the time trend analysis, dividing the dataset into three 15-year periods 1990-2004, 1998-2012, 2008-2020, and 12 regions. The use of overlapping periods was motivated by the need for sufficient periods for sound time trend analysis. We assess trends in sulphate (SO_4^{2-}), nitrate (NO_3^-), chloride (Cl^-), calcium (Ca^{2+}), magnesium (Mg^{2+}), acid neutralizing capacity (ANC), H^+, Organic anions (Org.$^-$), and bicarbonate (HCO_3^-).

A dedicated chapter of the report addresses cross-network differences in Ca^{2+} trends. There has been a consistent pattern of chemical recovery across a vast majority of the ICP Waters sites, characterized by decreasing SO_4^{2-} and NO_3^- and increasing pH and ANC. The principle of electroneutrality, where cation and anion charges must balance, suggests that Ca^{2+} levels might be expected to have fallen in response to the declining anion levels. In line with this, a global analysis confirms that downward temporal trends in Ca^{2+} dominate in base-cation-poor regions of the world receiving declining deposition of acid deposition (Weyhenmeyer et al., 2019), including the ICP Waters region.

However, there are exceptions to this pattern that remain not fully understood. In the Norwegian national 1000 lake survey in 2019 compared to 1995 (de Wit et al., 2023), as well as in a long-term annual survey of 78 lakes (i.e., "TrendLakes") (Vogt & Skancke, 2023), we noted an upward trend in Ca^{2+}, except for South Norway (the part of the country with historically the most acidified surface waters).

Understanding the major biogeochemical processes driving changes in base cation concentrations and an accurate description of catchment buffering of acidic deposition is pivotal, both for critical load calculations within process-oriented models and for predicting future recovery effects on aquatic organisms that are sensitive to low calcium levels. Gaining a better understanding of the biogeochemical controls of Ca^{2+} is therefore a key to understanding current trends and making predictions regarding future recovery of acidified surface waters. Moreover, the increase in Ca^{2+} concentrations challenge our models' predictions of recovery from acidification for lakes and rivers. This is thus investigated further in Chapter 3 based on the very extensive data from ICP Waters sites.

2 Trends in Surface Water Chemistry 1990 – 2020

Anthropogenic emissions of acid oxides have greatly declined in Europe and Norh America since 1990 (Fagerli et al., 2023). The decline in SO_4^{2-}, formerly the major non-marine anion in most surface waters in acid-sensitive regions, has been accompanied by a significant recovery in water chemistry. We report trends for sites that are grouped into regions defined by geographic location, acid sensitivity and rates of deposition. These regions adhere to those used in previous ICP Waters trend reports.

2.1 Methods

2.1.1. Selection of sites for analysis

The sites in the ICP Waters database have been selected by the Focal Centres. They should preferably be sensitive to acid deposition (e.g., have inherent low alkalinity) and have a short response time. Their catchments should also be relatively undisturbed and be without significant local sources of pollution (ICP Waters Programme Centre, 2010). The sites are thus predominantly headwaters, many of them located in protected environment areas. Sites with known contamination (e.g., from mining) were excluded[3]. National providers of the data used in this report are listed in Table A3.

Raw data were extracted for all ICP Waters sites and derived parameters (such as ANC, organic anions (Org.$^-$) and bicarbonate (HCO$_3^-$)) were calculated for each sample, where possible.

To gain a clearer understanding of potential shifts in temporal dynamics over time, the analysis considers four periods of interest: the whole period from 1990 to 2020, the initial period covering the years from 1990 to 2004, the middle period from 1998 to 2012, and the most recent period going from 2006 to 2020. To avoid spurious results due to missing data, we applied selection criteria for inclusion of the data from each site for each of these periods:

- At least one annual value within the first 5 years of the period.
- At least one annual value within the last 5 years of the period.
- Data available for at least 65% of years in the period (e.g., 1990 to 2020 is 31 years, so the data series must have at least $0.65 \cdot 31 = 20$ valid annual values).

These criteria were applied separately at each site for the following parameters: pH, TOC, base cations ([Ca^{2+}], [Mg^{2+}], [Na$^+$], [K$^+$], and [NH$_4^+$]), and strong acid anions (SO$_4^{2-}$, NO$_3^-$, and Cl$^-$), enabling the calculation of strong acid anions (SAA), acid neutralising capacity (ANC), Org.$^-$, and HCO$_3^-$ (Chapter 2.1.3). Sites were included in the final selection for each period only if the criteria were met for all parameters simultaneously. An exception was made for the lack of TOC data for sites in Italy and Switzerland as their waters do not contain significant levels of dissolved organic matter.

---

[3] The sites in Moldova (MD01 and MD02) and several sites in Germany (DE04, DE09, DE14, DE15, DE21, DE25, DE30 and DE31) were removed as we suspect these sites are affected by mining. Sites in Latvia and Estonia were removed due to that they are not acid sensitive. Edasjön (SE55) was removed as it is an outlier having a neutral pH (7.12), with high Ca^{2+} levels (1.02 mEq/L), driven by a high HCO$_3^-$ (0.95 mEq/L).

This yielded the following numbers of sites included in further analyses:

- 1990 to 2020:   430 sites (Figure 1)
- 1990 to 2004:   445 sites
- 1998 to 2012:   462 sites
- 2006 to 2020:   440 sites

Of these sites, 405 met the criteria for all four periods. This limited selection would provide the most coherent picture of changes over time, but for some regions, the number of sites is small or lacking completely (Figure 2). The main strength of the ICP Water database is the large number of sites, spanning large gradients in drivers and pressures. In this report, we draw from a variable population of sites for the different periods to maximise site diversity.
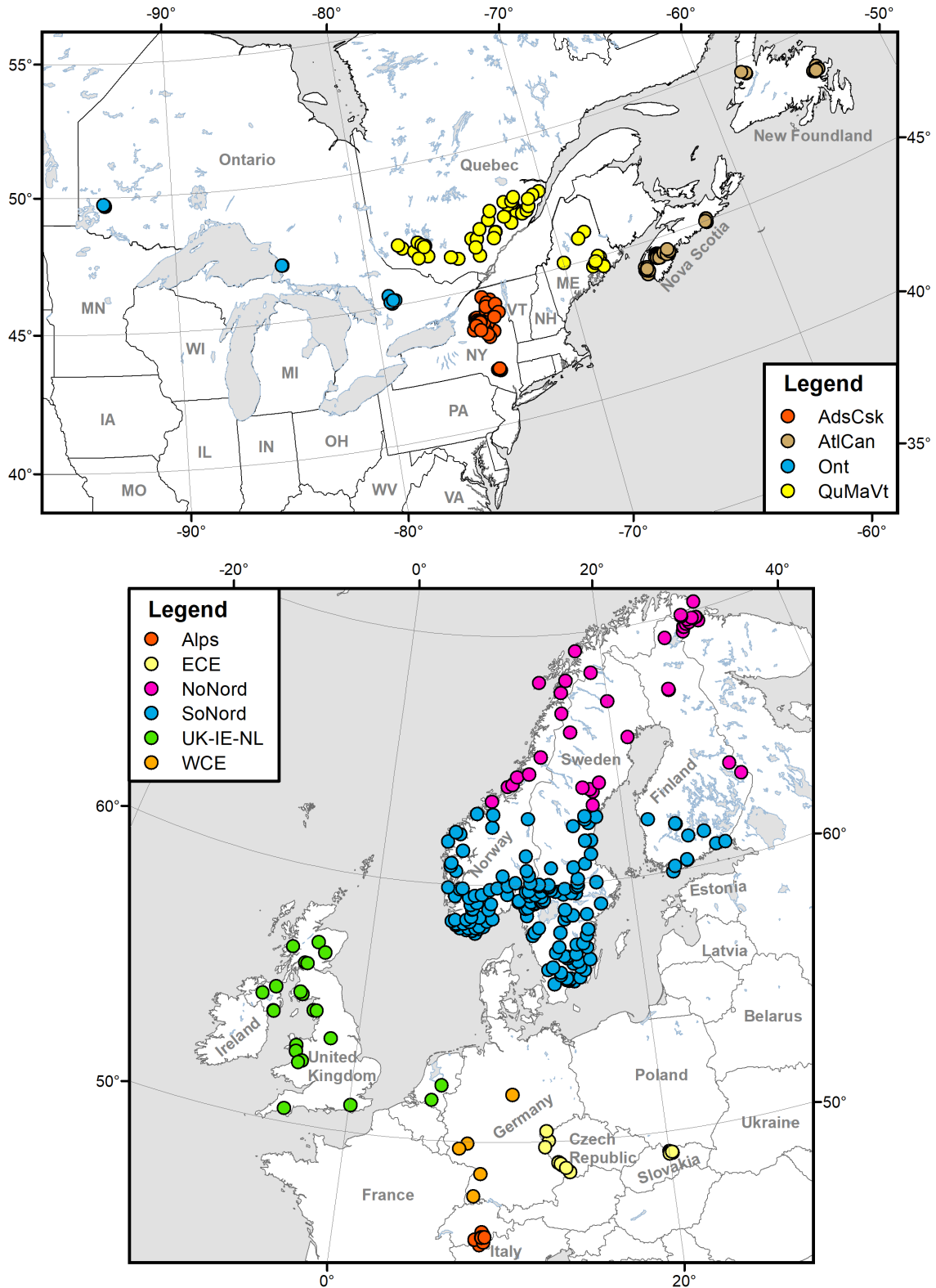
Figure 1. Maps showing the 430 sites that passed the criteria for estimating trends from 1990 to 2020. Region names are abbreviated as follows: NoNord = North Nordic; SoNord = South Nordic; UK-IE-NL = Great Britain/Ireland/Netherlands; WCE = West Central Europe; ECE=East Central Europe; AdsCsk = Adirondack/Catskill; AtlCan = Atlantic Canada; Ont = Ontario; QuMaVt = Quebec/Maine/Vermont.
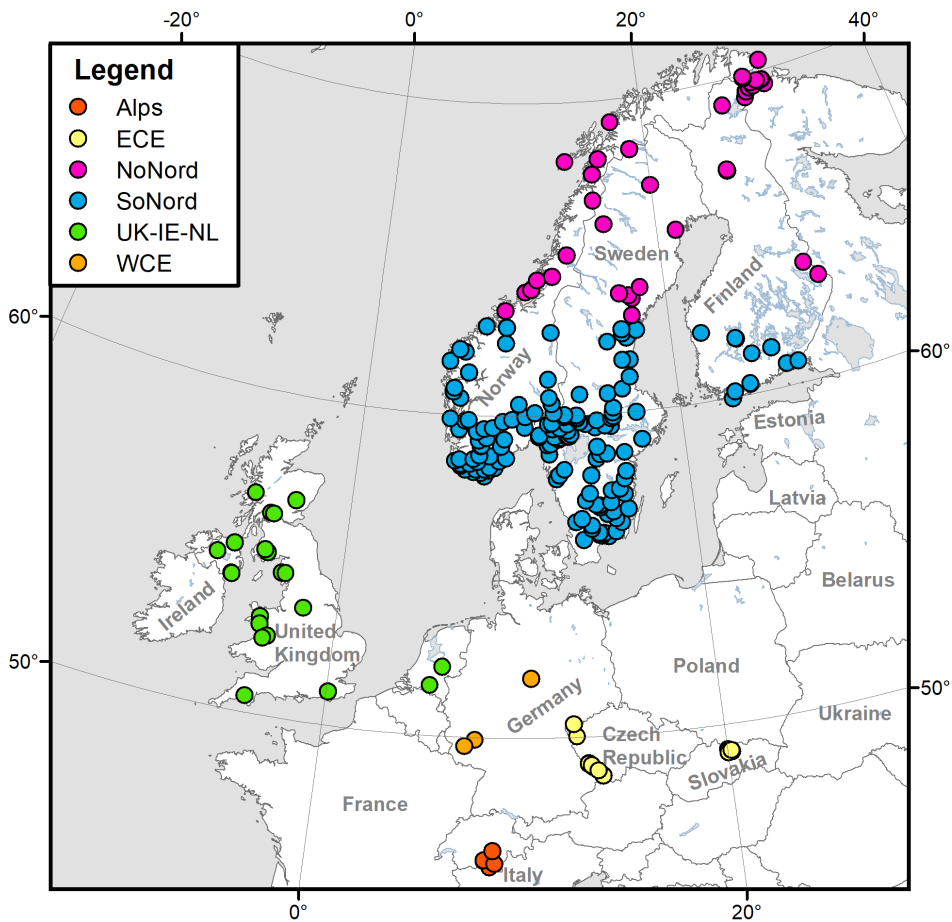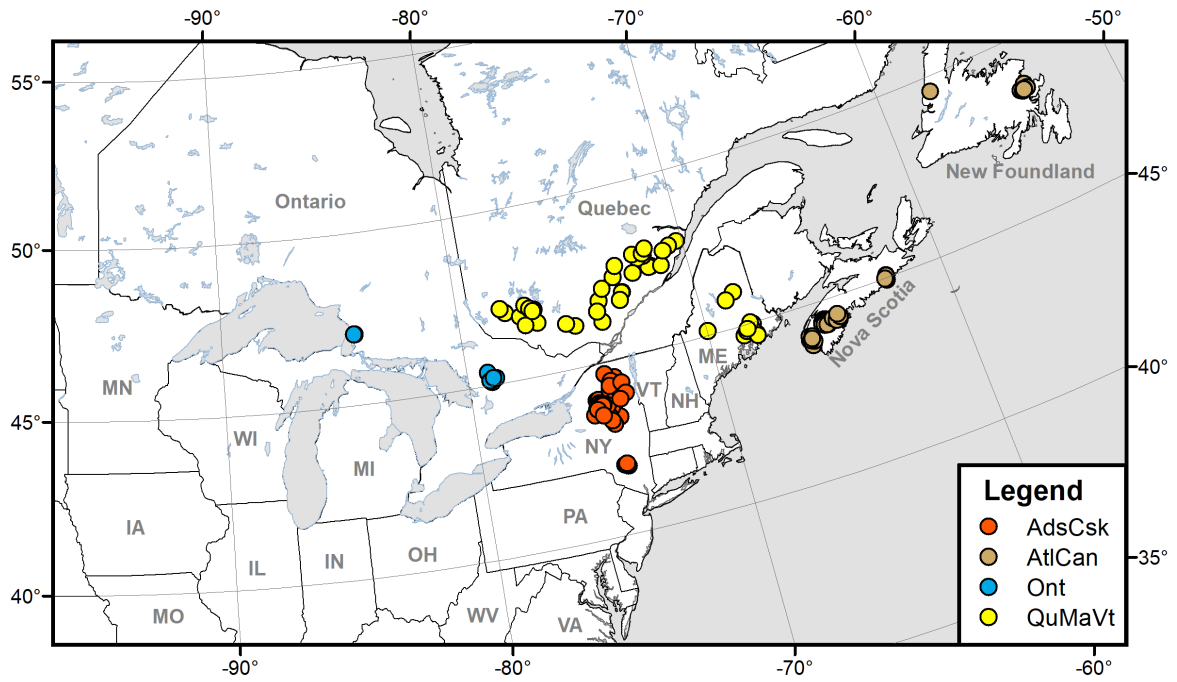
Figure 2. Map of the 405 sites that have data for all the three 15-year time series 1990-2004, 1998-2012, and 2008-2020. See the caption of Figure 1 for explanations or abbreviations.

2.1.2. Quality assurance of data

Standardization of sample collection and analytical methodologies are addressed in the ICP Waters Programme Manual (ICP Waters Programme Centre, 2010). Three levels of quality control (QC) of water chemistry data are distinguished: intra-laboratory controls in individual countries, inter-laboratory controls (Bryntesen, 2022) and QC of data reported to the National Focal Centres and forwarded to the Programme Centre at NIVA. The latter involves a technical procedure including ascertaining outliers. To identify and remove outliers, we used a "double Median Absolute Deviation" approach based on Hampel (1974). In this step, the "outlier threshold" was set to a conservative value of 5 – instead of the more common value of 2.5 to 3, to ensure only extreme outliers were removed. Annual medians for each parameter at each site were then calculated.

2.1.3. Variables and statistical methods

Our analysis is restricted to variables that play major roles in acidification and recovery:

1. **SO_4^{2-} and NO_3^-**, the acid anions of acidic deposition. Trends in the concentrations of these anions usually reflect recent trends in deposition (especially SO_4^{2-}) and in ecosystem response to long-term deposition (e.g., NO_3^-).

2. **Cl^-**, another acid anion that reflects the sea-salt influence, and in some regions (e.g., UK-IE-NL) anthropogenic emissions of hydrochloric acid.

3. **Ca^{2+} and Mg^{2+}** are divalent base cations. They are mobilised by weathering reactions and cation exchange that neutralise acids in watersheds. Deposition from air may also be a (usually minor) source.

4. **pH** is the negative log of the H^+ activity, reflecting the acidity of the water. All pH values were transformed to H^+ concentrations before any statistical analysis.

5. **Acid Neutralising Capacity (ANC)** is calculated as the difference between the equivalent sum of base cations (BC = $[Ca^{2+}]$ + $[Mg^{2+}]$ + $[Na^+]$ + $[K^+]$ + $[NH_4^+]$)[4] and strong acid anions (SAA = SO_4^{2-} + NO_3^- + Cl^-). Ammonium (NH_4^+) is assumed negligible where data are lacking (i.e., 27% of the samples). ANC reflects the water's ability to neutralize acid inputs. ANC can also be conceived equal to $[HCO_3^-]$ + $[Org.^-]$ - $[H^+]$ - $[Al^{n+}]$, i.e., the remaining ions constituting the charge balance. The aluminium ($[Al^{n+}]$) and bicarbonate (HCO_3^-) charge concentrations are assumed to be negligible in samples with pH above and below 5.5, respectively. The ANC is therefore conceived to be equal to the charge of $[HCO_3^-]$ + $[Org.^-]$ - $[H^+]$ in samples with pH above 5.5. Below pH 5.5 the ANC mainly includes $[Org.^-]$ - $[H^+]$ - $[Al^{n+}]$.

6. **Total organic carbon** (TOC) or dissolved organic carbon (DOC) - i.e., organic carbon measured in samples after filtering through, for example, a 0.45 μm filter. TOC and DOC are considered proxies for dissolved organic matter (DOM), mainly derived through the degradation of soil organic matter in catchment soils. The difference between TOC and DOC in headwaters is usually minor.

7. **Organic anions** ($Org.^-$) is the average charge of DOM, balancing a significant fraction of the positive ANC charge. It is estimated according to the tri-protic acid model by Hruška et al. (2003)[5], which generates similar results as the model by Oliver et al. (1983).

8. **Bicarbonate** (HCO_3^-) is also balancing a significant part of the positive ANC at pH above 5.5. It is estimated from the equivalent charge balance (i.e., ($[HCO_3^-]$ = ANC + $[H^+]$ – $[Org.^-]$), assuming the charge contribution by labile aluminium to be insignificant at pH above 5.5. Where HCO_3^- is calculated to be negative it is set to 0. At pH above 5.5 the HCO_3^- concentration becomes significant as more than 14% of carbonic acid present is deprotonated ($\frac{[H_2CO_3]}{[HCO_3^-]} = \alpha_1 = 0.86$).

---

[4] *The brackets refer to concentration in μEq/L. Ammonium concentration was set to zero where unavailable. ANC was not calculated if data on any of the other major ions were missing.*

[5] *The pKa values used in the model are $pK_1=3.04$, $pK_2=4.42$, $pK_3=6.70$, with a site density of 16.6 μEq/mg C.*

Analysis of trends in other important variables, such as labile aluminium and alkalinity, is hampered in the ICP Waters dataset by large differences in analytical methods between laboratories due to lack of standardisation (see e.g., Hovind, 1998).

The frequency of observations at each site varied from a single annual observation in some lakes to weekly sampling in some streams, and the frequency of observations for some sites differed between years. For each site, an annual median was therefore calculated for each variable, and used in the statistical analysis of trends from 1990 to 2020, and for the three 15-year periods. Thus, seasonality in the data only influenced the annual value and did not affect the power of the statistical tests.

The Mann-Kendall test (MKT) (Hirsch and Slack, 1984) is used to identify monotonic trends for individual sites for the periods 1990-2020, 1990-2004, 1998-2012, and 2008-2020 from the value of the test statistic (Z-score). The MKT is robust against outliers and missing data. Moreover, it does not require normal distribution of data. Slopes were calculated using the Sen's estimator (Sen, 1968). A paired t-test is used to test for differences between individual trend slopes for the partly overlapping periods. Regional trends in annual median values are assessed using the Regional Kendall Test (RKT) (Helsel and Frans, 2006), which provides median slopes and statistical significance of the trend. The RKT has similar strengths as the MKT and again does not require normal distribution of data. All time trend and slope analyses have been computed using Python 3.10 (Python Software Foundation, 2023), while multivariate statistics and regressions have been conducted in Minitab statistical software (Minitab, 2021).

2.2 Results

2.2.1. Data Characteristics

Statistical descriptors of all parameters were assessed with a varying population of sites for the different periods (Chapt. 2.1.1).

On average Ca^{2+} accounts for most of the cation charge, followed by Na^+ and Mg^{2+} (Figure 3). The anion charge is dominated by SO_4^{2-} followed closely by Cl^-, Org.$^-$ and HCO_3^- (Figure 3). Since the ICP Waters sites were selected to follow the effect on water chemistry caused by the decline in acid oxide emissions, the average of annual median SO_4^{2-} levels from 1990 to 2020 of the 430 sites are rather high (64.5) µEq/L, though there is a wide distribution among the samples (Figure 4). Although the ICP Water watersheds are acid-sensitive, the average of annual median ANC and Ca^{2+} concentrations are 69.8 µEq/L and 80.7 µEq/L, respectively. The dataset comprises several samples that are less acidic and

Figure 3. Grand average water ionic composition at the 73 656 ICP Waters samples from 1990 to 2020.

anthropogenically acidified (Figure 4). The average of annual median pH values (based on H^+ Eq.) is only 5.39, though more than 292 sites have average pH values above 5.5. Org.$^-$ and HCO_3^- are relatively high with averages of annual median concentrations of 66.6 µEq/L and 23.5 µEq/L, respectively.
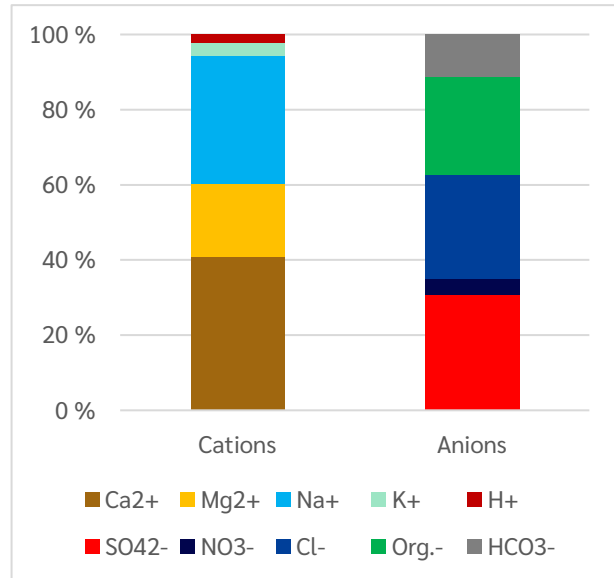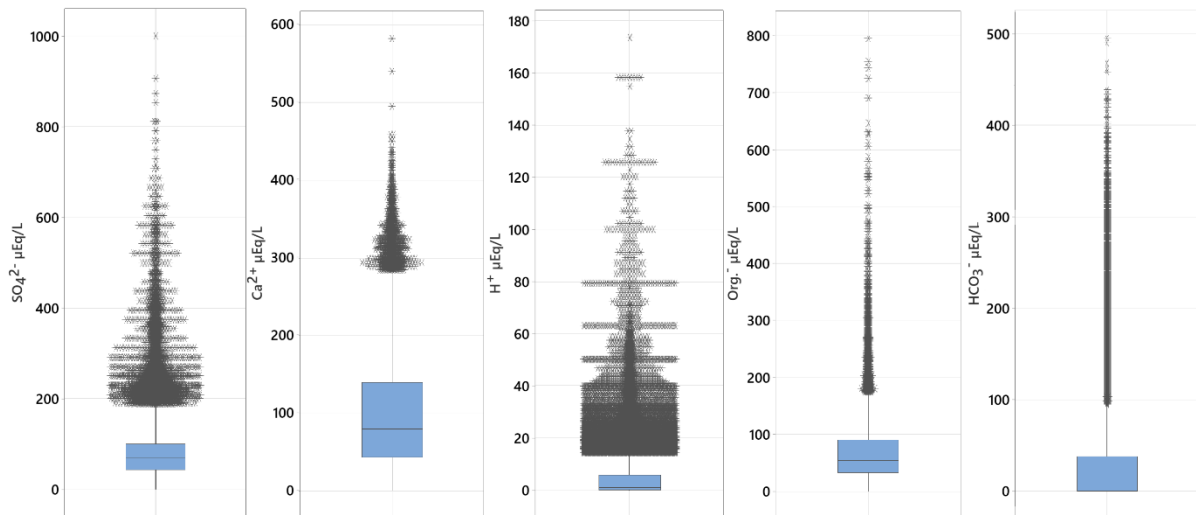

Figure 4. Box and whisker plots of the distribution of all data for SO_4^{2-}, Ca^{2+}, H^+, Org.$^-$ and HCO_3^- in the 73656 ICP Waters samples from 1990 to 2020, showing median, interquartile range box (50% of the data), whiskers (top and bottom 25%), and outliers (i.e., 1.5 times the interquartile range). Symbols for identical outlier values are distributed horizontally to reveal overlapping points.

2.2.2. Inter-parameter relationships

Grand inter-parameter relationships in time and space are analysed by studying the 73 656 water samples from the 430 ICP Waters sites assessed from 1990 to 2020 using Principal Component Analysis (PCA) and Cluster analysis. A PCA of only spatial variation, assessing the median values of the 440 sites with data from 2006 to 2020, is depicted in Appendix Figure A1. Since the ranges in spatial variations are considerably larger than temporal changes this figure shows very similar inter-parameter relationships to the grand relationships shown in Figure 5a. The main principal component (PC1) (Figure 5a) of the PCA, is an ionic strength gradient, explaining 37.2% of the variation in the data. Although mainly driven by spatial differences, this ionic strength gradient may also be interpreted as a temporal component as the ionic strength has declined with decreasing acid deposition. All parameters except H^+ have positive loading, although this is weak for NO_3^-. That H^+ has a negative loading along the PC1 reflects the tendency for waters with lower ionic strength to have lower buffering capacity and hence be more likely to be acidic and/or acidified. Nitrate has a weak PC1 loading since, as a nutrient, it is also regulated by other drivers. The second principal component (PC2), explaining an additional 20.8% of the variance, reflects an acid sensitivity and marine gradient and may be interpreted more as a spatial component. Here the acid parameters hydrogen ion (H^+), and sea salts (Na^+ and Cl^-) have a strong negative loading as opposed to the more alkaline parameters Ca^{2+} and HCO_3^- that have strong positive loadings. Notably, the SO_4^{2-}, along with Org.$^-$, Mg^{2+}, and K^+, have weak loadings along this spatial gradient. That the sulphate and Org.$^-$ have weak loading as opposed to the strong loading of HCO_3^- along an acid spatial gradient, reflects the increasing importance of carbonate buffering at sites with pH above 5.5. The sample score plot (Figure 5b) reveals an even distribution of the samples.

The cluster analysis (Figure 6) reflects the parameter grouping in the PCA (Figure 5a), and reveals a cluster of SO_4^{2-}, Mg^{2+} and K^+, along with the Na^+ and Cl^- indicative of sea salt sources. Again, we find that HCO_3^- clusters with Ca^{2+}. Moreover, the weak link between SO_4^{2-} and Ca^{2+} is noteworthy. Having an opposite loading to H^+ on the PC2 HCO_3^- is a strong contributing factor to the variation in Ca^{2+}. Notably, Ca^{2+} differs from Mg^{2+} in that Ca^{2+} follows HCO_3^-, while Mg^{2+} is associated with the SO_4^{2-}. This may partly be due to that both sulphate and magnesium are more linked to sea salts than calcium.
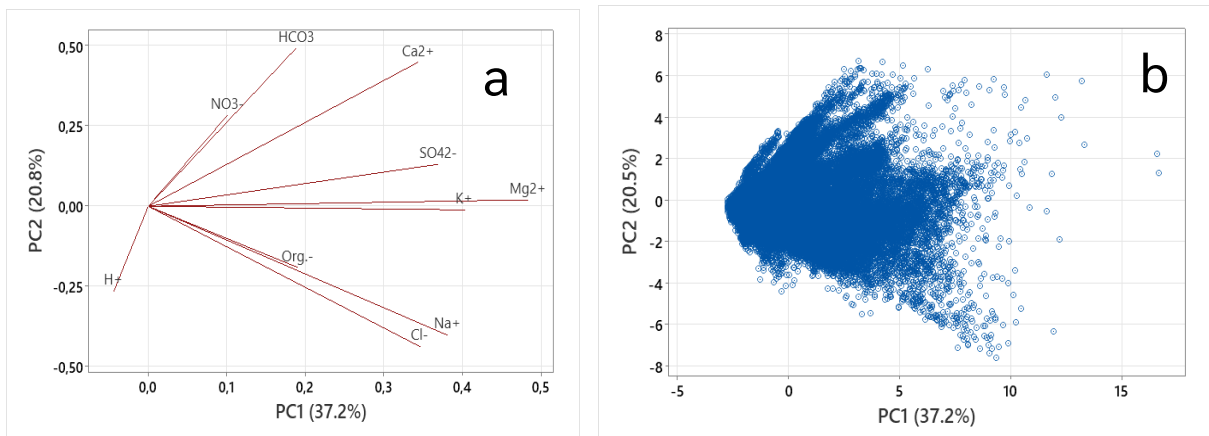

Figure 5. PCA parameter loading plot (a) and sample score plot (b) of the major descriptive parameter's loadings along the two main principal components.
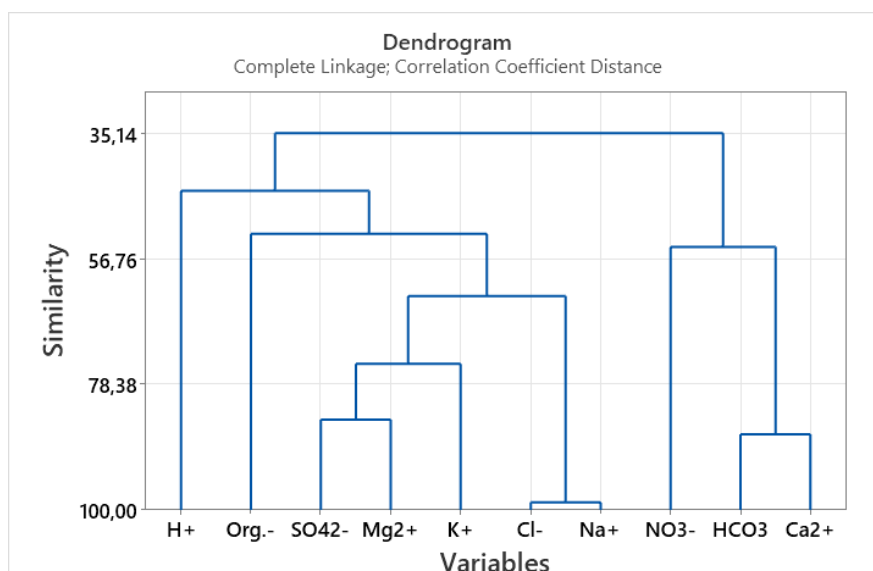
Figure 6. Dendrogram showing parameter clustering based on correlation coefficient distance of data from 1990 to 2020.

Differences in Ca^{2+} are much more closely correlated with HCO_3^- than SO_4^{2-}, as would be expected from temporal relationships alone. This is partly because the multivariate analysis is based on a grand mix of samples in space and time. Still, assessing only the spatial variation we find that the variation in annual median concentrations of Ca^{2+}, at the 430 sites with data from 1990 to 2020, is better explained by the variation in HCO_3^- (54.4%), than by SO_4^{2-} (32.9%) or $Org.^-$ (13.1%), as deduced by the coefficient of determination (R^2) in simple trendline analysis (Figure A2). This is also reflected in the loadings of these parameters along the PC2 (Figure 5a). The mainly spatial correlation between nitrate and bicarbonate (conf. Figure A1) could be due to those catchments with higher levels of NO_3^-, are less N limited, therefore relatively more productive - with more root respiration resulting in higher CO_2 production and hence more HCO_3^-. Still, the focus of this report is the temporal trends at the sites, where the declines in SAA likely play a more significant role. This analysis nevertheless points out that the effects of temporal trends are contingent on spatial differences in site characteristics.

2.2.3. Regional patterns and temporal trends
Surface water chemistry of the acid sensitive ICP Waters headwater catchments has changed markedly across Europe and North America (Figure 7), owing to the reductions in emissions to the atmosphere of sulphur and nitrogen oxides achieved under the CLRTAP (2023). Most evident is the 34% and 28% regional average declines in SO_4^{2-} and NO_3^- concentrations, respectively, between the periods 1990-2004 and 2006-2020 (Table 2) and an increase in pH and ANC across a majority of the sites (Table 3).

Of the 430 sites assessed from 1990 to 2020, 427 show decreasing SO_4^{2-} trends. The Swedish site Abiskojaure is the only one to show an increasing trend (possibly due to melting glaciers leading to exposure of sulfidic shale minerals), while two sites (Svardalsvatnet in Norway and Stor-Tjulträsket in Sweden) show no SO_4^{2-} trend (Table 3). Reductions in NO_3^- concentrations, especially in absolute values, were smaller and more subtle in most regions than for SO_4^{2-}. Slightly more sites showed a decrease in NO_3^- (238), than no trend (178), whereas increases were rare (14) across all regions (Table 3). Cl^-, another acid anion, has also decreased at many (163) sites, though it also increased slightly at 29 sites. These overall changes in strong acid anions are the major drivers of general reductions in base cation concentrations. Lower concentrations of mobile acid anions draining through the catchment soils lead to lower amounts of base cations (BC) being released and leached from the soil. However, Ca^{2+} trends were not universally negative as its concentrations did not change significantly at 164 sites and even increased at 36 of the

sites. The sites with increasing Ca^{2+} occur mainly in the regions NoNord (17 sites), SoNord (9 sites) and AtlCan (6 sites). That BCs have decreased less than the acid anions is due to buffering mechanisms in the soils, resulting in widespread increases in ANC and pH. Organic acids (Org.$^-$) have increased at 77% of the sites. However, the change in the balance of acid and base cations, in terms of equivalence, is lower than the change in the balance between strong and weak acid anions. The resulting anionic charge surplus is conceived to be made up of bicarbonate. The weak organic and carbonic acids have partially replaced the strong mineral acids and thus counteracted the decline in BC and increase in pH. In other words, a more pronounced rise in ANC compared to the increase in Org.$^-$ relative to the decrease in H$^+$ and acid cations (e.g., LAl) implies increased bicarbonate (HCO$_3^-$) concentrations at 34% of the sites. In the NoNord region, the Regional Kendall Test (RKT) showed increasing trends for HCO$_3^-$ at 75% of the sites.

The strength of trends in chemical parameters varies between the sub-periods analysed (Table 4). In Europe, the decline in SO$_4^{2-}$ has become less pronounced in later years, whereas in North America the trend slopes are generally more pronounced after 2006 (purple in Table 4). The historically very heavily polluted Western Central Europe (WCE) is unusual in that median sulphate values show a 4% increase between the periods 1990 – 2004 and 2006 – 2020 (Table 2). The median value declined from 191 µEq/L in 1990 – 2004, to 119 µEq/L during 1998 – 2012, but then increased again to 199 µEq/L in 2006 – 2020 (Table A1). This is an artefact due to varying site selection of a limited number of sites between the periods (Chapt. 2.1.1). The deviations could have been caused by e.g., oxidation of sulphide from legacy S in wetlands after droughts. Still, there is an overall significant (p < 0.01) decreasing trend according to RKT and a strong negative Sen's slope (-2.3) in this region (Figure 8). In most regions of North America, the positive slopes in ANC have become steeper (more positive, i.e. orange in Table 4). In the next chapters, we take a closer look at the magnitude of the trends in these parameters and how they differ between regions.

Table 2. Regional median levels for the whole period 1990-2020, as well as the per cent change between the periods 1990 – 2004 and 2006 – 2020. The median levels are the average annual median values for all the sites in each region. See Table A1 in the Appendix for median concentration values for 1990-2004, 1998 – 2012, and 2006 – 2020. NA denotes not analysed.

	SO$_4^{2-}$	NO$_3^-$	Cl$^-$	Org.$^-$	HCO$_3^-$	Ca^{2+}	Mg^{2+}	H$^+$	ANC	TOC
Region					µEq/L					mg C/L
NoNord	37.5	0.57	62.1	28.0	14.9	54.9	39.9	0.54	45.0	2.10
SoNord	61.5	3.04	88.0	85.2	0.0	73.4	48.0	1.58	67.1	7.00
UK-IE-NL	57.1	8.25	202	39.3	0.0	45.9	52.6	2.28	19.0	3.70
WCE	145	35.7	82.9	47.6	14.2	122	132	1.00	51.9	4.38
ECE	48.5	21.8	6.12	14.0	4.08	87.2	14.2	1.95	29.6	1.26
Alps	34.8	23.1	4.23	4.72	29.3	57.2	10.2	0.28	32.5	NA
Ont	95.8	4.05	8.86	51.1	47.0	120	40.2	0.32	95.2	3.87
AdsCsk	71.7	7.98	7.83	52.6	0.0	72.5	25.4	1.72	31.5	4.37
QuMaVt	58.3	2.36	9.87	56.4	9.76	73.4	29.9	0.49	62.1	4.45
AtlCan	37.9	1.43	111	70.3	0.0	35.9	32.9	2.38	42.4	6.40
Average	64.8	10.8	58.3	44.9	11.9	74.3	42.5	1.25	47.6	3.79
Region					%					
NoNord	-27	-45	-9	14	140	3	0	-24	62	10
SoNord	-42	-21	0	27	0	-22	-14	-34	31	24
UK-IE-NL	-36	-15	-7	67	0	-7	-2	-69	291	39
WCE	4	-21	48	90	-100	4	15	157	49	66
ECE	-50	-40	-31	39	0	2	-13	-86	287	24
Alps	-54	-52	-84	NA	-68	-56	-81	34	-66	NA
Ont	-31	20	-21	3	-17	-11	-13	28	2	2
AdsCsk	-42	-44	-18	21	0	-17	-16	-52	128	15
QuMaVt	-35	-58	0	14	96	-15	-12	-31	24	7
AtlCan	-30	0	4	24	0	1	0	-62	38	16
Average	-34	-28	-12	0	0	-12	-14	-14	85	0

Table 3. The number of sites showing significant (p < 0.05) positive or negative Mann-Kendall trends (MKT) in SO_4^{2-}, NO_3^-, Cl^-, Org.$^-$, HCO_3^-, Ca^{2+}, H^+, ANC, and TOC, between 1990 and 2020. The "+" and "-" signs represent increasing and decreasing trend, respectively. No trend is abbreviated "n.t.". NA denote not analysed.

	SO_4^{2-}			NO_3^-			Cl^-			Org.$^-$			HCO_3^-		
Regions	-	+	n.t.	-	+	n.t.	-	+	n.t.	-	+	n.t.	-	+	n.t.
NoNord	38	1	1	23	0	17	16	0	24	0	24	16	1	30	9
SoNord	145	0	1	82	6	58	46	7	93	0	133	13	8	40	98
UK-IE-NL	23	0	0	12	2	9	16	0	7	0	21	2	2	8	13
WCE	5	0	0	3	0	2	0	0	5	0	3	2	0	1	4
ECE	24	0	0	20	0	4	13	0	11	0	21	3	0	11	13
Alps	10	0	0	8	0	2	5	2	3	NA	NA	NA	0	3	7
Ont	15	0	0	4	1	10	11	1	3	0	12	3	0	7	8
AdsCsk	55	0	0	45	0	10	44	3	8	0	45	10	0	28	27
QuMaVt	51	0	0	28	1	22	9	1	41	3	33	15	2	14	35
AtlCan	61	0	0	13	4	44	3	15	43	0	30	31	1	5	55
Sum	427	1	2	238	14	178	163	29	238	3	332	95	14	147	269

	Ca^{2+}			Mg^{2+}			H^+			ANC			TOC		
Regions	-	+	n.t.	-	+	n.t.	-	+	n.t.	-	+	n.t.	-	+	n.t.
NoNord	7	17	16	5	6	29	22	1	17	0	37	3	0	19	21
SoNord	103	9	34	114	4	28	99	2	45	2	134	10	0	129	17
UK-IE-NL	18	1	4	17	0	6	16	0	7	0	22	1	0	19	4
WCE	2	0	3	1	0	4	5	0	0	0	4	1	1	3	1
ECE	15	3	6	13	2	9	23	0	1	0	22	2	0	16	8
Alps	7	0	3	8	0	2	6	0	4	0	6	4	NA	NA	NA
Ont	11	0	4	13	0	2	5	1	9	0	13	2	0	11	4
AdsCsk	51	0	4	51	0	4	32	2	21	0	50	5	0	39	16
QuMaVt	38	0	13	44	0	7	39	0	12	0	32	19	6	24	21
AtlCan	14	6	41	20	1	40	45	0	16	0	38	23	0	14	47
Sum	266	36	128	286	13	131	292	6	132	2	358	70	7	284	139
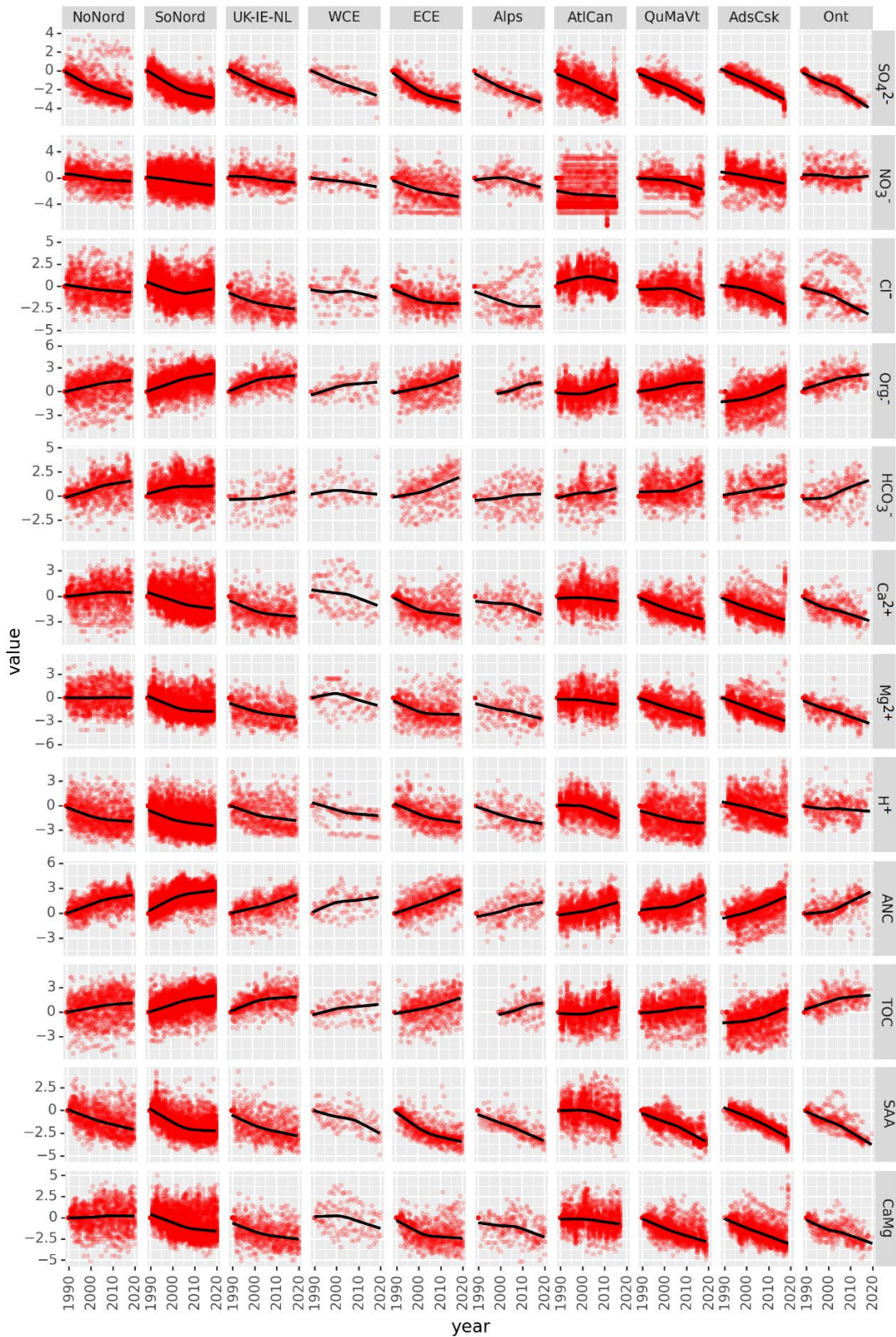
Figure 7. Time series trends (μEq/L/yr) between 1990 and 2020 for SO$_4^{2-}$, NO$_3^-$, Cl$^-$, Org.$^-$, HCO$_3^-$. Ca^{2+}, Mg^{2+}, H$^+$, ANC, TOC, SAA and CaMg. Each point represents the difference between the annual median value and the annual median of the first year in the time series, divided by the standard deviation. The solid lines indicate the moving average and represent Locally Weighted Scatterplot Smoothing (LoWeSS) smoothers. The plots allow direct comparison across regions and variables. Note that the scales on the y-axis are different for different variables.

Table 4. Overview of changes in Sen's slopes and change in direction of RKT trends. Blue and purple colour indicates negative Sen's slopes and red and orange indicate positive slopes. Plus, and minus represent increasing and decreasing RKT trends, respectively, over the whole period. White and "n.t." refer to zero slope and no trend. n.d. denote No data. Purple and orange denote whether differences in Sen's slopes for the last period (2006-2020) compared to the first period (1990 – 2004) diverge from the overall trend by being more negative, or more positive, respectively.

Continent	Region	SO_4^{2-}	NO_3^-	Cl^-	$Org.^-$	HCO_3^-	Ca^{2+}	Mg^{2+}	H^+	ANC	TOC
Europe	NoNord	-	-	-	+	+	+	n.t.	-	+	+
	SoNord	-	-	-	+	+	-	-	-	+	+
	UK-IE-NL	-	-	-	+	+	-	-	-	+	+
	WCE	-	-	n.t.	+	+	-	-	-	+	+
	ECE	-	-	-	+	+	-	-	-	+	+
	Alps	-	-	n.t.	+	n.d.	-	-	-	+	n.d
N America	Ont	-	-	-	+	+	-	-	-	+	+
	AdsCsk	-	-	-	+	+	-	-	-	+	+
	QuMaVt	-	-	-	+	+	-	-	-	+	+
	AtlCan	-	-	+	+	+	-	-	-	+	+

Legends:

-    Decreasing RKT trend   +   Increasing RKT trend

[blue] Negative Sen's slope   [purple] Neg. Sen's slope except during the last period

[red] Positive Sen's slope   [orange] Pos. Sen's slope except during the last period

There were 81 (18%) sites with negative median ANC values during the first period from 1990 to 2004, while only 17 (4%) still had negative median ANC values during the last period of 2006 – 2020. Since the calculated ANC corresponds to the difference in the equivalent sum of BC and SAA this implies a dominance of SAA over BC at these sites. Alternatively, the charge balance can be expressed in terms of the sum of weak acid anions (i.e., [Org.$^-$] and [HCO$_3^-$]) subtracted for the sum of acid cations (i.e., [H$^+$] and [Al^{n+}]), so in the case of these sites with negative ANC the equivalent sum of acid cations (i.e., H$^+$ and mainly Al^{n+}) remains greater than the sum of weak acid anions (i.e., Org.$^-$ and HCO$_3^-$). At the other end of this spectrum, 216 (49%) of the sites contained significant carbonate alkalinity (i.e., ANC + H$^+$ - Org.$^-$ > 0) during the last period. The average median pH at these sites is 6.3, implying a negligible aluminium and hydrogen ion charge. The calculated ANC thus corresponds to the sum of [Org.$^-$] and [HCO$_3^-$] (average values of 61 and 71 µEq/L, respectively).

2.2.3.1. Trends in sulphate concentrations across regions

From 1990 to 2020, SO_4^{2-} concentrations declined across all regions (Figure 8). As expected, the strongest decreases occurred in regions most heavily burdened by acid deposition, such as the AdsCsK, WCE, and Ont, while the declines were less pronounced in regions with lower sulphur deposition, such as NoNord and AtlCan (Table 2).
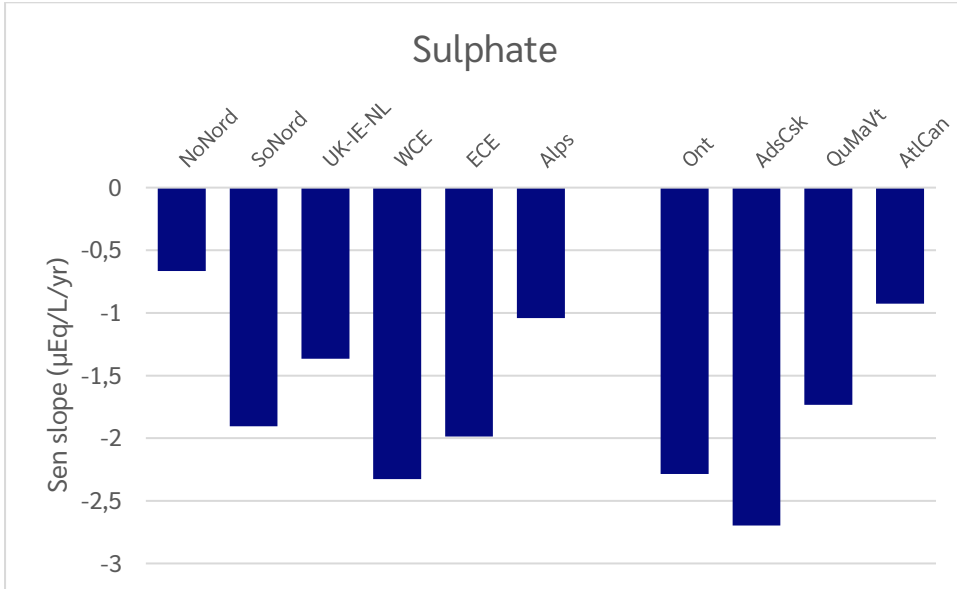

Figure 8. Median regional Sen's slopes in sulphate concentration for the period 1990-2020. All are statistically significant at p < 0.01 according to the Regional Kendall test for trend.

A comparison of SO_4^{2-} Sen's slope between the three 15-year periods (1990–2004, 1998–2012, and 2006–2020) within the ten regions (Figure 9) shows that rates of decline have become gentler in most European regions, except for WCE. Conversely, the trend has become steeper in North America. One may speculate that the steeper declines in sulphate concentrations in WCE may be attributed to a decline in the desorption of sulphate from soils that were previously heavily loaded with sulphur.
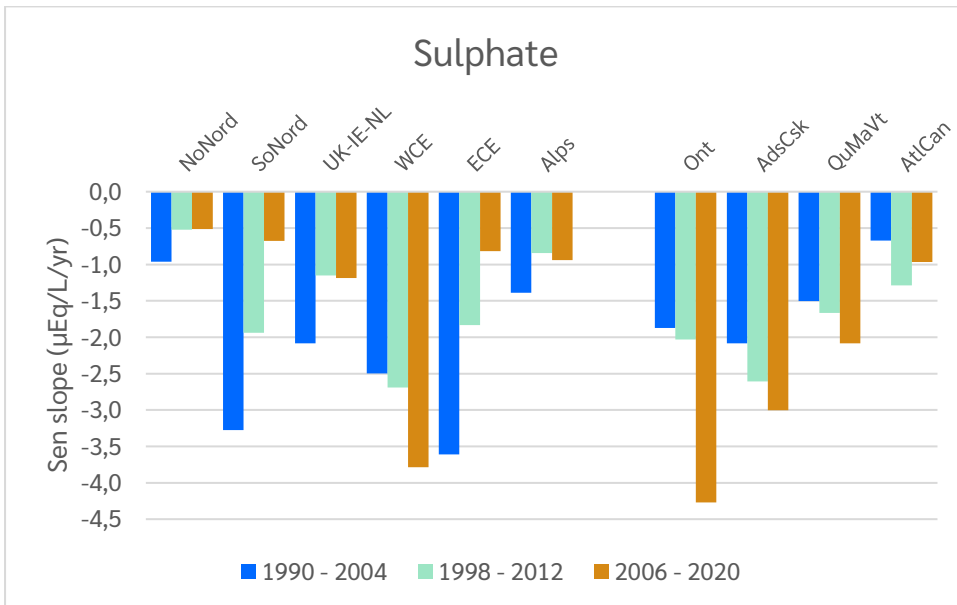

Figure 9. Median regional Sen's slopes in sulphate concentration for the three 15-year periods 1990-2004, 1998-2012, and 2006-2020.

The steeper trend with time in North America can be linked to differences in the timing of abatement policies and economic recessions that have led to strong reductions in emissions on both continents (Monks et al. 2009; Strock et al. 2014). Emissions reductions in Europe slowed around the turn of the millennium, while they became more pronounced in North America around 2005 (Garmo et al., 2014).

2.2.3.2. Trends in nitrate concentrations across regions

According to the regional Mann-Kendall test (RKT), NO_3^- concentrations exhibited a consistent decrease in all regions over the entire period 1990-2020 (Table 4). However, it is noteworthy that while there is a general decline, there has been an absolute increase in median nitrate values in Ont and no discernible change in AtlCan between the periods of 1990-2004 and 2006-2020 (Table 2). The Sen's slopes are accordingly zero at QuMaVt and AtlCan and low (-0.01) in Ont and NoNord (Figure 10). In common with the trends in SO_4^{2-}, the regions with the highest median NO_3^- levels, namely WCE, ECE and Alps (Table 2), displayed the steepest reduction in concentrations.

While reduced deposition of sulphur is the main driver behind the substantial decline of freshwater SO_4^{2-}, NO_3^- concentration levels are influenced more by the biogeochemical cycling of nitrogen (N) in soils. Various factors affecting soil processes can consequently impact nitrate leaching (Austnes et al., 2022). Long-term deposition of N and associated soil enrichment of N, leading to reductions in the carbon to nitrogen ratio (C/N) ratio in soil organic matter, have in the long run been hypothesized to lead to ''N saturation'', with elevated leaching of NO_3^- to surface waters (Aber et al., 1998). As data from a large share of ICP Waters sites show decreasing NO_3^- trends and an increase in the C/N ratio of DOM in surface waters (Austnes et al., 2022), there are few indications that N saturation is occurring here and now.

Moreover, climate change is likely to influence changes in N uptake into terrestrial and aquatic biomass. Furthermore, it is important to note that insect attacks on vegetation can introduce significant temporal fluctuations in NO_3^- concentrations, as evidenced by observations in sites in Quebec and the East Central European region (Eshleman et al., 1998; Houle et al., 2009; Oulehle et al., 2019). Despite these potential confounding factors, the consistent decline in NO_3^- concentrations observed at the regional level strongly suggests that reductions in long-range transported air pollutants have been effective in reducing nitrate levels in surface waters.
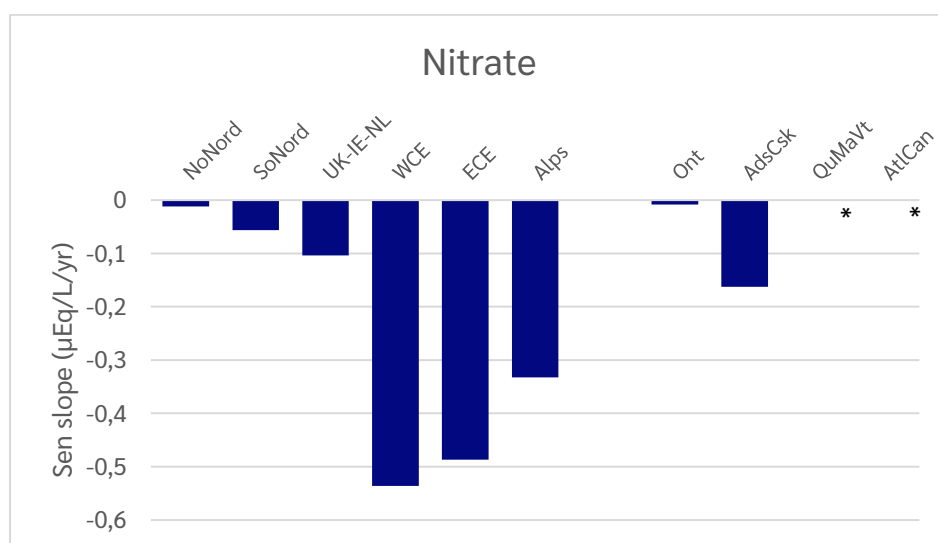

Figure 10. Median regional Sen's slopes in nitrate concentration for the period 1990-2020. All are statistically significant at p< 0.01 according to the Regional Kendall test for trend. Asterisks denote that the RKT indicates a decreasing trend (Table 4) although the Sen's slope shows no trend.

Rates of change in NO_3^- concentrations vary between the three 15-year periods: 1990-2004, 1998-2012, and 2008-2020, and between regions (Figure 11). In the Alps, NO_3^- continued to increase until 2004, reflecting heavy pollution from the Po Valley (Rogora et al., 2016), after which steep declines can be seen in Figure 7. The steep decline in NO_3^- concentrations within the more heavily impacted regions (Table 2) appears to have stabilized since 1998. Conversely, there is little indication of shifts in rates of change in NO_3^- in regions with historically low NO_3^- levels, such as the NoNord, QuMaVt, and AtlCan regions. A recent slight increase in the leaching of NO_3^- in the Ontario region (Ont) (Figure 11) may be linked to insect damage to forests.
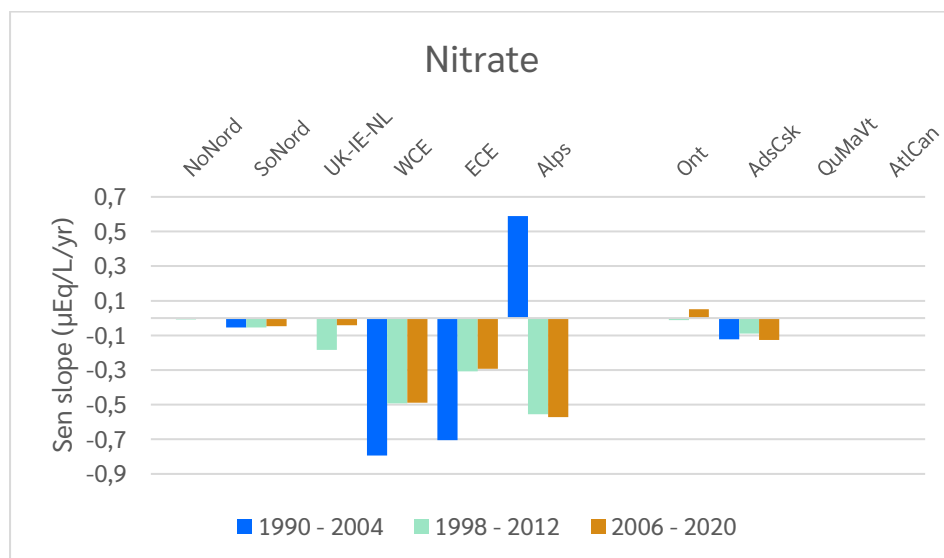

Figure 11. Median regional Sen's slope trends in nitrate concentration for the three 15-year periods 1990-2004, 1998-2012, and 2008-2020.

2.2.3.3. Trends in chloride concentrations across regions

Chloride (Cl^-), as compared to SO_4^{2-} and NO_3^-, exhibits greater mobility in soil, rendering hydrochloric acid (HCl) a highly potent acidifying agent for surface waters. However, chloride has historically received less attention as a potential long-range acidifying factor, primarily due to its substantially natural origin and variability stemming from the dispersion of sea-salt aerosols carried inland from breaking waves on the ocean surface. This predominant natural source has potentially obscured discernible trends in regions close to the sea. Moreover, dechlorination of sea salt aerosols, following interactions with sulphate and nitrate ions from anthropogenic emissions, can further complicate the link between chloride emission and chloride deposition (Evans et al., 2011).

Abatement measures aimed at reducing emissions of sulphur oxides, such as substituting coal with gas and flue-gas scrubbing, have also clearly been limiting anthropogenic emissions of HCl. Consequently, anthropogenic emissions of HCl have declined in parallel with S emissions. Recent reports have highlighted decreasing trends in chloride levels in headwaters, both in the UK (Evans et al., 2011) and in Central Europe (Kopáček et al., 2015; Oulehle et al., 2017).

The monitoring data show declining Cl^- trends (RKT) (Table 4) and negative Sen's slopes (Figure 12) in seven of ten regions. Moreover, in the SoNord region, the decline in chloride (-0.23 µEq/L/yr) was larger than that of nitrate (-0.06 µEq/L/yr). Although the steep median slope in the UK-IE-NL region (-1.53 µEq/L/yr) is within the range of values presented by Evans et al. (2011) for the UK, the values for the other regions are comparatively lower. Out of the 23 sites included in the UK-IE-NL regions, 21 are in the UK, with the remaining two in the Netherlands. The Dutch sites demonstrate the steepest declines in Cl^- (i.e., -9.87 µEq/L/yr at Achterste Goorven and -4.52 µEq/L/yr at Gerritsfles). This is in line with the original conclusion by Lightowlers and Cape (1988) that HCl is likely to be deposited close to emission sources due

to its high solubility and reactivity. The WCE and Alps regions show no significant change in Cl⁻, whereas concentrations have increased significantly in the AtlCan region (Figure 12), possibly reflecting increased sea salt deposits resulting from more extreme weather.
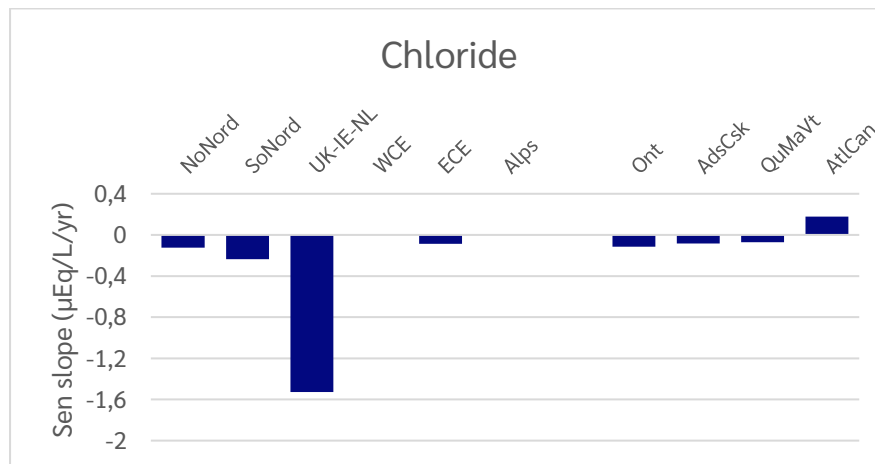

Figure 12. Median regional Sen's slopes in chloride concentration for the period 1990-2020. All are statistically significant at p < 0.01 according to the RKT for trend, except for WCE (i.e., p > 0.05).

A comparison of trends in Cl⁻ concentrations between the three 15-year periods (1990-2004, 1998-2012, and 2008-2020) within the ten regions (Figure 13) reveals a tendency towards more gentle declines in Cl⁻ over time in UK-IE-NL where levels have been high historically (Table 2). This pattern mirrors the trends observed for SO_4^{2-} and NO_3^-, which reflect the decline in anthropogenic emissions of SO_2, NOx and HCl consistent with a dominance of shared sources for these pollutants. An extreme event in 1989, with a strong westerly rainless storm, caused an unusually high dry deposition of sea salts over southern Sweden (Franzén, 1990). This produced a pronounced peak in Cl⁻ concentration in the early 90-ies in many south Swedish sites and probably accounts for the negative trend from 1990 to 2020. In the SoNord and WCE regions, the direction of change in Cl⁻ has changed from a decline to an increase, possibly due to the more recent effect of climate change with stronger winds. The apparent increase in the AtlCan region (Table 4, Figure 12) is on the other hand primarily attributed to a substantial rise during the first period (1990 – 2004) (Figures 7 and 13).
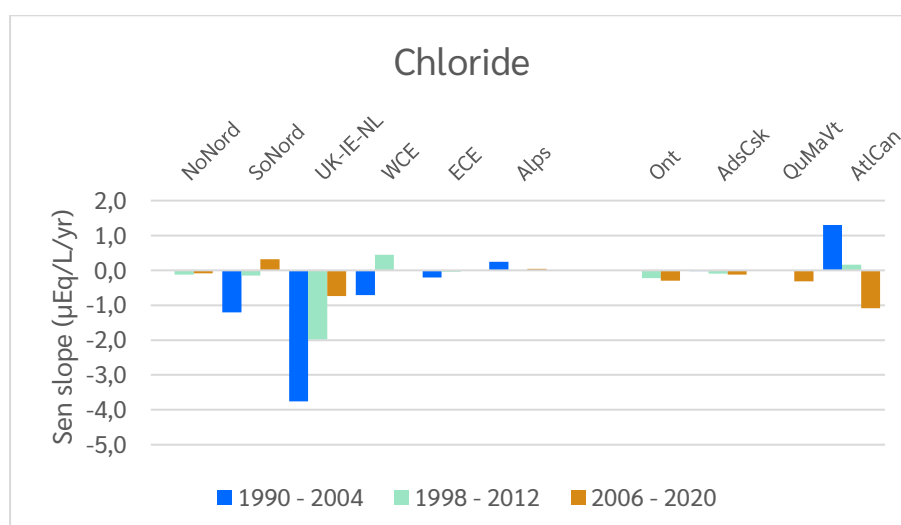

Figure 13. Median regional Sen's slopes in chloride concentration for the three 15-year periods 1990-2004, 1998-2012, and 2008-2020.

27

One of the anticipated responses of catchments to the decline in strong acid inputs is the reduced leaching of divalent base cations (Ca^{2+} and Mg^{2+}) because of less leaching of mobile strong acid anions. Across all regions, with the important exception of the NoNord region, there is an overall pattern of decline in Ca^{2+} and Mg^{2+} between 1990 and 2020 (Figure 14). As demonstrated in the multivariate analysis (Chapt. 2.2.2) of all samples from all sites, Mg^{2+} was most correlated with SO_4^{2-}, indicative of a temporal relationship reflecting declines in S deposition, whereas Ca^{2+} was more strongly linked with HCO_3^- because of spatial differences in alkalinity production. On the other hand, in a purely temporal context, rates of decline in Ca^{2+} were strongly correlated with those for SO_4^{2-} ($R^2 = 0.94$) and not to HCO_3^- ($R^2 = 0.07$) (Figure A3). Notably, the NoNord region showed a small but significant increase in Ca^{2+} but not for Mg^{2+}. Similarly, the AtlCan region experienced very small declines in both Ca^{2+} and Mg^{2+} over the whole period from 1990 to 2020 (Figure 14, a and b). These changes seem partly decoupled from recent trends in acid deposition since the concentrations of SAA have been consistently decreasing also at these sites (Figures 7, 8, 10 & 12, Table 2). As concentrations of Mg^{2+} tend to be lower than for Ca^{2+}, absolute slopes (i.e., µEq/L/yr) are inherently gentler (Figure 14). The percentage reductions in Mg^{2+} are on average about half of that for Ca^{2+} (Table 2), but with large differences in relative declines in Ca^{2+} and Mg^{2+} between the regions.

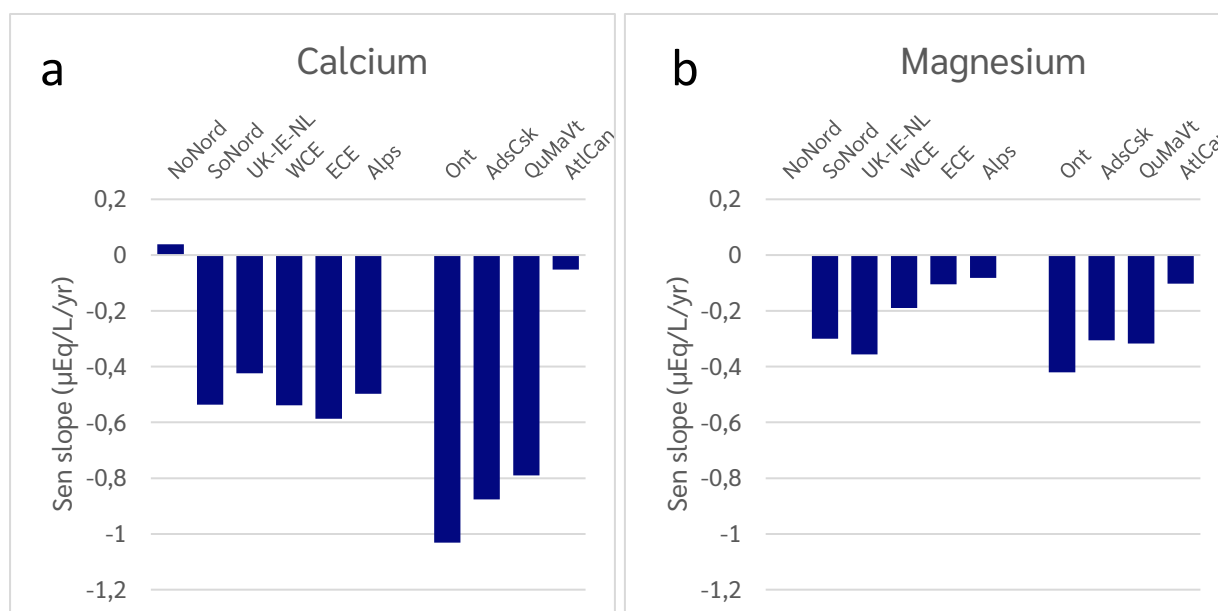*Figure 14. Median regional Sen's slopes Ca^{2+} (a) and Mg^{2+} (b) concentration for the period 1990-2020. All slopes are statistically significant at p < 0.01 according to the Regional Kendall test for trend.*

Differences in Sen's slopes for Ca^{2+} between the three 15-year periods 1990-2004, 1998-2012, and 2008-2020 within the ten regions are depicted in Figure 15a. These differences generally indicate that the most substantial declines in Ca^{2+} occurred during the initial period of decreasing acid deposition inputs. The exception again for Europe is for NoNord. Here Ca^{2+} increased during the middle period, before falling slightly during the last period (Figure 15a), despite a more monotonic long-term reduction in SO_4^{2-} (Figure 9). Among the 44 sites monitored in NoNord during the middle period, only 11% had negative slopes of Ca^{2+} while 25% displayed no slope. The rest demonstrated positive slopes, with some reaching up to 3.42 µEq/L/yr (i.e., Abiskojaure in Sweden). This is consistent with the hypothesis that the drivers of temporal trends in Ca^{2+} are more complicated than trends in other ions, as indicated by the PCA and cluster analysis (Chapt. 2.2.2).

It is noteworthy that reductions in Ca^{2+} in the European sites were consistently very small (> -0.2 µEq/L/yr) during the last period, and indeed smaller than for SO_4^{2-} (i.e., from -0.82 to -3.78 µEq/L/yr, Figure 9). The exception is for the Alps region, where Ca^{2+} leaching increased during the middle period before showing a

strong decline in the last period. This may reflect the importance of Saharan dust deposition as a source of calcium in the Alps region (Rogora et al., 2016). As dust episodes are highly sporadic, they tend to introduce a large variability in Ca^{2+} concentrations. The Ont and AtlCan regions of North America provide exceptions. In Ont, Ca^{2+} declined most steeply during the last period (Figure 15a), while Ca^{2+} levels increased in the early period only in AtlCan (in contrast to the later increase in NoNord). Mg^{2+} slopes generally followed the trends found for Ca^{2+} in Europe (Figure 15b). The exception here is again for the heavily polluted WCE region, where there was no significant trend during the first period. In ECE, Mg^{2+} increased during the last period. In the North American regions, there was no clear pattern in the difference in Sen's slopes between the periods. Notably, there was an increase in Mg^{2+} in AtlCa during the first period.

In summary, these data show that Ca^{2+} concentrations in general have declined less rapidly than those for SO_4^{2-}, and for a minority of sites show the reverse trend. This aspect will be explored further in Chapter 3.

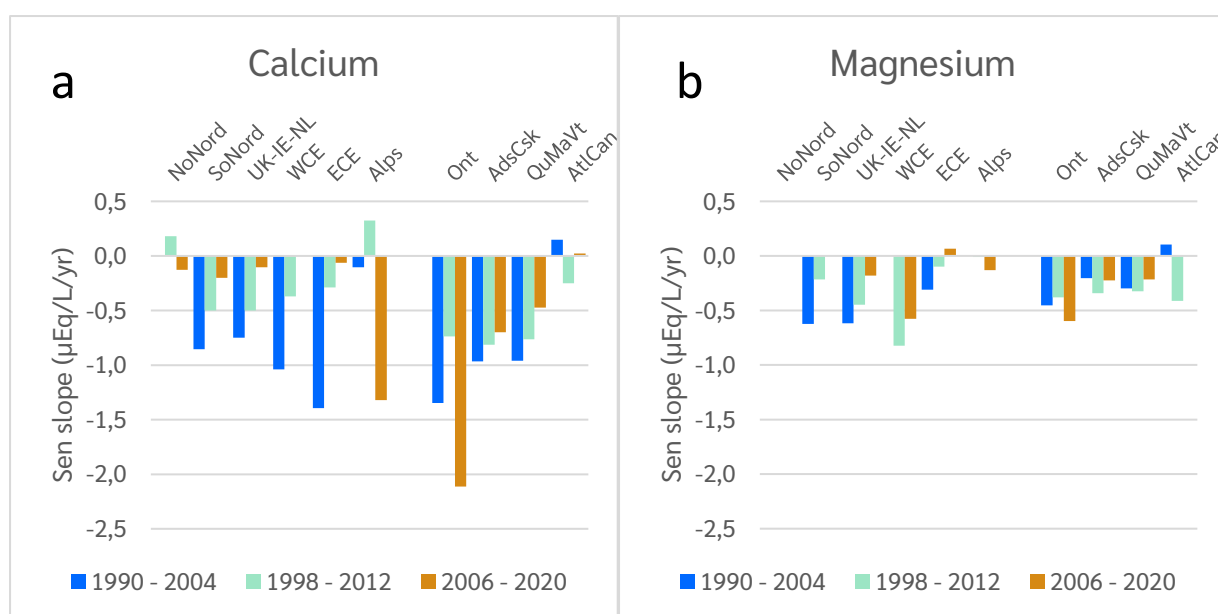*Figure 15. Median regional Sen's slopes Ca^{2+} (a) and Mg^{2+} (b) concentration for the three 15-year periods 1990-2004, 1998-2012, and 2008-2020.*

2.2.3.5. Trends in ANC across regions

Adhering to the principle of charge neutrality, larger reductions in SO_4^{2-}, NO_3^- and Cl^- concentrations (Figures 8, 10 & 12), relative to divalent base cations Ca^{2+} and Mg^{2+} (Figure 14), along with Na^+ and K^+ (Table A2), must result in increased ANC. Indeed, all regions show positive regional trends in ANC between 1990 and 2020 (Figure 16), signalling the chemical recovery of the surface waters from acidification in all ten regions. As anticipated, the greatest improvements were found among the regions that endured the heaviest acid deposition loadings (i.e., WCE) (Table 2). The regional Sen's slopes in ANC were thus negatively correlated to regional Sen's slopes in SO_4^{2-} ($R^2 = 0.84$, Figure A4). Still, the ANC response is also dependent on the acid sensitivity of the region. In regions with more acidic soils, Ca^{2+} concentrations tend to be relatively low, as this is generally indicative of the soil's susceptibility to acidity. This is exemplified by a positive correlation ($R^2 = 0.56$) between the regional temporal slopes in ANC for 2006 – 2020 (Figure 16, Table A2) and the regional median levels of Ca^{2+} for the same period (Table 2, A1). In the regions in North America, the increases in ANC are more moderate than in Europe, reflecting the gentler decline in SAA (Figures 8, 10 and 12).
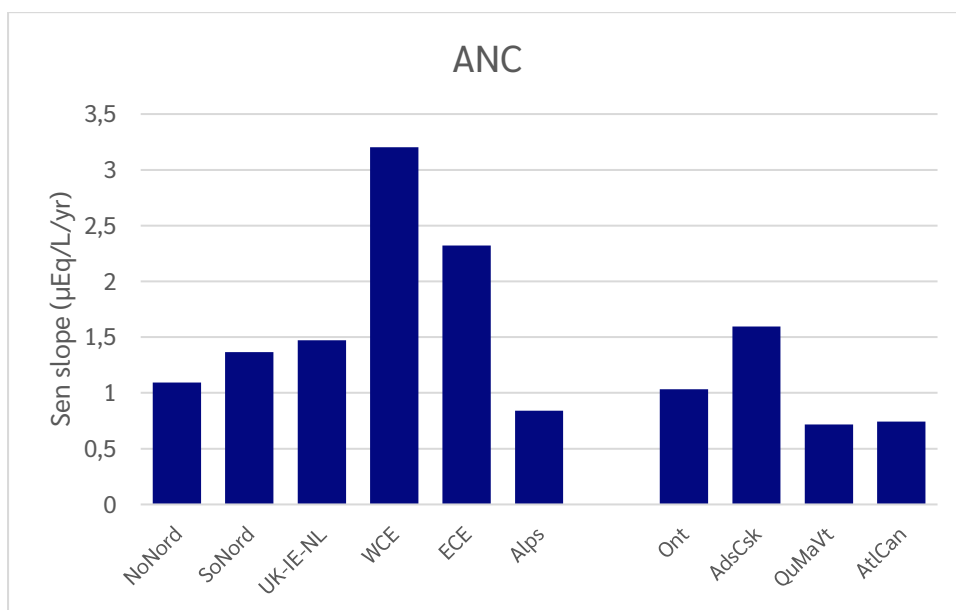
Figure 16. Median regional Sen's slopes in ANC for the period 1990-2020. All are statistically significant at p < 0.01 according to the Regional Kendall test for trend.

Significant differences in ANC slopes between the three 15-year periods (1990-2004, 1998-2012, and 2008-2020) and the ten regions are evident in Figure 17. Generally, the trends reveal that the ANC increase has decelerated in Europe over the past three decades, aligning with the declining trends observed in SAA slopes. However, an exception is observed in the more heavily impacted UK-IE-NL and WCE regions, where there has been an increase in ANC over the most recent period. This enhanced recovery is caused by the less steep declining slopes in Ca^{2+} and Mg^{2+} (Figure 15) concurrent with increasing negative slopes for sulphate (Figure 9). Conversely, in the North American regions, the rate of ANC increase has accelerated, as expected, in conjunction with the increased reduction in sulphate levels (Figure 9) over the three 15-year periods from 1990 to 2020 (Figure 17).
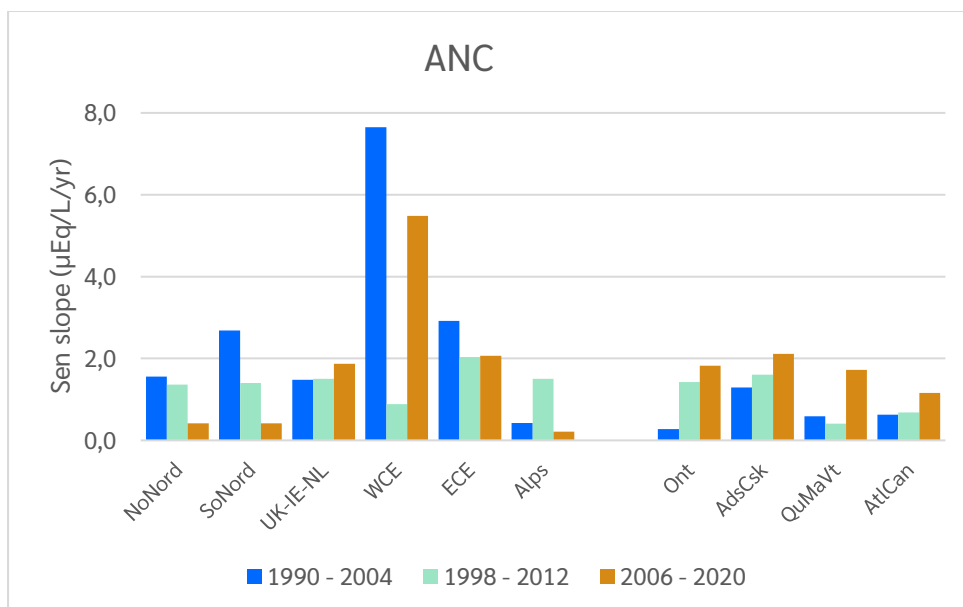

Figure 17. Median regional Sen's slopes in ANC for the three 15-year periods 1990-2004, 1998-2012, and 2008-2020.

2.2.3.6. Trends in hydrogen ion concentrations across regions

Most biogeochemical processes in natural aqueous systems are highly influenced by pH. The concentration of hydrogen ions (H^+) or pH (expressed as pH = $-\log\{H^+\}$) is thus a key parameter for understanding the biological ramifications of acid deposition. Whereas ANC (and alkalinity) is a capacity factor indicating susceptibility or degree of acidification, pH (and inorganic aluminium fractions) is an intensity factor, more directly linked to toxic effects. In Figure 18 it is evident that all regions exhibited a significant decrease in H^+ concentration between 1990 and 2020. This increasing pH is a clear sign of chemical recovery from acidification, entailing an improvement in habitat conditions for vulnerable biota. Regional differences in H^+ slopes primarily arise from differences in rates of decline in SO_4^{2-}, although this relationship is strongly moderated by the buffering capacity of the catchment soils and weak acids. Thus, no strong correlations are found between the slopes in H^+ and those of other parameters. This is reflected by the low loading and lack of clustering by H^+ concentrations in the multivariate analysis (Chapt. 2.2.2), reflecting mainly spatial differences. Instead, regional temporal trends in H^+ are strongly inversely correlated with median regional H^+ concentrations ($R^2 = 0.91$, Figure A5). Hence the steepest declines in H^+ occur in the more acidic regions with the most acidic waters. This may relate to carbonate in the soils of some regions (e.g., Alps and Ont) buffering the pH (rendering high HCO_3^- and pH in the runoff, Table 2), while carbonic acid does not contribute to the buffering in waters with a pH below 5.5.
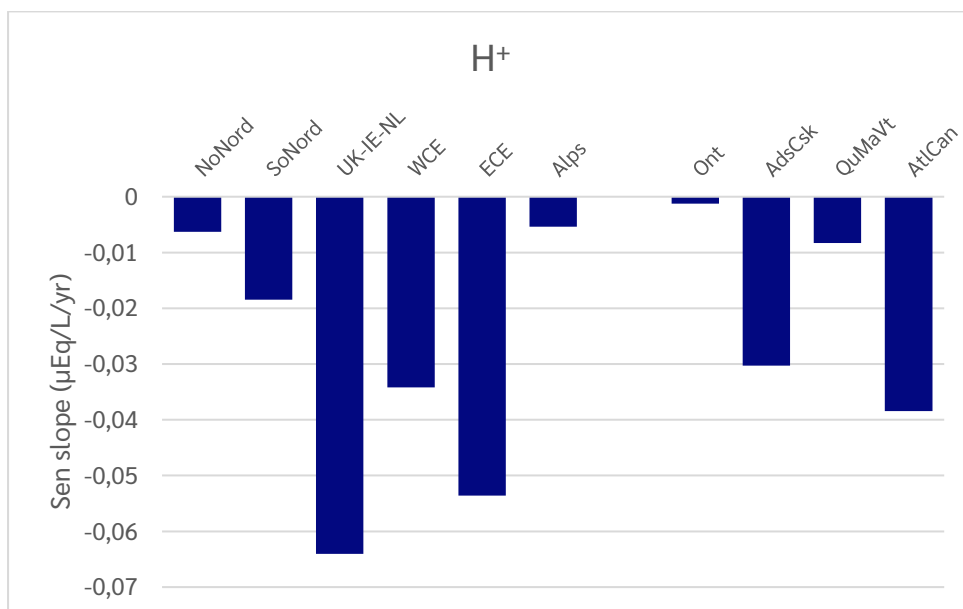

Figure 18. Median regional Sen's slopes in hydrogen ion concentration for the period 1990-2020. All are statistically significant at p < 0.01 according to the Regional Kendall test for trend.

A comparison of trends in H^+ between the three 15-year periods 1990-2004, 1998-2012, and 2008-2020 and across the ten regions (Figure 19) shows that the decrease in H^+ is slowing down or has halted in Europe, consistent with the sulphate levelling off. During the last period, the decline in H^+ in the European regions was less than 0.013 µEq/L/yr while SO_4^{2-} declined by more than -0.51 µEq/L/yr. The disparity is likely due to a concomitant increase in buffering by weak organic and carbonic acids as addressed below. The pH of sites in the Alps declined slightly during the first period, possibly due to a continued increase in NO_3^- (Figure 11). In North America, declines in H^+ have not been as strong, except for the two last periods in the AtlCan, prior to which no trend was evident (Figure 19).
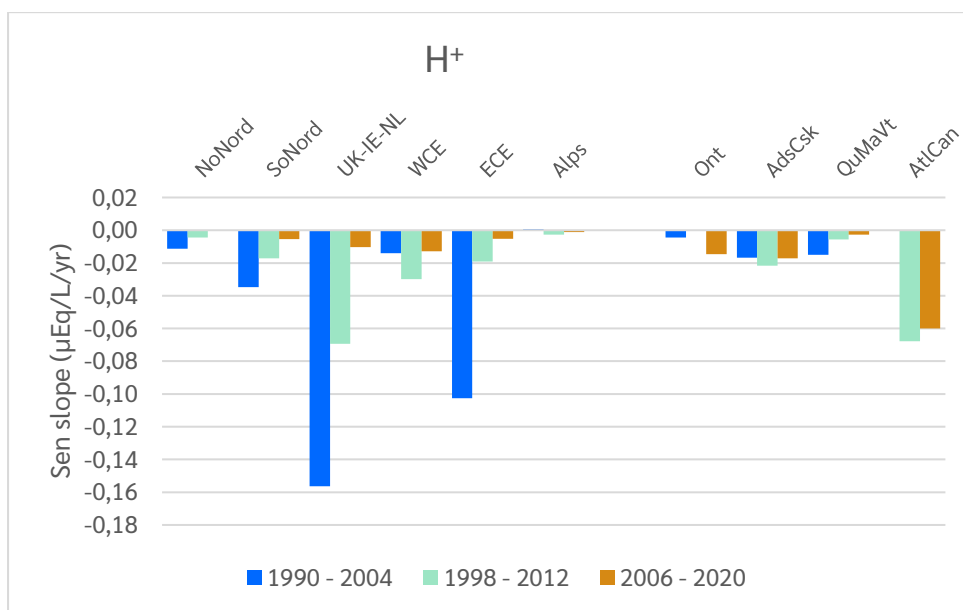
Figure 19. Median regional Sen's slopes in hydronium ion concentration for the three 15-year periods 1990-2004, 1998-2012, and 2008-2020.

2.2.3.7. Trends in organic anions and TOC concentrations across regions

Natural organic acidity holds a pivotal role in acid-sensitive regions with detectable levels of TOC. In the high-altitude Alps region, levels of TOC are insignificant (Table 2) as a consequence of scarce soil cover and limited availability of terrigenous organic matter. The data from the Alps sites are therefore not included in this assessment. The anionic charge of DOM (Org.$^-$), resulting from the deprotonation of weak organic acids, is estimated based on TOC concentration and pH (Hruška et al., 2003). Along with inorganic bicarbonate, these organic acids counterbalance a positive ANC, to support a surplus of BC over SAA.

All regions experienced positive and statistically significant trends (Figure 20; Table 4) in Org.$^-$ and TOC between 1990 and 2020, though the median slopes vary greatly between regions from 0.21 to 0.85 µEq/L/yr for Org.- and from 0.013 to 0.061 mg C/L/yr for TOC (Figure 20 a and b). Several environmental pressures drive this upward trend in Org.$^-$ and TOC. Assessments of ICP Waters data have established a strong correlation between TOC trends, trends in acid deposition, and acid sensitivity of the catchment (specifically, the stores of base cations in the soil) (Monteith et al., 2007). Decreasing ionic strength of the soil solution, resulting from reduced acid deposition, has a strong impact on the solubility of dissolved organic matter (DOM) (de Wit et al., 2007; Haaland et al., 2023; Monteith et al., 2023) by expanding the thickness of the diffuse double layer (DDL) around DOM molecules. A thicker DDL at lower ionic strength leads to reduced DOM flocculation and less precipitation from the solution. This can lead to an increase in TOC even in non-acidified catchments (Hruška et al. 2009). In addition, lower concentrations of labile aluminium (LAl), as well as iron (Fe^{3+}) have resulted in reduced complexation with DOM (Vogt et al., 1994; Vogt et al., 2001). Furthermore, there has been an increase in deprotonation due to a slight increase in pH (Tipping et al., 2011) (Figure 18), which has led to an increased charge density of the organic matter (de Wit et al., 2007). This enhances its hydrophilicity and thereby its solubility, leading to increased TOC.

De Wit et al. (2021) found that climate and increased biomass also play important roles in contributing to the increase in DOM. Air temperatures have increased globally by 1.1 °C since 1850 - 1900 (IPCC, 2022), with an above-average increase at higher latitudes (Hanssen-Bauer et al., 2017). This warming has been most distinct during spring and autumn. Consequently, the growing season has expanded practically everywhere in northern Europe (Aalto et al., 2022). According to the sixth IPCC assessment report (IPCC, 2022), annual precipitation has on average increased in middle, northern and eastern Europe. Moreover, precipitation extremes have increased both in intensity and frequency in northern and eastern Europe

(e.g., Monteith et al., 2016). These changes in climate, with longer and wetter growing seasons, are likely to boost primary production generating more biomass, i.e., commonly referred to as "Greening" (Finstad et al., 2016). This is augmented by less outfield grazing, and increased forest planting as a nature-based solution for carbon capture and sequestration (Vogt et al., 2022), along with accumulating reactive nitrogen (N) in the catchments (Austnes et al., 2022) and increased level of CO_2 in the ambient air (Comstedt et al., 2006; Terrer et al., 2021). On a regional scale, this Greening is evident and especially prominent in the boreal biomes. Over the period 1990 to 2007, the cumulative C sink into the world's forests regrowing was equivalent to 60% of cumulative fossil emissions in that period (Pan et al., 2011). The growth of EU forests, covering approximately 42% of its land area, is thus contributing at least temporarily to mitigating climate change by annually increasing biomass equivalent to about 10% of Europe's fossil fuel emissions. Likewise, the land use, land use change and forestry sectors (LULUCF) in Finland, Sweden and Norway have roughly balanced between 20-40% of their annual national anthropogenic CO_2 emissions since 1990 through increased biomass (see Vogt et al., 2022 and references therein). Notably, forest biomass in Norway has increased by about 50% since 1990 (Breidenbach et al., 2020; De Wit et al., 2015), a trend also observed in Sweden, Finland and elsewhere in Europe (Luyssaert et al., 2010). Concurrently, treelines have risen mainly because of reduced outfield grazing and timbering (Bryn & Potthoff, 2018). Eisfelder et al. (2023), studying vegetation trends during growing seasons in Europe over 30 years, found significant positive trends in NDVI (0.15 NDVI units) for 55% of Europe. In particular, the western, central, southern, and northeastern Europe show widespread significant positive NDVI trends. Negative NDVI trends for the growing season were only observed in 2.2% of the land area. This "Greening", signifying increases in terrestrial primary productivity and afforestation, can cause an increase in DOM and colour (referred to as "Browning") over longer timeframes (Finstad et al., 2016; Škerlep et al., 2020; Kritzberg et al., 2020; Crapart et al., 2023). Still, an increase in biomass (document by e.g., changes in Normalized Difference Vegetation Index (NDVI)) in the ICP Waters sites has been difficult to detect due to that the catchments mainly are small (median 3.41 ha) and forested (median 73%). Moreover, most of the ICP Water sites would probably not support an increase in biomass as they are nutrient-limited and most have cold climates. This is further addressed in Chapter 3.4.

Climatic factors also exert influence on seasonal and interannual variations in DOM (Clark et al., 2010) and may also affect temporal trends in DOM (de Wit et al., 2016). However, the linkage between rising DOM and declining sulphate concentrations indicates that rising TOC concentrations are integral to the process of chemical recovery from acidification. The partial replacement of strong mineral acidity by weak organic acidity helps explain why pH responses are more muted than initially anticipated (Chapt. 2.2.3.6; Battarbee et al., 2005; Erlandsson et al., 2010). The effect of the resulting minor declines in H^+ (Figure 18) on increased Org.$^-$ caused by deprotonation is therefore limited. The regional differences in Sen's slopes for TOC explain 98% of the variation in the slopes for Org.$^-$ (Figure A6), which is unsurprising given that Org.$^-$ is estimated based on the TOC and H^+ with weak temporal trends. There is a notable difference in rates of increase in Org.$^-$ between NoNord and SoNord regions, primarily driven by the differences in declines of acid deposition, which in turn influence changes in TOC levels. However, when considering all ten regions, there is no significant correlation between the slopes of Org.$^-$ and SO_4^{2-} (R^2 = 0.06, Figure A7a). Correlating instead to the slopes of all SAA (i.e., SO_4^{2-} + Cl^- + NO_3^-, µEq/L/yr) improves the explanatory value slightly (R^2 = 0.19, Figure A7b). This discrepancy may be partly attributable to the large spatial differences in land cover and climate between the regions. Correlating instead the temporal slopes of Org.$^-$ and SO_4^{2-} from 1990 to 2020 for each of the 420 sites, gives as expected a negative correlation (Figure A8) explaining 58.9% of the variation in the slopes of Org.$^-$.
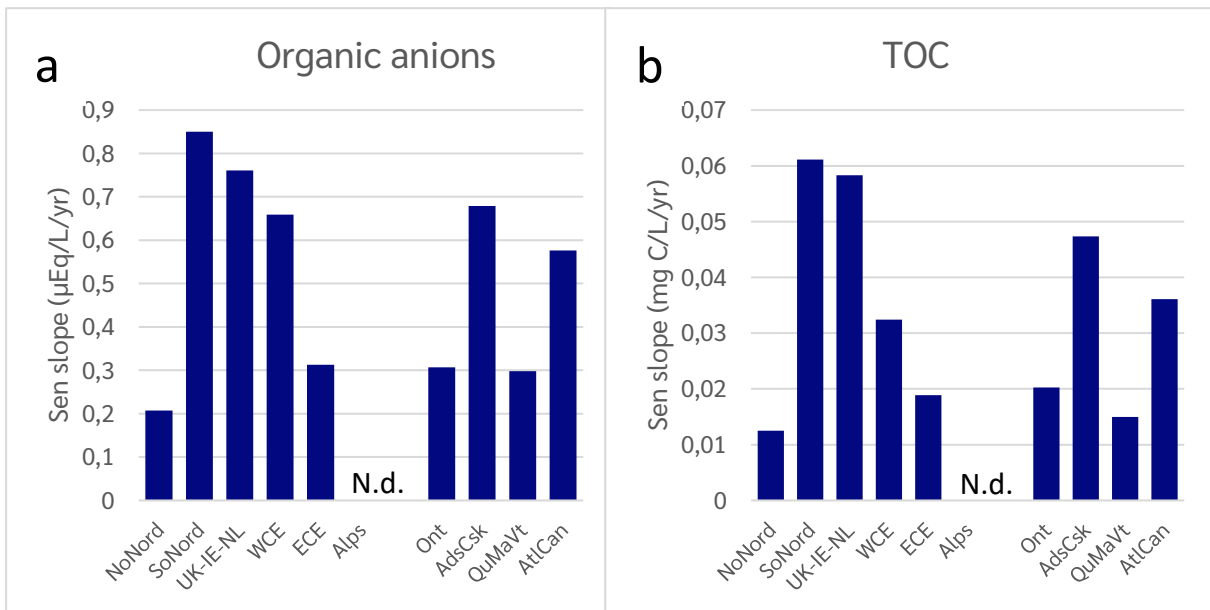
Figure 20. Median regional Sen's slopes in Org.⁻ (a) and TOC (b) concentration for the period 1990-2020. All are statistically significant at p < 0.01 according to the Regional Kendall test for trend. N.d. denote No data.

A comparison of trends in Org.⁻ and TOC between the three 15-year periods (1990-2004, 1998-2012, and 2008-2020) and across the ten regions, is depicted in Figure 21 a and b. This shows that the increase in Org.⁻ and TOC has decelerated over time in the Nordic regions (NoNord and SoNord) and even reversed in UK-IE-NL. In North America, the patterns are less clear, although in these regions as well, the increase in Org.- and TOC during the last period (2006 – 2020) is lower than the preceding period in three of the four regions. Central Europe (WCE and ECE) and AdsCsk are the only regions where rates of change in Org.⁻ and TOC have accelerated in the last period. In WCE and AdsCsk this can potentially be attributed to the steeper decline in sulphate during the most recent period, as well as climatic factors, such as changes in precipitation.
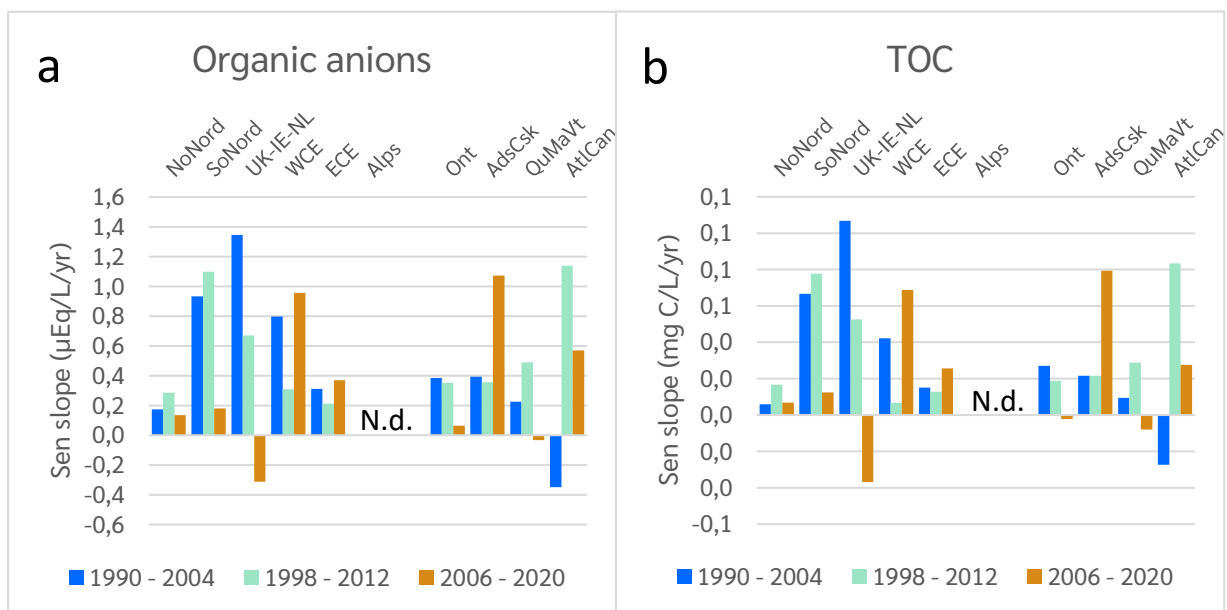

Figure 21. Median regional Sen's slopes in Org.⁻ (a) and TOC (b) concentrations for the three 15-year periods 1990-2004, 1998-2012, and 2008-2020. N.d denote No data.

2.2.3.8. Trends in bicarbonate concentrations across regions

Bicarbonate concentrations are commonly estimated from Alkalinity data, though this is not possible in the ICP Waters dataset due to large deviations in analytical methods between laboratories. Moreover, these calculations are hampered by uncertainties due to several methodical assumptions (Vogt et al., 2023). Instead, we here estimated the bicarbonate concentration based on charge balance, including the contribution of BC, SAA, H^+ and $Org.^-$ as outlined in Chapter 2.1.3. This method for calculating the HCO_3^- is also problematic as it is a small value based on the difference between large sums. Moreover, there are uncertainties both in all the analytical data as well as the modelled $Org.^-$.

In less acid-sensitive regions, where pH is above 5.5, HCO_3^- contributes significantly to the anionic charge (Figure A9). Still, only the NoNord, Alps and Ont regions showed significant increases in bicarbonate for the whole period from 1990 to 2020 (Figure 22). This is mainly because the other regions had low, or no bicarbonate concentrations (Table 2). Nevertheless, all regions have positive RKT trends (Table 4) for HCO_3^- between 1990 and 2020, indicating that a slight increasing trend in bicarbonate in all regions. Several factors drive this upward trend in HCO_3^-, as discussed further in Chapter 3.
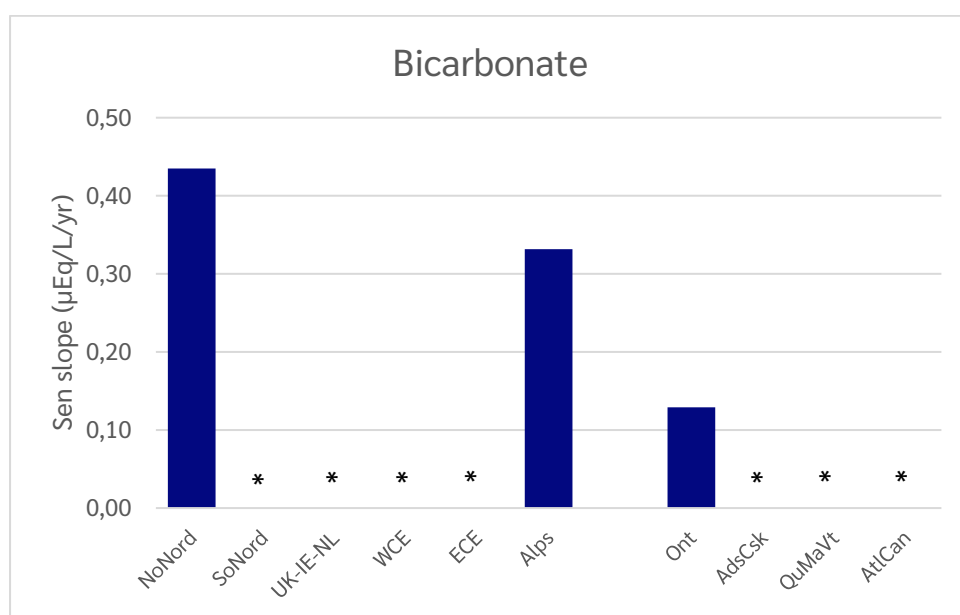

Figure 22. Median regional Sen's slopes in HCO_3^- concentration for the period 1990-2020. All are statistically significant at p < 0.01 according to the Regional Kendall test for trend. Asterisks denote that the RKT indicate an increasing trend (Table 4) although the Sen's slope shows no trend.

Differences in rates of change in HCO_3^- between the three 15-year periods (1990-2004, 1998-2012, and 2008-2020) within the ten regions, as depicted in Figure 23, show that the increase in HCO_3^- appears to have levelled off in the NoNord region as there was no Sen's slope during the most recent period. Still, the MKT trend is increasing (Table 4). On the other hand, in the Alps where pH and HCO_3^- concentrations are relatively high (Table 2), HCO_3^- increased from the first to the second period and decreased slightly during the last period. The overall positive slope in Ont is due to an increase only during the last period. Positive slopes were also found for WCE and QuMaVt during the first and last periods, respectively, though these regions do not show an increase in HCO_3^- across the whole period. Still, with pH during these periods of 5.65 and 6.40, respectively (i.e., > 5.5; Table A1), relatively steep ANC slopes (Figure 17), while weaker slopes for $Org.^-$, it is not unlikely that bicarbonate has increased as indicated.
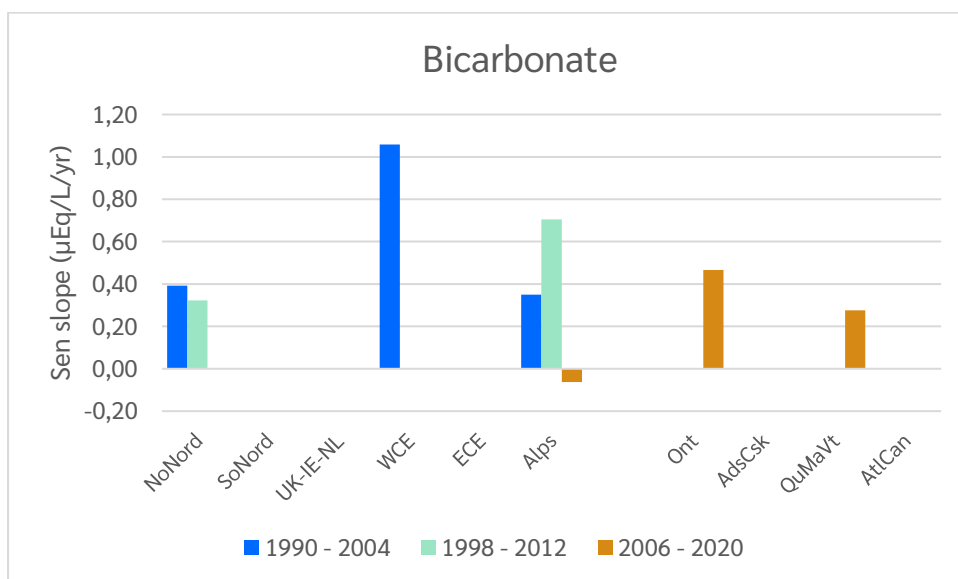
Figure 23. Median regional Sen's slopes in HCO$_3^-$ concentrations for the three 15-year periods 1990-2004, 1998-2012, and 2008-2020.

2.3 Conclusions regarding chemical trends

Sulphate concentrations have declined at 427 of the 430 sites (Table 3). In 9 of the 10 regions, the decline has been more than 27% from the initial period (1990 – 2004) to the most recent period (2006 – 2020) (Table 2). The declines for sulphate were steeper In Nordic regions and ECE during the 1990s than after the turn of the century (Figure 9), while the opposite was the case for WCE, as well as the regions in North America. Nitrate concentrations also declined in all regions, except for QuMaVt and AtlCan in North America (Figure 10), although the RKT shows a decreasing trend even in these regions (Table 4). Among the 430 sites, 55% show no trend in NO$_3^-$, while a few (14 sites) show a slight increase, possibly due to N saturation or local factors such as insect attacks (Table 3). Chloride concentrations declined in 7 out of the 10 regions (Figure 12). In the UK-IE-NL region, the negative slope for chloride is larger than for sulphate (Figure 8), possibly due to the concurrent large decline in UK emissions of hydrochloric acid.

The average regional Sen's slopes for the sum of divalent base cation concentrations decreased by -0.82 µEq/L/yr. This is half the average Sen's slope for SO$_4^{2-}$ (-1.69 µEq/L/yr) (Table A2). Noteworthy, in the less acid deposition influenced NoNord region, there is an overall positive increase in calcium (Figure 14). More widely in Europe, except for the Alps, rates of decline in Ca^{2+} have slowed down with slopes less than 0.2 µEq/L/yr for the last 15-year period (2006 – 2020) (Figure 15). This decline is especially low relative to the concurrent decline in sulphate, with slope values between -0.52 and -3.78 µEq/L/yr (Figure 9). All regions have experienced an increase in ANC between 1990 and 2020 (Figure 16), mainly reflecting the regional Sen's slopes for sulphate (Figure 8). pH has also increased in all regions (Figure 18), as declines in mineral acidity cannot be fully compensated by weak organic acidity (Monteith et al., 2007) and carbonic acid. Still, the increase is minimal in NoNord, Alps and Ont, where the pH and bicarbonate levels are high (Table 2). The trajectories of SO$_4^{2-}$, ANC and pH indicate that recovery has decelerated in Europe and accelerated in North America. This difference can be attributed to the varying timing of regulatory measures, which have nevertheless resulted in significant reductions in emissions on both continents. Still, comparisons between periods with varying populations of sites may not always reflect the actual differences in trend. Differences in site distribution are depicted by comparing Figures 1 and 2.

3 Spatially diverging temporal trends in calcium concentrations

3.1 Background

As pointed out in the multivariate spatiotemporal analysis of water chemistry parameters (Chapt. 2.2.2), concentrations of Ca^{2+} are mainly governed by spatial differences in HCO_3^-, while Mg^{2+} are more correlated with SO_4^{2-}. Despite this, in a strictly temporal context, regional slopes in Ca^{2+} and Mg^{2+} were strongly correlated with regional slopes for SO_4^{2-} and not HCO_3^- (Chapt. 2.2.3.4). Notably, the NoNord region showed a small but significant increase in Ca^{2+}. Since concentrations of SAA have been consistently decreasing also at these sites, albeit slowly, the increase in Ca^{2+} cannot be attributed to an upsurge in acid deposition. This warrants a closer inspection of the factors governing the temporal trends in Ca^{2+}.

On a global scale, the spatial distribution of freshwater Ca^{2+} concentrations is closely and proportionally linked to the levels of carbonates, as both are governed by the amount of carbonate minerals present in the soils. However, in terms of temporal changes, Weyhenmeyer et al. (2019) pointed out a decoupling of the relationship between Ca^{2+} concentrations and carbonate alkalinity. Their global analysis showed a declining trend in Ca^{2+} concentrations in regions sensitive to acidification, as also documented in previous ICP Waters reports (Garmo et al., 2020). This decline was attributed to reduced loading of acid deposition, following the principle of electroneutrality, where the cationic charge balances the anionic charge.

Regional declines in the deposition of strong acid anions (SAA) are the main explanatory factors for the temporal trends in Ca^{2+} concentrations observed at the ICP Waters sites (Chapter 2). Still, there are also other regional trends in important confounding drivers and pressures that likely influence the temporal trends of Ca^{2+}, though their relative importance differs between sites. Figure 24 provides a conceptual framework illustrating the cause/response relationship that, to a varying degree, may counteract the effects of decreased SAA leaching on temporal trends in Ca^{2+}.

Decreased acid deposition has led to a strong decline in SAA and inherently a decline in ionic strength, increase in pH and decline in inorganic labile aluminium (LAl). This increases the solubility and thereby the leaching of dissolved organic matter (DOM) and its associated weak organic acid anions (Org.$^-$) (Chapt. 2.2.3.7). Climate change, with rising temperatures causing warmer and longer growing seasons, along with land-use changes, accumulation of reactive N, and increased atmospheric CO_2, all potentially contributing to increased biomass that over time contributes to elevated levels of Org.$^-$ (Chapt. 2.2.3.7). This potentially contributes to the leaching of cationic Ca^{2+} by counterbalancing the weak organic acid anion charge.

Moreover, enhanced vegetation growth, along with a longer growing season, can boost chemical weathering and the release of Ca^{2+} from soil minerals (de Wit et al., 2023) by increased respiration, increasing the partial pressure of CO_2, leading to more carbonic acid, and the secretion of fulvic acids by plant roots in the soil (van Schöll et al., 2008). Reduced snow cover length may promote weathering due to more exposed soil surface and freeze-thaw cycles (Kopaćek et al., 2017). Moreover, a one-degree increase in soil temperature can accelerate weathering rates by 10% (Houle et al., 2020). On the other hand, increased biomass means that more Ca^{2+} is stored in the biosphere. Moreover, some of the released Ca^{2+} will also be retained in the soil to build up the depleted base saturation (%BS) of the ion exchanger. The potential impact of higher weathering rates on the leaching of Ca^{2+} could thus be masked. Regardless, these proposed mechanisms for the increase in Ca^{2+} cannot be tested as we lack data documenting, increased biomass, increased partial pressure of CO_2 in the soils and enhanced weathering at our ICP Water sites.
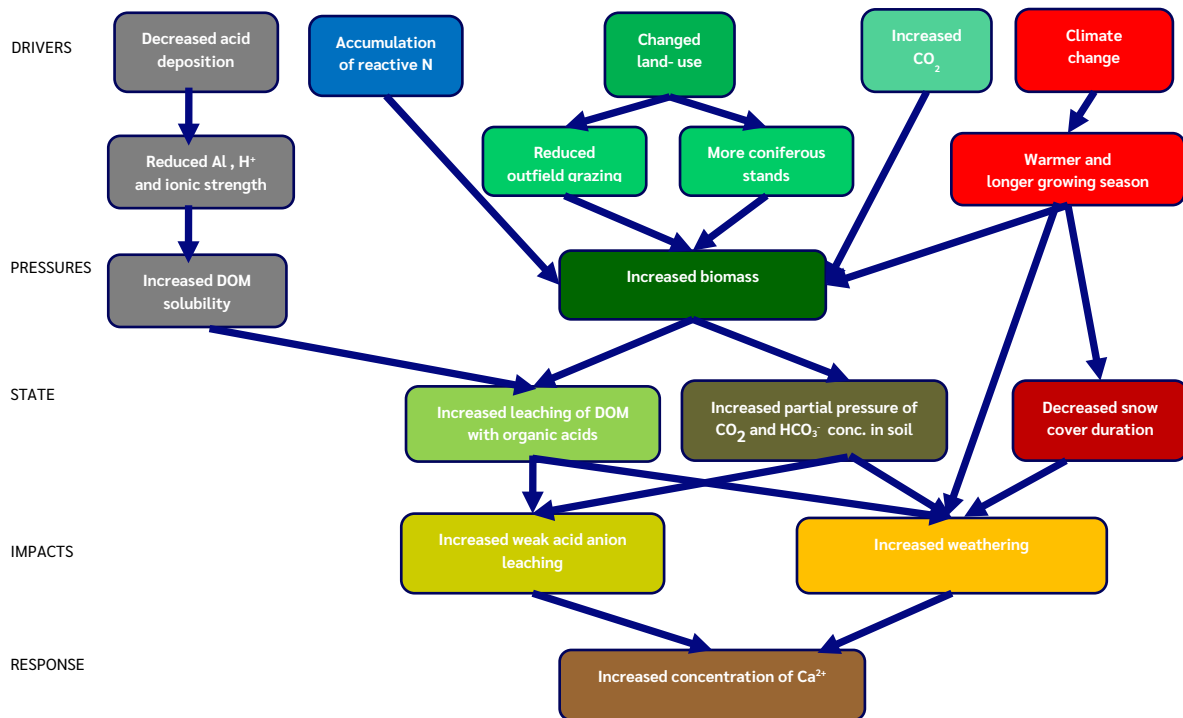
Figure 24. Conceptual cause effect relationship between drivers, pressures, state, impacts and responses regarding counteracting the effect of decreased SAA concentrations on temporal trends in Ca^{2+}.

3.2 Aim

3.2.1. Purpose and approach

In the current era of low acid deposition in Europe and North America, SAA concentrations are approaching pre-industrial levels. As the influence of acid deposition diminishes, the weathering processes and natural weak acids are likely to become more important for changes in base cation concentrations. Quantifying the weathering process and the retention of base cations in the soil cation exchanger (Reuss and Johnsen, 1986) is a complex task. Nevertheless, these processes hold great importance for the recovery of our watercourses and thus also for biogeochemical models used to predict recovery from acidification (e.g., MAGIC (Wright et al., 1990; Austnes et al., 2020) and Forsafe (Wallman et al., 2005)). Moreover, Ca^{2+} is an essential element for most organisms, as Ca^{2+} concentrations ≤ 1.5 mg L^{-1} are considered a critical threshold for the survival of many Ca-demanding organisms.

The role of weak acids in governing the levels of Ca^{2+} is simpler to assess and may have the potential to shed some light on the weathering processes. It thus becomes essential to deepen our understanding of how Ca^{2+} respond to increased levels of $Org.^{-}$ and HCO_3^{-}. The aim of this study is hence to first assess the overall relative importance of temporal changes in SO_4^{2-}, $Org.^{-}$ and HCO_3^{-} on the trends in Ca^{2+}. This is addressed by comparing sites with negative and positive slopes in Ca^{2+}, and by employing a set of different correlation analyses to identify explanatory parameters for the temporal variation in Ca^{2+}, as well as regression analysis to unravel the relative importance of the explanatory variables. Then the role of spatial differences in site characteristics (e.g., acidity and land cover) is assessed. This knowledge is a prerequisite for identifying the spatial site-specific characteristics that determine the varying roles of the different explanatory parameters, collectively shaping temporal trends in calcium concentrations, and to better understand the effects of confounding factors on the time required for chemical recovery.

3.2.2. Hypothesis

Based on the assessments of trends and inter-parameter relationships in water chemistry (Chapter 2.2.2), the trends in potential drivers, as outlined in Chapt. 2.2.3, and informed by the conceptual rationale of the Ca^{2+} biogeochemistry (Chapt. 3.1), the following two hypotheses are postulated to explain the spatial differences in temporal trends in Ca^{2+}:

1. Trends in Ca^{2+} are determined by the size of decline in SO_4^{2-} relative to counteracting increases in $Org.^-$ and HCO_3^-.
2. Spatial differences in catchment characteristics, such as land cover, historic acid deposition loading, and acid sensitivity, dictate the relative importance of the processes governing Ca^{2+} trends.

3.3 Results and discussion

3.3.1. Distribution of sites with different trends in SO_4^{2-} and Ca^{2+}

The trend analysis, described in Chapter 2.2.3, depicted a consistent pattern of declining SO_4^{2-} concentrations (Table 4). This is further exemplified by the distribution of Sen's slopes for SO_4^{2-} from 1990 to 2020 (Figure 25A), which shows negative trends at nearly all sites. However, 34 sites had low or negligible negative Sen's slopes, falling within the range of 0 to -0.5 µEq/L/yr (orange bars). Moreover, in the European regions, the declines in SAA have been levelling off in recent years (see Figures 9, 11, 13, and Table 4). In contrast, the distribution of Sen's slopes for Ca^{2+} (Figure 25B) displays a more skewed pattern with a substantial portion of sites (142 sites, or 33%) having very gradual slopes (i.e. between 0 and -0.5 µEq/L/yr (orange bars)). Furthermore, 128 sites (30%) showed no Mann-Kendall trends in Ca^{2+} (Table 3). Remarkably, 84 sites (20%) show an increase in Ca^{2+} (red bars). Among these, 13 sites had slopes that were steeper than +0.5 µEq/L/yr, six of which exceeded +1.0 µEq/L/yr, which amounts to increases in Ca^{2+} concentration of more than 30 µEq/L over the assessed 30-year period. Trends in weak acid anions $Org.^-$ and HCO_3^- were skewed in the opposite direction, with more sites having positive slopes (Figure 25c and d). More than half of the sites had no trend in bicarbonate since HCO_3^- concentrations in samples stayed 0 since the ANC was negative or the pH was below 5.5, while more than 37% of the sites experienced an increase.

The fact that more than 50% of the stations either showed no decline or an increase in Ca^{2+} (Figure 25b), despite a practically universal decline in SO_4^{2-} (Figure 25a), highlights the role of the increasing levels of weak acids (Figure 25 c and d) as drivers significantly counteracting the effect of declining levels of strong acids. Furthermore, on a regional scale, the equivalent sum of Ca^{2+} and Mg^{2+} declined by approximately half the equivalent change in sulphate concentration (Chapter 2.3) (Table A2). Moreover, the overall increase in $Org.^-$ concentrations in all regions (Figure 20, Table 4) and in more than 92% of the sites (Figure 25c) indicates that weak organic acidity has, to some extent, replaced the previous dominant strong mineral acidity from acid deposition. A continued increase in DOM and thus $Org.^-$ - beyond declining acid deposition - is apparent by the continued ongoing browning of many of our boreal freshwater systems in regions where declines in SAA have levelled off (Finstad et al., 2016; de Wit et al., 2016; 2021). However, it is worth noting that widespread browning in numerous watercourses across Sweden ceased around 20 years ago (Eklöf et al., 2021). Likewise, as highlighted in Chapt. 2.2.1.3, the increase in $Org.^-$ at the ICP Water sites has decelerated in the Nordic regions (NoNord and SoNord) and even reversed in UK-IE-NL (Figure 21).

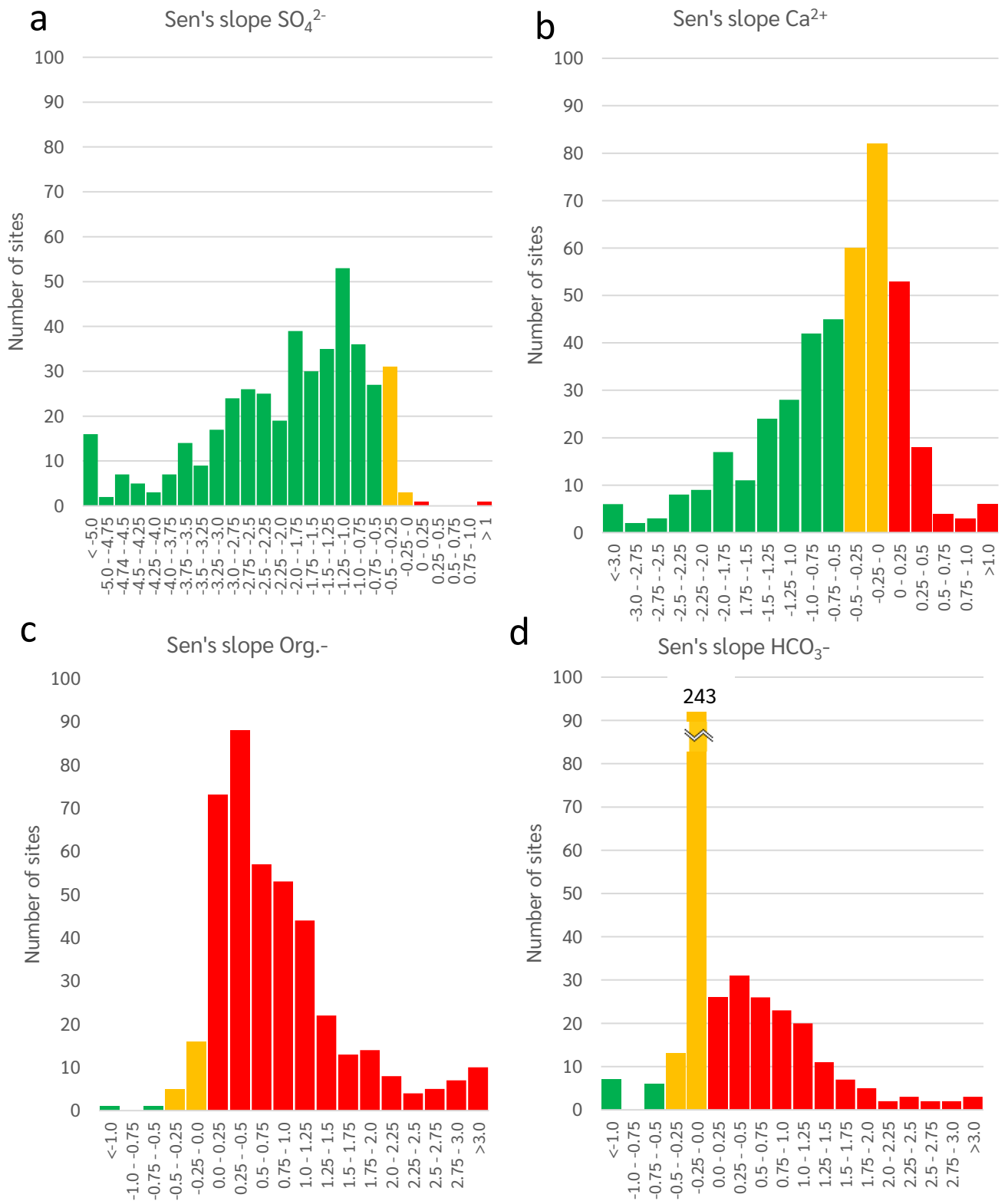*Figure 25. Distribution of Sen's slopes for the whole period from 1990 to 2020 of SO_4^{2-} (a), Ca^{2+} (b), $Org.^-$ (c), and HCO_3^- (d). Sites with weak negative slopes (i.e., -0.5 – 0 µEq/L/yr) are marked in orange. Sites with positive trends (> 0 µEq/L/yr) are marked in red, while negative slopes (< -0.5 µEq/L/yr) are in green.*

3.3.2. Significant differences between sites with positive and negative Ca^{2+} Sen's slopes

A comparison of average site median concentrations (µEq/L) of key parameters between sites with positive and negative trends in Ca^{2+} for the whole period (1990 – 2020) is presented in Table 5 and Figure 26. Sites with increasing Ca^{2+} concentrations had significantly lower median SO_4^{2-}, NO_3^-, H^+, and $Org.^-$ concentrations, and higher levels of HCO_3^-, implying that these sites were less acidified or acidic, and less humic. There were no differences in ANC (Table 5) between sites with contrasting trends in Ca^{2+} since the weak acid anion charge had only shifted from $Org.^-$ to HCO_3^-. Sites with increasing Ca^{2+} underwent relatively gradual changes in both SO_4^{2-} and $Org.^-$, but larger increases in HCO_3^-. The trends presented in Table 5 also show that at the sites where Ca^{2+} is rising, HCO_3^- has been increasing more rapidly than organic acids, indicating that bicarbonate buffering exceeds buffering from organic acidity. Thus, the main driver for positive temporal increases in Ca^{2+} is the increase in HCO_3^-. For the group of sites with increasing levels of Ca^{2+}, rates of change in HCO_3^- explain 43% of the variation in trends in Ca^{2+} (Figure A10).

Table 5. Median values (µEq/L) and Sen's slopes (µEq/L/yr) for sites with positive and negative Ca^{2+} Sen's slopes, and their Mann-Withey P value for the significant difference of the key parameters (data from 1990 to 2020)

	Ca^{2+} slope	SO_4^{2-}	NO_3^-	Cl^-	$Org.^-$	HCO_3^-	Ca^{2+}	Mg^{2+}	H^+	ANC	Ca^{2+}/SO_4^{2-}
Median	Neg. Slp.	71.9	6.61	82.8	70.5	20.3	83.6	44.4	4.41	67.9	1.26
	Pos. Slp.	38.6	5.22	84.2	52.8	34.9	70.5	36.9	3.06	76.5	1.84
	p-Value	**0.000**	**0.000**	0.056	**0.000**	**0.001**	**0.001**	0.070	**0.008**	0.621	**0.000**
Sen slp.	Neg. Slp.	-2.41	-0.13	-0.35	0.94	0.14	-0.90	-0.44	-0.14	1.33	0.35
	Pos. Slp.	-0.85	-0.08	-0.01	0.45	0.76	0.37	0.04	-0.08	1.45	0.30
	p-Value	**0.000**	0.070	**0.001**	**0.000**	**0.000**	**0.000**	**0.000**	0.462	0.926	**0.000**

Spatially, with respect to the sites with increasing Ca^{2+} median annual Ca^{2+} concentrations show a strong positive correlation with median annual HCO_3^- concentrations ($R^2 = 0.78$), and weaker relationships with SO_4^{2-} ($R^2 = 0.38$) and $Org.^-$ ($R^2 = 0.05$) (Figure 27). Importantly, however, HCO_3^-, being pH dependent, has only risen significantly in the less acidic regions (Figure 22).

Sites with contrasting trends in Ca^{2+} show similar rates of increase in ANC (Table 5), suggesting that similar rates of chemical recovery from acidification. Despite this, the dominant underlying cause of the ANC trends differs between the two groups. At sites with strongly negative Ca^{2+} slopes (<-2.5 µEq/L/yr), the increase in ANC can be attributed to a larger decline in the strong acid anion SO_4^{2-} than in Ca^{2+}, mainly compensated by an increase in organic anions (Figure 28) and a decline in acid cations. In contrast, the ANC increase at sites with increasing Ca^{2+} is best explained by the increase in HCO_3^-, balancing the increase in Ca^{2+} (Figure 29) as the sites have pH that is high enough to allow for carbonic acid deprotonation.
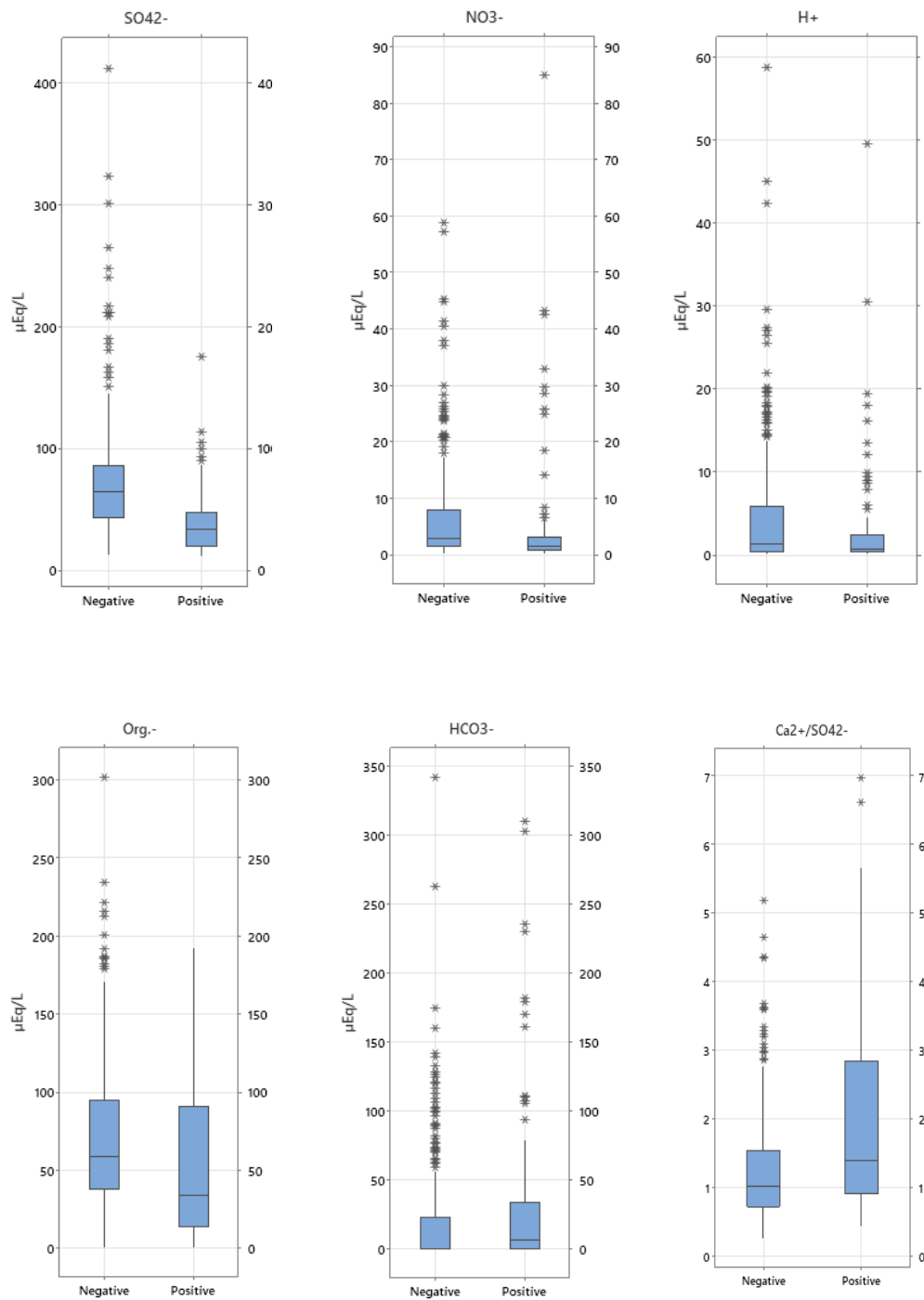
Figure 26. Boxplots depicting significant differences in median concentrations of SO_4^{2-}, NO_3^-, H^+, Org.$^-$, and HCO_3^- concentrations, and ratios of SO_4^{2-}/Ca^{2+}, between sites with positive and negative Ca^{2+} Sen's slopes.
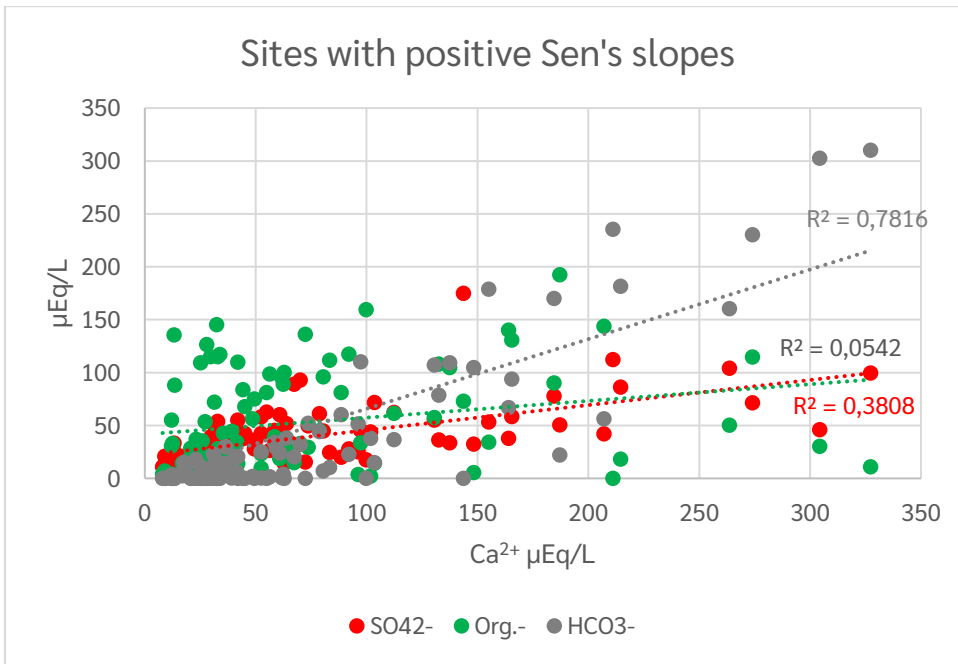
Figure 27. Relationship between median Ca^{2+} and SO_4^{2-} (red), Org.- (green) and HCO_3^- (grey) concentrations in samples at sites with positive Ca^{2+} slopes.

Figure 29. Figure 28. Relationship between Sen's slopes of SO_4^{2-} (red), Org.- (green), Ca^{2+} (blue), and HCO_3^- (grey) vs. the slope of ANC at sites with very negative Ca^{2+} slopes (<-2).

Figure 28. Figure 29. Relationship between Sen's slopes of SO_4^{2-} (red), Org.- (green), Ca^{2+} (blue), and HCO_3^- (grey) vs. the slope of ANC at sites with positive Ca^{2+} slopes. Blue line indicates the 1:1 relationship between ANC and bicarbonate.

Multiple linear regression models for the Ca^{2+} Sen's slope, using SO_4^{2-}, HCO_3^- and $Org.^-$ slopes as predictors, illustrate the differences in the relative roles of the predictors in the datasets from all sites, and for sites with negative and positive Ca^{2+} slopes (Table 6). As could be expected, the inclusion of all predictors at all sites generates the strongest explanatory value (i.e., 70.8%). At the sites with negative Ca^{2+} slopes the SO_4^{2-} needs 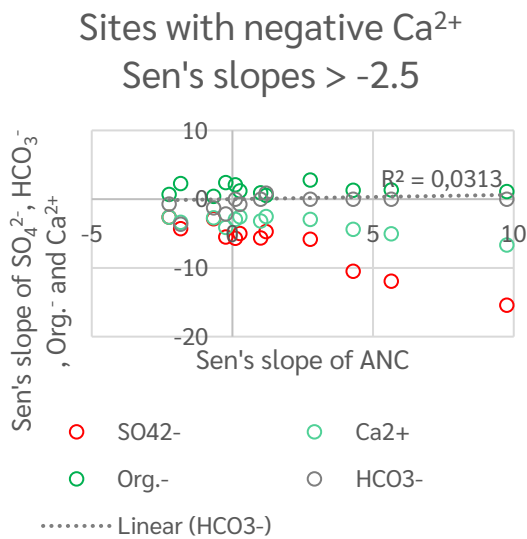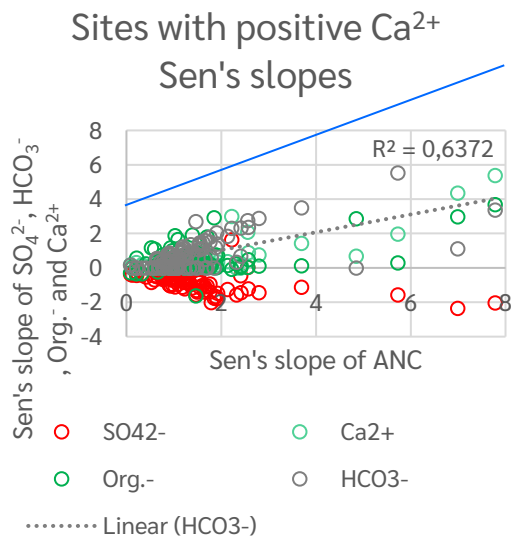to be included to achieve a model with a significant explanatory value. Focusing on the data from the sites with positive Ca^{2+} slopes, a model including only HCO_3^- and $Org.^-$ as prediction variables have a significant explanatory value (40.8%). In this model the HCO_3^- and the $Org.-$ have similar coefficients, implying that together they have a similar governing strength on the Ca^{2+} slopes, although the temporal trends in HCO_3^- at these sites with positive ANC are much greater than for $Org.^-$. Including SO_4^{2-} in the model improves the regression at sites with positive Ca^{2+} trends to $R^2 = 0.446$.

Table 6 Regression analysis for the Sen's slope of Ca_{2+} based on HCO_3^- and $Org.^-$ as predictors on all the sites, and the sites with negative and positive Ca^{2+} slopes. $Ca^{2+} = aSO_4^{2-} + bHCO_3^- + cOrg.^- + d$.

Sen's slope model:	Coeff. SO_4^{2-} (a)	P value	Coeff. HCO_3^- (b)	P value	Coeff. $Org.^-$ (c)	P value	Const. (d)	P value	R^2
All sites	0.4851	0.000	0.5696	0.000	0.3434	0.000	-0.0610	0.177	0.7078
			0.5881	0.000	-0.1129	0.029	-0.6882	0.000	0.2069
Sites with negative Ca^{2+} slopes	0.4376	0.000	0.4007	0.000	0.2158	0.000	-0.1048	0.025	0.7028
			0.3152	0.000	-0.1891	0.000	-0.7663	0.000	0.0962
Sites with positive Ca^{2+} slopes	0.3399	0.000	0.5724	0.000	0.7136	0.000	-0.0936	0.283	0.4456
			0.5150	0.000	0.5305	0.000	-0.2566	0.002	0.4076

De Wit et al. (2023) considered that the increase in biomass and respiration rate, induced by climate change, may affect weathering rates, and thereby change the water chemistry. However, assessing changes in water chemistry in 1000 Norwegian lakes from 1995 to 2019 they found no correlations between temporal trends in Ca^{2+} and the widespread increase in SiO_2, which is often regarded as a proxy for the degree of weathering of the silicate rocks. This indicated that the Ca^{2+} increase was not only a consequence of increased weathering of primary minerals. De Wit et al. proposed instead that the rise in Ca^{2+}, and its close association with alkalinity, is related to increasing terrestrial productivity that results in more root exudation of organic acids and root respiration (i.e., Increased terrestrial pump of CO_2 to the root zone) (Comstedt et al., 2006). This study agrees with this hypothesis. On the other hand, more biomass due to increased productivity will lead to increased tree uptake of Ca^{2+}, which can mask the increase in Ca weathering rates of granitic bedrock Marty et al. (2021).

Since 2017 the declines in non-marine sulphate have levelled off in the 78 Norwegian acid-sensitive freshwater lakes that are a part of this study (Vogt and Skancke, 2023). Trends in the sum of non-marine calcium and magnesium differ between the different regions of the country, from decreasing in the more acid deposition-affected southern- and Southeastern Norway, to increasing in the less polluted northwestern-, Central-, and Northern Norway. TOC concentration has increased as acidification has decreased. However, there are signs that these trends are levelling off in the regions that have been most exposed to acidification. A continued increase in other parts of the country may be due to climate change and increased biomass as discussed in Chapters 2.2.3.7.

Summing up, sites where Ca^{2+} has been increasing are characterized by being less acidified (lower median concentrations of SAA and pH above 5.5) and having higher HCO_3^- concentrations. These sites have gentler decreasing slopes in SO_4^{2-}, lower increases in $Org.^-$, and steeper increasing slopes of HCO_3^-. The increase in HCO_3^- is the most important factor governing the increases in Ca^{2+} at these sites.

3.4 Possible causes for spatial differences in HCO_3^- and $Org.^-$ trends

Spatial variation in maximum HCO_3^- and $Org.^-$ concentrations is partially linked to the fraction of forest land cover in the watersheds (Figure 30), though there is a large variation in their median concentration at sites with more than 50% forest cover.
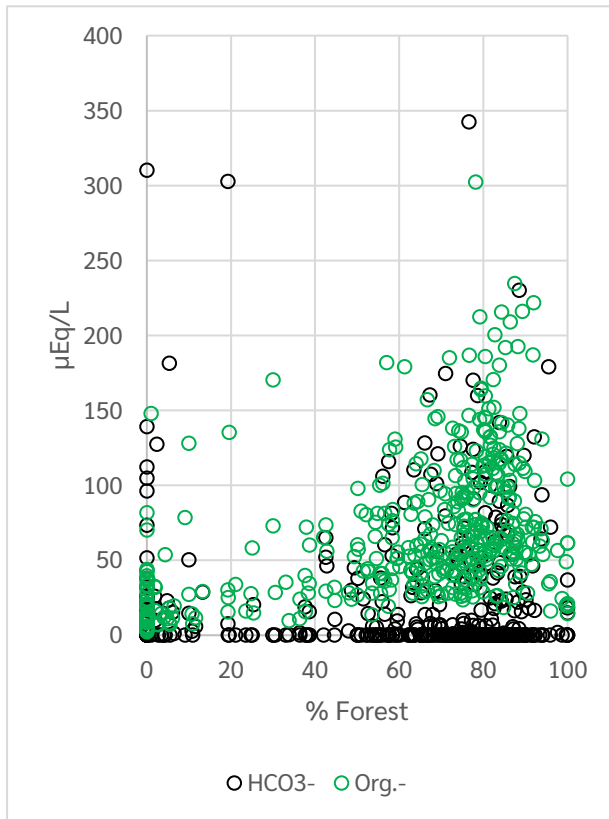

Figure 30. Spatial relationship between the levels of HCO_3^- (black) and $Org.^-$ (green) in the drainage water and the percent forest coverage in the watershed.(green) in the drainage water and the percent forest coverage in the watershed

In the most acid-sensitive and anthropogenically acidified regions, the average pH (i.e., 5.02 in 1995 and 5.38 in 2019 (de Wit et al., 2023)) remains so low that the carbonate is predominantly in the form of protonated carbonic acid and CO_2 (aq.) (i.e., $\alpha_0 = \frac{[H_2CO_3]}{[HCO_3^-]} = 0.95$ and 0.83, respectively), exerting minimal influence on Ca^{2+} transport processes. Generally, at sites with pH below 5.5, the levels of bicarbonate remain insignificant regardless of forest cover. Still, the increase in bicarbonate in less acidic forested sites may thus be driven by the prolonged growing season (as described in Chapt. 3.1) increasing soil respiration and atmospheric CO_2 (CO_2 pump) (Comstedt et al., 2006), leading to increased carbonate alkalinity, weathering, and cation concentrations (Andrews and Schlesinger, 2001). On the other hand, these experiments have used exaggerated CO_2 levels and lack a documentation of long-term effects. Moreover, many of the ICP Water sites would likely not support extra biomass growth as they are too nutrient-limited and are located in cold climates, particularly those with the increasing Ca^{2+} trends situated in the NoNord region.

Still, the spatial differences in median levels of $Org.^-$ are related to the relative forest coverage (Figure 30). This may be due to the high biomass in forests generating more allochthonous DOM.

On average in our dataset, sites with negative Sen's slopes for Ca^{2+} are dominated by forests (66%), mainly coniferous, while sites with positive slopes have less forest cover (43%), and instead a significant land cover of heathland, sparsely vegetated land, and bare rock (37%).

Moreover, in the most acid-sensitive and anthropogenically acidified regions, Ca^{2+} on the soil's cation exchanger were depleted (i.e., %BS < 20%, Reuss and Johnson, 1985). Where the critical load is not exceeded, it is hypothesized that these pools are being replenished (Lawrence et al., 1999, 2015; Hazlett et al., 2020). Refilling this soil pool of Ca^{2+} is thus also limiting the leaching of Ca^{2+} to surface waters at these sites.

3.5 Conclusions regarding calcium trends

Differences between sites with respect to temporal trends in Ca^{2+} levels are, as hypothesized, mainly due to differences in rates of decline in SO_4^{2-} vs. rates of increase in $Org.^-$ and HCO_3^-, which in turn are governed by acid deposition loading and catchment characteristics, soil buffering capacity and land cover.

Within regions with moderate or low acid deposition, spatial differences in pH and forest cover may together explain variation in the extent to which trends in $Org.^-$ and HCO_3^- modify the Ca^{2+} response relative to declines in SO_4^{2-}. Since HCO_3^- concentrations are negligible in waters with a pH below 5.5, increases in HCO_3^- will only be detectable in less acidic systems. In more acidic and more acid-rain-impacted sites, the effect of increases in $Org.^-$ is outweighed by strong declines in SO_4^{2-} and depleted base saturation limiting Ca^{2+} release from the soil.

The significance of these results in an air pollution policy context is that, although increasing ANC trajectories have slowed down in Europe in recent years, the chemical recovery of less acidified freshwaters with a pH above 5.5 is occurring more rapidly than current biogeochemical models predict. We hypothesize that climate-induced increases of weathering rates may explain the increases in Ca^{2+} and thereby chemical recovery, at least for less acid-sensitive sites. If this is correct, we should consider incorporating this effect in the process description of the models used to predict future chemical recovery.

4 References

Aber, J. D., K. J. Nadelhoffer, P. Steudler and J. M. Melillo (1989). Nitrogen Saturation in Northern Forest Ecosystems: Excess nitrogen from fossil fuel combustion may stress the biosphere. BioScience **39**(6): 378-386. https://doi.org/10.2307/1311067

Andrews, J. A., and W. H. Schlesinger (2001). Soil CO_2 dynamics, acidification, and chemical weathering in a temperate forest with experimental CO_2 enrichment, Global Biogeochem. Cycles, 15(1), 149–162, https://doi.org/10.1029/2000GB001278

Austnes, K., Hjermann, D. Ø., Sample, J. E., Wright, R. F., Kaste, Ø. & de Wit, H. (2022). Nitrogen in surface waters: time trends and geographical patterns explained by deposition levels and catchment characteristics. (NIVA-rapport 7728-2022). Norsk institutt for vannforskning. https://hdl.handle.net/11250/2997096

Austnes, K., Wright, R. F., Sample, J. E., & Clayer, F. (2020). Critical loads and the MAGIC model. Evaluating the country-scale applications in Norway using data from the 2019 national lake survey (NIVA Report, Issue. https://niva.brage.unit.no/niva-xmlui/handle/11250/2725461

Battarbee, R.W., Monteith, D.T., Juggins, S., Evans, C.D., Jenkins, A., Simpson, G.L. (2005). Reconstructing pre-acidification pH for an acidified Scottish loch: A comparison of palaeolimnological and modelling approaches. Environ. Pollut. 137, 135–149. http:/doi.org/10.1016/j.envpol.2004.12.021

Breidenbach, J., Granhus, A., Hylen, G., Eriksen, R., & Astrup, R. (2020). A century of National Forest Inventory in Norway - informing past, present, and future decisions [Article]. Forest Ecosystems, 7(1), 19, Article 46. https://doi.org/10.1186/s40663-020-00261-0

Bryn, A., & Potthoff, K. (2018). Elevational treeline and forest line dynamics in Norwegian mountain areas - a review [Review]. Landscape Ecology, 33(8), 1225-1245. https://doi.org/10.1007/s10980-018-0670-8

Bryntsen, T., 2022. Intercomparison 2236: pH, Conductivity, Alkalinity, NO_3-N, Cl, SO_3, Ca, Mg, Na, K, TOC, Tot-P, Tot-N, Al, Fe, Mn, Cd, Pb, Cu, Ni, and Zn. ICP Waters report 151/2022. 7792-2022. https://www.icp-waters.no/2022/

Clark, J.M., Bottrell, S.H., Evans, C.D., Monteith, D.T., Bartlett, R., Rose, R., Newton, R.J., Chapman, P.J. (2010). The importance of the relationship between scale and process in understanding long-term DOC dynamics. Sci. Total Environ. 408, 2768–2775. https://doi.org/10.1016/j.scitotenv.2010.02.046

CLRTAP, 2023. Mapping critical loads for ecosystems, Chapter 5 of Manual on methodologies and criteria for modelling and mapping critical loads and levels and air pollution effects, risks and trends. UNECE Convention on Long-range Transboundary Air Pollution; accessed 25 September 2023 at www.umweltbundesamt.de/en/cce-manual

Comstedt, D., Bostrom, B., Marshall, J. D., Holm, A., Slaney, M., Linder, S., & Ekblad, A. (2006). Effects of elevated atmospheric carbon dioxide and temperature on soil respiration in a boreal forest using

delta C-13 as a labeling tool [Article]. Ecosystems, 9(8), 1266-1277. https://doi.org/10.1007/s10021-006-0110-5

Crapart, C., Finstad, A. G., Hessen, D. O., Vogt, R. D., & Andersen, T. (2023). Spatial predictors and temporal forecast of total organic carbon levels in boreal lakes. Science of the Total Environment, 870, 161676. https://doi.org/https://doi.org/10.1016/j.scitotenv.2023.161676

De Wit, H. A., Austnes, K., Hylen, G., & Dalsgaard, L. (2015). A carbon balance of Norway: terrestrial and aquatic carbon fluxes. Biogeochemistry, 123(1-2), 147-173. https://doi.org/10.1007/s10533-014-0060-5

De Wit, H. A., Garmo, Ø. A., Jackson-Blake, L. A., Clayer, F., Vogt, R. D., Austnes, K., Kaste, Ø., Gundersen, C. B., Guerrerro, J. L., & Hindar, A. (2023). Changing Water Chemistry in One Thousand Norwegian Lakes During Three Decades of Cleaner Air and Climate Change. Global Biogeochemical Cycles, 37(2), e2022GB007509. https://doi.org/https://doi.org/10.1029/2022GB007509

De Wit, H. A., Mulder, J., Hindar, A., & Hole, L. (2007). Long-Term Increase in Dissolved Organic Carbon in Streamwaters in Norway Is Response to Reduced Acid Deposition Environmental Science & Technology, 41(22), 7706-7713. https://doi.org/10.1021/es070557f

De Wit, H. A., J. L. Stoddard, D. T. Monteith, J. E. Sample, K. Austnes, S. Couture, J. Fölster, S. N. Higgins, D. Houle, J. Hruška, P. Krám, J. Kopáček, A. M. Paterson, S. Valinia, H. Van Dam, J. Vuorenmaa and C. D. Evans (2021). "Cleaner air reveals growing influence of climate on dissolved organic carbon trends in northern headwaters." Environmental Research Letters 16(10): 104009. http://doi.org/10.1088/1748-9326/ac2526

De Wit, H. A., Valinia, S., Weyhenmeyer, G. A., Futter, M. N., Kortelainen, P., Austnes, K., Hessen, D. O., Räike, A., Laudon, H., & Vuorenmaa, J. (2016). Current Browning of Surface Waters Will Be Further Promoted by Wetter Climate. Environmental Science & Technology Letters, 3(12), 430-435. https://doi.org/10.1021/acs.estlett.6b00396

Eisfelder, C., Asam, S., Hirner, A., Reiners, P., Holzwarth, S., Bachmann, M., Gessner, U., Dietz, A., Huth, J., Bachofer, F., & Kuenzer, C. (2023). Seasonal Vegetation Trends for Europe over 30 Years from a Novel Normalised Difference Vegetation Index (NDVI) Time-Series—The TIMELINE NDVI Product. Remote Sensing, 15(14), 3616. https://www.mdpi.com/2072-4292/15/14/3616

Eklöf, K., von Brömssen, C., Amvrosiadi, N., Fölster, J., Wallin, M. B., & Bishop, K. (2021). Brownification on hold: What traditional analyses miss in extended surface water records. Water Res, 203, 117544. https://doi.org/10.1016/j.watres.2021.117544

Erlandsson, M., Cory, N., Köhler, S., Bishop, K., (2010). Direct and indirect effects of increasing dissolved organic carbon levels on pH in lakes recovering from acidification. J. Geophys. Res. 115, 8 PP. hppt://doi.org/ 10.1029/2009JG001082

Eshleman, K.N., Morgan, R.P., Webb, J.R., Deviney, F.A., Galloway, J.N. (1998). Temporal patterns of nitrogen leakage from mid-Appalachian forested watersheds: Role of insect defoliation. Water Resour. Res. 34, 2005–2016. https://doi.org/10.1023/A:1006427401665

Evans, C.D., Monteith, D.T., Fowler, D., Cape, J.N., and Brayshaw, S. (2011). Hydrochloric Acid: An Overlooked Driver of Environmental Change. Environmental Science & Technology 45 (5), 1887-1894. http://doi.org/10.1021/es103574u

Fagerli, H., Benedictow, A. M. K., van Caspel, W., Gauss, M., Ge, Y., Jonson, J. E., Klein, H., Nyiri, A., Simpson, D., Tsyro, S., Valdebenito, A., Wind, P., Aas, W., Hjellbrekke, A.-G., Solberg, S., Tørseth, K., Yttri, K. E., Matthews, B., Schindlbacher, S., . . . Wegener, R. (2023). Transboundary particulate matter, photo-oxidants, acidifying and eutrophying components (EMEP Report, Issue 1/2023. EMEP_Status_Report_1_2023.pdf

Finstad, A. G., Andersen, T., Larsen, S., Tominaga, K., Blumentrath, S., de Wit, H. A., Tømmervik, H., & Hessen, D. O. (2016). From greening to browning: Catchment vegetation development and reduced S-deposition promote lake organic carbon load on decadal time scales. Scientific Reports, 6(31944). https://doi.org/10.1038/srep31944

Franzén, L. G. (1990). Transport, Deposition and Distribution of Marine Aerosols over Southern Sweden during Dry Westerly Storms. Ambio 19(4): 180-188. https://www.jstor.org/stable/4313690

Garmo, Ø. A., Øyvind, K., Arle, J., Austnes, K., de Wit, H., Fölster, J., Houle, D., Hruška, J., Indriksone, I., Monteith, D., Rogora, M., Sample, J. E., Steingruber, S., Stoddard, J. L., Talkop, R., Trodd, W., Ulańczyk, R. P., & Vuorenmaa, J. (2020). Trends and patterns in surface water chemistry in Europe and North America between 1990 and 2016, with particular focus on changes in land use as a confounding factor for recovery. ICP Water report 142-2020, NIVA report 7479. https://niva.brage.unit.no/niva-xmlui/handle/11250/2649682

Garmo, Ø.A., De Wit, H., Fjellheim, A. (2015). Chemical and biological recovery in acid-sensitive waters: trends and prognosis. ICP Waters report 119/2015, NIVA report 6847. https://niva.brage.unit.no/niva-xmlui/handle/11250/282920

Garmo, Ø. A., Skjelkvåle, B. L., Wit, H. A., Colombo, L., Curtis, C., Fölster, J., Hoffmann, A., Hruška, J., Høgåsen, T., Jeffries, D. S., Keller, W. B., Krám, P., Majer, V., Monteith, D. T., Paterson, A. M., Rogora, M., Rzychon, D., Steingruber, S., Stoddard, J. L., Vuorenmaa, J., Worsztynowicz, A. (2014). Trends in Surface Water Chemistry in Acidified Areas in Europe and North America from 1990 to 2008 [journal article]. Water, Air, & Soil Pollution, 225(3), 1-14. https://doi.org/10.1007/s11270-014-1880-6

Hampel, F.R. (1974). The Influence Curve and its Role in Robust Estimation. Journal of the American Statistical Association, 69:346, 383-393. http://doi.org/10.1080/01621459.1974.10482962

Hanssen-Bauer, I., Førland, E., Haddeland, I., Hisdal, H., Lawrence, D., Mayer, S., Nesje, A., Nilsen, J., Sandven, S., & Sandø, A. (2017). Climate in Norway 2100 – a knowledge base for climate adaptation. NCCS report, 1, 2017. MDir report M-741. https://www.miljodirektoratet.no/globalassets/publikasjoner/M741/M741.pdf

Hazlett, P., Emilson, C., Lawrence, G., Fernandez, I., Ouimet, R., Bailey, S. (2020). Reversal of Forest Soil Acidification in the Northeastern United States and Eastern Canada: Site and Soil Factors Contributing to Recovery. Soil Syst. 2020, 4, 54. https://doi.org/10.3390/soilsystems4030054

Helsel, D.R., Frans, L.M. (2006). Regional Kendall Test for Trend. Environ. Sci. Technol. 40, 4066–4073. https://doi.org/10.1021/es051650b

Hirsch, R.M., Slack, J.R. (1984). A nonparametric trend test for seasonal data with serial dependence. Water Resour. Res. 20, 727–732. https://doi.org/10.1029/WR020i006p00727

Houle, D., Duchesne, L., Boutin, R. (2009). Effects of a spruce budworm outbreak on element export below the rooting zone: a case study for a balsam fir forest. Ann. For. Sci. 66, 707–707. https://doi.org/10.1051/forest%2F2009057

Houle, D., Marty, C., Augustin, F., Dermont, G., & Gagnon, C. (2020). Impact of Climate Change on Soil Hydro-Climatic Conditions and Base Cations Weathering Rates in Forested Watersheds in Eastern Canada. Frontiers in Forests and Global Change, 3, 535397. https://doi.org/10.3389/ffgc.2020.535397

Hovind, H. (1998). Intercomparison 9812. pH, conductivity, alkalinity, nitrate + nitrite, chloride, sulfate, calcium, magnesium, sodium, potassium, total aluminium, reactive and non-labile aluminium, dissolved organic carbon, and chemical oxygen demand. ICP Waters report 49/1998, NIVA report 3939. https://niva.brage.unit.no/niva-xmlui/handle/11250/210134

Haaland, S., Eikebrokk, B., Riise, G., & Vogt, R. D. (2023). Browning of Scottish surface water sources exposed to climate change. PLOS Water, 2(9), e0000172. https://doi.org/10.1371/journal.pwat.0000172

Hruška, J., Köhler, S., Laudon, H., & Bishop, K. (2003). Is a Universal Model of Organic Acidity Possible: Comparison of the Acid/Base Properties of Dissolved Organic Carbon in the Boreal and Temperate Zones. Environmental Science & Technology, 37(9), 1726-1730. https://doi.org/10.1021/es0201552

Hruška, J., Krám, P., McDowell, W.H., Oulehle, F. (2009). Increased dissolved organic carbon (DOC) in Central Europe streams is driven by reduction in ionic strength rather than climate change or decreasing acidity. Environmental Science and Technology 43 (12), 4320-4326. https://doi.org/10.1021/es803645w

ICP Waters Programme Centre (2010). ICP Waters Programme Manual. ICP Waters Report 105/2010. NIVA report 6074. http://hdl.handle.net/11250/215220.

IPCC. (2022). Climate Change 2022: Impacts, Adaptation, and Vulnerability. Contribution of Working Group II to the Sixth Assessment Report of the Intergovernmental Panel on Climate Change (H.-O. Pörtner, D.C. Roberts, E.S. Poloczanska, K. Mintenbeck, M. Tignor, A. Alegría, M. Craig, S. Langsdorf, S. Löschke, V. Möller, A. Okem., B. Rama (eds.)). https://www.ipcc.ch/report/ar6/wg2/

Kopáček, J., Bičárová, S., Hejzlar, J., Hynštová, M., Kaňa, J., Mitošinková, M., Porcal, P., Stuchlík, E., Turek, J. (2015). Catchment biogeochemistry modifies long-term effects of acidic deposition on chemistry of mountain lakes. Biogeochemistry 125, 315–335. https://doi.org/10.1021/es5058743

Kopáček, J., Kaňa, J., Bičárová, S., Fernandez, I.J., Hejzlar, J., Kahounová, M., Norton, S.A., and Stuchlík, E. (2017). Climate Change Increasing Calcium and Magnesium Leaching from Granitic Alpine Catchments. Environmental Science & Technology 51, 159-166. https://doi.org/10.1021/acs.est.6b03575

Kritzberg, E. S., Hasselquist, E. M., Škerlep, M., Löfgren, S., Olsson, O., Stadmark, J., Valinia, S., Hansson L.-A., and Laudon H. (2020). Browning of freshwaters: Consequences to ecosystem services, underlying drivers, and potential mitigation measures. Ambio 49(2), 375–390. https://doi.org/10.1007/s13280-019-01227-5

Lawrence, G. B., David, M. B., Lovett, G. M., Murdoch, P. S., Burns, D. A., Stoddard, J. L., Baldigo, B. P., Porter, J. H., & Thompson, A. W. (1999). Soil calcium status and the response of stream chemistry to changing acidic deposition rates [Article]. Ecological Applications, 9(3), 1059-1072. https://doi.org/10.1890/1051-0761(1999)009[1059:Scsatr]2.0.Co;2

Lawrence, G. B., Hazlett, P.W., Fernandez, I.J., Ouimet, R., Bailey, S.W., Shortle, W.C., Smith, K.T., Antidormi, M.R. (2015). Declining Acidic Deposition Begins Reversal of Forest-Soil Acidification in the Northeastern U.S. and Eastern Canada. *Environmental Science & Technology* **49**, 13103-13111. https://doi.org:10.1021/acs.est.5b02904

Lightowlers, P. J., & Cape, J. N. (1988). Sources and fate of atmospheric HCl in the U.K. and Western Europe. Atmospheric Environment (1967), 22(1), 7-15. https://doi.org/https://doi.org/10.1016/0004-6981(88)90294-6

Luyssaert, S., Ciais, P., Piao, S. L., Schulze, E. D., Jung, M., Zaehle, S., Schelhaas, M. J., Reichstein, M., Churkina, G., Papale, D., Abril, G., Beer, C., Grace, J., Loustau, D., Matteucci, G., Magnani, F., Nabuurs, G. J., Verbeeck, H., Sulkava, M., . . . Team, C.-I. S. (2010). The European carbon balance. Part 3: forests [Review]. Global Change Biology, 16(5), 1429-1450. https://doi.org/10.1111/j.1365-2486.2009.02056.x

Marty, C., Duchesne, L., Couture, S., Gagnon, C. & Houle, D. (2021). Effects of climate and atmospheric deposition on a boreal lake chemistry: A synthesis of 36 years of monitoring data. Science of The Total Environment 758, 143639. https://doi.org:https://doi.org/10.1016/j.scitotenv.2020.143639

Minitab, LLC. (2021). Minitab. Retrieved from Minitab website. Data Analysis Software | Statistical Software Package | Minitab

Monks, P.S., Granier, C., Fuzzi, S., Stohl, A., Williams, M.L., Akimoto, H., Amann, M., Baklanov, A., Baltensperger, U., Bey, I., Blake, N., Blake, R.S., Carslaw, K., Cooper, O.R., Dentener, F., Fowler, D., Fragkou, E., Frost, G.J., Generoso, S., Ginoux, P., Grewe, V., Guenther, A., Hansson, H.C., Henne, S., Hjorth, J., Hofzumahaus, A., Huntrieser, H., Isaksen, I.S.A., Jenkin, M.E., Kaiser, J., Kanakidou, M., Klimont, Z., Kulmala, M., Laj, P., Lawrence, M.G., Lee, J.D., Liousse, C., Maione, M., McFiggans, G., Metzger, A., Mieville, A., Moussiopoulos, N., Orlando, J.J., O'Dowd, C.D., Palmer, P.I., Parrish, D.D., Petzold, A., Platt, U., Pöschl, U., Prévôt, A.S.H., Reeves, C.E., Reimann, S., Rudich, Y., Sellegri, K., Steinbrecher, R., Simpson, D., ten Brink, H., Theloke, J., van der Werf, G.R., Vautard, R., Vestreng, V., Vlachokostas, Ch., von Glasow, R. (2009). Atmospheric composition change – global and regional air quality. Atmospheric Environment, ACCENT Synthesis 43(33): 5268–5350. https://doi.org/10.1016/j.atmosenv.2009.08.021

Monteith, D. T., Henrys, P. A., Hruška, J., de Wit, H. A., Krám, P., Moldan, F., Posch, M., Räike, A., Stoddard, J. L., Shilland, E. M., Pereira, M. G., & Evans, C. D. (2023). Long-term rise in riverine dissolved organic carbon concentration is predicted by electrolyte solubility theory. Science Advances, 9(3), eade3491. https://doi.org/10.1126/sciadv.ade3491.

Monteith, D., Henrys, P., Lindsay, B., Smith, R., Morecroft, M., Scott, T., Andrews, C., Beaumont, D., Benham, S., Bowmaker, V., Corbett, S., Dick, J., Dodd, B., Dodd, N., McKenna, C., McMillan, S., Pallett, D., Pereira, G., Rennie, S., Rose, R., Schafer, S., Sherrin, L., Turner, A., Watson, H., Poskitt, J. and Tang, S. (2016). Trends and variability in weather and atmospheric deposition at UK Environmental Change Network sites (1993-2012). Ecological Indicators, 68, 21-35. http://doi.org/10.1016/j.ecolind.2016.01.061.

Monteith, D.T., Stoddard, J.L., Evans, C.D., De Wit, H.A., Forsius, M., Høgåsen, T., Wilander, A., Skjelkvåle, B.L., Jeffries, D.S., Vuorenmaa, J. and Keller, B. (2007). Dissolved organic carbon trends resulting from changes in atmospheric deposition chemistry. Nature, 450(7169), p.537. https://doi.org/10.1038/nature06316

Oulehle F, Wright R.F, Svoboda M, Bače R, Matějka K, Kaňa J, Hruška J, Couture RM, Kopáček J. (2019). Effects of bark beetle disturbance on soil nutrient retention and lake chemistry in glacial catchment. Ecosystems. 22(4):725-41. https://doi.org/10.1007/S10021-018-0298-1

Oulehle, F., Chuman, T., Hruška, J., Krám, P., McDowell, W.H., Myška, O., Navrátil, T., Tesař, M. (2017). Recovery from acidification alters concentrations and fluxes of solutes from Czech catchments. Biogeochemistry 132, 251–272. https://doi.org/10.1007/s10533-017-0298-9

Oliver, B. G., Thurman, E. M., & Malcolm, R. L. (1983). The contribution of humic substances to the acidity of colored natural waters. Geochimica et Cosmochimica Acta, 47(11), 2031-2035. https://doi.org/http://dx.doi.org/10.1016/0016-7037(83)90218-1

Pan, Y., Birdsey, R. A., Fang, J., Houghton, R., Kauppi, P. E., Kurz, W. A., Phillips, O. L., Shvidenko, A., Lewis, S. L., Canadell, J. G., Ciais, P., Jackson, R. B., Pacala, S. W., McGuire, A. D., Piao, S., Rautiainen, A., Sitch, S., & Hayes, D. (2011). A Large and Persistent Carbon Sink in the World's Forests. Science, 333(6045), 988-993. https://doi.org/doi:10.1126/science.1201609

Python Software Foundation. Python Language Reference, version 2.7. Available at http://www.python.org

Reuss, J. O., & Johnson, D. W. (1985). Effect of soil processes on the acidification of water by acid deposition. J. Environ. Qual., 14, 26-31. https://doi.org/10.2134/jeq1985.00472425001400010005x

Rogora, M., Colombo, L., Marchetto, A., Mosello, R. & Steingruber, S. (2016). Temporal and spatial patterns in the chemistry of wet deposition in Southern Alps. Atmospheric Environment 146, 44-54. https://doi.org/10.1016/j.atmosenv.2016.06.025

Sen, P.K. (1968). Estimates of the regression coefficient based on Kendall's tau. J. Am. Stat. Assoc. 63, 1379–1389. https://doi.org/10.1080/01621459.1968.10480934

Škerlep, M., Steiner, E., Axelsson, A.-L., & Kritzberg, E. S. (2020). Afforestation driving long-term surface water browning. Global Change Biology, 26(3), 1390-1399. https://doi.org/https://doi.org/10.1111/gcb.14891

Skjelkvåle, B.L., de Wit, H. (2007). Trends in surface water chemistry and biota; The importance of confounding factors. ICP Waters report No. 87/2007, NIVA reprt 5385. https://niva.brage.unit.no/niva-xmlui/handle/11250/213562

Skjelkvåle B.L. and de Wit, H. (eds.) 2011. Trends in precipitation chemistry, surface water chemistry and aquatic biota in acidified areas in Europe and North America from 1990 to 2008. NIVA report SNO 6218-2011. ICP Waters report 106/2011, NIVA report 6218. https://niva.brage.unit.no/niva-xmlui/handle/11250/215591

Strock, K.E., Nelson, S.J., Kahl, J.S., Saros, J.E., McDowell, W.H. (2014). Decadal Trends Reveal Recent Acceleration in the Rate of Recovery from Acidification in the Northeastern U.S. Environ. Sci. Technol. 48, 4681–4689. https://doi.org/10.1021/es404772n

Terrer, C. (2021). Balancing carbon storage under elevated CO2. Nature. https://doi.org/10.1038/s41586-021-03306-8

Tipping, E., Loft, S., & Sonke, J. E. (2011). Humic Ion-Binding Model VII: a revised parameterisation of cation-binding by humic substances. Environ. Chem., 8, 225-235. https://doi.org/10.1071/EN 11016

van Schöll, L., Kuyper, T. W., Smits, M. M., Landeweert, R., Hoffland, E., & Breemen, N. v. (2008). Rock-eating mycorrhizas: their role in plant nutrition and biogeochemical cycles. Plant and Soil, 303(1), 35-47. https://doi.org/10.1007/s11104-007-9513-0

Vogt, R. D., Ø. A. Garmo, A. K. Schartau and S. L. Haaland (2023). Methods for calculating the Acid neutralizing capacity of water (ANC) for classification of acidification state. In Norwegian. Vann 02(58): 105-117.

Vogt, R. D., Gjessing, E., Andersen, D. O., Clarke, N., Gadmar, T., Bishop, K., Lundstrøm, U., & Starr, M. (2001). Natural Organic Matter in the Nordic countries. http://www.nordtest.info/index.php/technical-reports/item/natural-organic-matter-in-the-nordic-countries-nt-tr-479.html

Vogt, R. D., de Wit, H., & Koponen, K. (2022). Case study on impacts of large-scale re-/afforestation on ecosystem services in Nordic regions [Rapport](Quantifying and deploing responsible negative emissions in climate resilient pathways. , Issue. N. project. https://www.negemproject.eu/wp-content/uploads/2022/06/NEGEM_D3.6_Case-study-on-impacts-of-large-scale-re-afforestation-on-ecosystem-services-in-Nordic-regions.pdf

Vogt, R. D., Ranneklev, S. B., & Mykkelbost, T. C. (1994). The impact of acid treatment on soil water chemistry at the HUMEX site [10.1016/0160-4120(94)90111-2]. Environ. Int., 20(3), 277-286. https://doi.org/10.1016/0160-4120(94)90111-2

Vogt, R.D., & Skancke, L.B., (2024). Overvåkning av langtransportert luft og nedbør, Årsrapport - Vannkjemiske effekter. 2022. MDir report M-2572. https://www.miljodirektoratet.no/publikasjoner/2023/november-2023/overvaking-av-langtransportert-forurenset-luft-og-nedbor.-arsrapport-vannkjemiske-effekter-2022

Wallman, P., Svensson, M. G. E., Sverdrup, H., & Belyazid, S. (2005). ForSAFE—an integrated process-oriented forest model for long-term sustainability assessments. Forest Ecology and Management, 207(1), 19-36. https://doi.org/https://doi.org/10.1016/j.foreco.2004.10.016

Weyhenmeyer, G. A., Hartmann, J., Hessen, D. O., Kopacek, J., Hejzlar, J., Jacquet, S., Hamilton, S. K., Verburg, P., Leach, T. H., Schmid, M., Flaim, G., Noges, T., Noges, P., Wentzky, V. C., Rogora, M., Rusak, J. A., Kosten, S., Paterson, A. M., Teubner, K., . . . Zechmeister, T. (2019). Widespread diminishing anthropogenic effects on calcium in freshwaters. Scientific Reports, 9, 10, Article 10450. https://doi.org/10.1038/s41598-019-46838-w

Aalto, J., Pirinen, P., Kauppi, P. E., Rantanen, M., Lussana, C., Lyytikainen-Saarenmaa, P., & Gregow, H. (2022). High-resolution analysis of observed thermal growing season variability over northern

Europe [Article]. Climate Dynamics, 58(5-6), 1477-1493. https://doi.org/10.1007/s00382-021-05970-y

Wright, R., Cosby, B., Flaten, M. et al. (1990). Evaluation of an acidification model with data from manipulated catchments in Norway. Nature 343, 53–55. https://doi.org/10.1038/343053a0

5 Appendix

Table A1. Regional median levels for the periods 1990-2004, 1998 – 2012, and 2006 – 2020. The median levels are of the annual median values for all the sites in each region.

		SO_4^{2-}	NO_3^-	Cl^-	$Org.^-$	HCO_3^-	Ca^{2+}	Mg^{2+}	H^+	ANC	TOC
						µEq/L					mg C/L
1990 - 2004	NoNord	42.7	0.79	56.4	27.3	10.3	58.4	41.1	0.55	38.4	2.10
	SoNord	82.9	3.36	86.0	77.2	0.00	83.0	51.9	1.95	57.9	6.40
	UK-IE-NL	69.7	9.29	226	36.0	0.00	53.4	55.9	3.63	9.37	3.50
	WCE	192	45.1	95.2	34.8	20.8	161	131	2.20	42.9	3.95
	ECE	67.4	29.0	8.07	12.2	0.00	86.9	15.2	5.29	14.0	1.18
	Alps	70.8	43.9	25.4	NA	176	178	65.8	0.12	176	NA
	Ont	108	4.88	9.70	50.1	45.2	124	42.6	0.39	89.7	3.77
	AdsCsk	93.1	10.9	8.46	47.4	0.00	78.3	27.5	2.68	18.5	4.10
	QuMaVt	70.8	2.36	9.87	52.7	8.04	80.0	32.7	0.57	59.1	4.25
	AtlCan	44.3	1.43	111	65.4	0.00	37.2	33.3	3.39	38.1	6.05
1998-2012	NoNord	35.3	0.64	45.1	31.7	19.7	60.6	41.5	0.46	60.4	2.40
	SoNord	58.0	3.11	78.3	90.2	0.00	71.9	46.9	1.51	72.7	7.45
	UK-IE-NL	56.2	8.57	202	46.2	0.00	43.8	52.1	2.68	14.7	4.23
	WCE	119	36.2	84.4	52.1	37.4	136	129	0.75	68.3	4.20
	ECE	43.4	21.4	5.10	10.3	4.65	84.5	12.0	1.48	28.4	0.80
	Alps	47.9	31.6	5.13	NA	67.0	102	15.5	0.15	72.0	NA
	Ont	96.5	3.94	8.91	52.4	46.0	118	39.7	0.36	95.1	3.92
	AdsCsk	75.9	8.19	7.83	50.6	0.00	71.4	25.4	1.71	28.6	4.21
	QuMaVt	59.3	2.36	11.3	57.2	7.89	71.9	30.1	0.48	59.2	4.48
	AtlCan	37.0	1.43	115	70.3	0.00	36.1	32.5	2.82	42.3	6.35
2006-2020	NoNord	31.0	0.43	51.1	31.2	24.8	59.9	41.1	0.42	62.4	2.30
	SoNord	47.9	2.64	85.6	98.1	0.00	64.9	44.7	1.29	75.8	7.95
	UK-IE-NL	45.0	7.93	209	60.2	0.00	49.9	55.0	1.13	36.6	4.88
	WCE	199	35.7	141	66.1	0.00	168	150	5.66	64.1	6.55
	ECE	33.8	17.4	5.58	17.0	10.5	88.8	13.1	0.73	54.4	1.46
	Alps	32.4	21.1	4.01	NA	55.7	79.3	12.3	0.15	59.9	NA
	Ont	74.7	5.86	7.63	51.6	37.5	110	37.1	0.50	91.9	3.86
	AdsCsk	54.2	6.08	6.91	57.1	0.00	64.8	23.0	1.29	42.3	4.72
	QuMaVt	45.8	1.00	9.87	60.3	15.8	67.9	28.8	0.39	73.4	4.54
	AtlCan	31.2	1.43	116	80.9	0.00	37.7	33.3	1.29	52.4	7.00

Table A2. Regional Sen's slopes for the periods 1990-2004, 1998 – 2012, and 2006 – 2020.N.d. denote no data. Units for all parameters except TOC is µEq/L/yr. For TOC the unit is mg C/L/yr. NA denote not analysed.

Sen slp		SO$_4^{2-}$	NO$_3^-$	Cl$^-$	Org.$^-$	HCO$_3^-$	Ca^{2+}	Mg^{2+}	H$^+$	ANC	TOC	CaMg
						µEq/L/yr					mg C/L/yr	µEq/L/yr
1990 - 2020	NoNord	-0.67	-0.01	-0.13	0.21	0.43	0.04	0.00	-0.01	1.09	0.01	0.03
	SoNord	-1.91	-0.06	-0.24	0.85	0.00	-0.54	-0.30	-0.02	1.37	0.06	-0.86
	UK-IE-NL	-1.37	-0.10	-1.53	0.76	0.00	-0.42	-0.36	-0.06	1.47	0.06	-0.78
	WCE	-2.33	-0.54	0.00	0.66	0.00	-0.54	-0.19	-0.03	3.20	0.03	-1.24
	ECE	-1.99	-0.49	-0.09	0.31	0.00	-0.59	-0.10	-0.05	2.32	0.02	-0.75
	Alps	-1.04	-0.33	0.00	NA	0.33	-0.50	-0.08	-0.01	0.84	NA	-0.57
	Ont	-2.28	-0.01	-0.12	0.31	0.13	-1.03	-0.42	0.00	1.03	0.02	-1.49
	AdsCsk	-2.70	-0.16	-0.08	0.68	0.00	-0.88	-0.31	-0.03	1.60	0.05	-1.25
	QuMaVt	-1.73	0.00	-0.07	0.30	0.00	-0.79	-0.32	-0.01	0.72	0.02	-1.12
	AtlCan	-0.93	0.00	0.18	0.58	0.00	-0.05	-0.10	-0.04	0.74	0.04	-0.17
1990 - 2004	NoNord	-0.96	0.00	0.00	0.17	0.39	0.00	0.00	-0.01	1.56	0.01	0.00
	SoNord	-3.27	-0.05	-1.21	0.93	0.00	-0.86	-0.62	-0.03	2.69	0.07	-1.50
	UK-IE-NL	-2.08	0.00	-3.76	1.35	0.00	-0.75	-0.62	-0.16	1.48	0.11	-1.47
	WCE	-2.50	-0.79	-0.71	0.80	1.06	-1.04	0.00	-0.01	7.65	0.04	-0.56
	ECE	-3.61	-0.71	-0.21	0.31	0.00	-1.39	-0.31	-0.10	2.92	0.02	-2.07
	Alps	-1.39	0.59	0.25	NA	0.35	-0.10	0.00	0.00	0.42	NA	-0.08
	Ont	-1.87	0.00	0.00	0.39	0.00	-1.35	-0.45	0.00	0.27	0.03	-1.80
	AdsCsk	-2.08	-0.12	-0.02	0.39	0.00	-0.97	-0.20	-0.02	1.29	0.02	-1.21
	QuMaVt	-1.50	0.00	0.00	0.23	0.00	-0.96	-0.30	-0.01	0.59	0.01	-1.29
	AtlCan	-0.67	0.00	1.30	-0.35	0.00	0.15	0.10	0.00	0.62	-0.03	0.29
1998 - 2012	NoNord	-0.52	-0.01	-0.12	0.28	0.32	0.18	0.00	0.00	1.36	0.02	0.39
	SoNord	-1.94	-0.05	-0.15	1.10	0.00	-0.50	-0.21	-0.02	1.40	0.08	-0.75
	UK-IE-NL	-1.15	-0.18	-1.97	0.67	0.00	-0.50	-0.45	-0.07	1.50	0.05	-0.94
	WCE	-2.69	-0.49	0.44	0.31	0.00	-0.37	-0.82	-0.03	0.88	0.01	-2.50
	ECE	-1.83	-0.31	-0.04	0.21	0.00	-0.29	-0.10	-0.02	2.04	0.01	-0.39
	Alps	-0.84	-0.56	0.00	NA	0.70	0.32	-0.01	0.00	1.50	NA	0.32
	Ont	-2.03	-0.01	-0.22	0.35	0.00	-0.74	-0.38	0.00	1.43	0.02	-1.19
	AdsCsk	-2.61	-0.09	-0.10	0.36	0.00	-0.81	-0.34	-0.02	1.60	0.02	-1.18
	QuMaVt	-1.67	0.00	0.00	0.49	0.00	-0.76	-0.32	-0.01	0.41	0.03	-1.10
	AtlCan	-1.29	0.00	0.16	1.14	0.00	-0.25	-0.41	-0.07	0.68	0.08	-0.72
2006 - 2020	NoNord	-0.52	0.00	-0.09	0.13	0.00	-0.13	0.00	0.00	0.42	0.01	-0.25
	SoNord	-0.68	-0.05	0.32	0.18	0.00	-0.20	0.00	-0.01	0.42	0.01	-0.18
	UK-IE-NL	-1.19	-0.04	-0.74	-0.31	0.00	-0.10	-0.18	-0.01	1.87	-0.04	-0.56
	WCE	-3.78	-0.49	0.00	0.96	0.00	0.00	-0.58	-0.01	5.48	0.07	-0.88
	ECE	-0.82	-0.29	-0.01	0.37	0.00	-0.06	0.07	-0.01	2.07	0.03	0.00
	Alps	-0.94	-0.57	0.05	NA	-0.06	-1.32	-0.13	0.00	0.21	NA	-1.46
	Ont	-4.27	0.05	-0.29	0.06	0.47	-2.11	-0.60	-0.01	1.82	0.00	-2.69
	AdsCsk	-3.00	-0.13	-0.12	1.07	0.00	-0.70	-0.22	-0.02	2.11	0.08	-1.02
	QuMaVt	-2.08	0.00	-0.31	-0.03	0.28	-0.47	-0.22	0.00	1.72	-0.01	-0.69
	AtlCan	-0.96	0.00	-1.09	0.57	0.00	0.02	0.00	-0.06	1.16	0.03	0.06

Table A3. National data providers.

Country	Institution	Contact person
Canada	Environment and Climate Change Canada	Daniel Houle
		Kara Chan
	International Institute for Sustainable Development -Experimental Lakes Area	Scott Higgins
		Chris Ray
	Ontario Ministry of the Environment, Dorset Environmental Science Centre	Andrew Paterson
Czech Republic	Czech Geological Survey	Jakub Hruška
Finland	Finnish Environment Institute	Jussi Vuorenmaa
Germany	German Environment Agency	Jens Arle
Italy	CNR Water Research Institute (IRSA)	Michela Rogora
Netherlands	Water and nature	Herman van Dam
	Bargerveen Foundation (Stichting Bargerveen)	Louise Franssen
Norway	Norwegian Institute for Water research	Heleen de Wit
Poland	Institute of Environmental Protection – National Research Institute	Rafał Ulańczyk
		Agnieszka Kolada
Slovakia	Institute of Hydrobiology, CAS	Jiří Kopáček
Sweden	Swedish University of Agricultural Sciences	Jens Fölster
Switzerland	Section of air, water and soil protection, Department of the territory of the Canton of Ticino (TI-SPAAS)	Sandra Steingruber
United Kingdom	UK Centre for Ecology & Hydrology	Don Monteith
United States	United States Environmental Protection Agency	John Stoddard
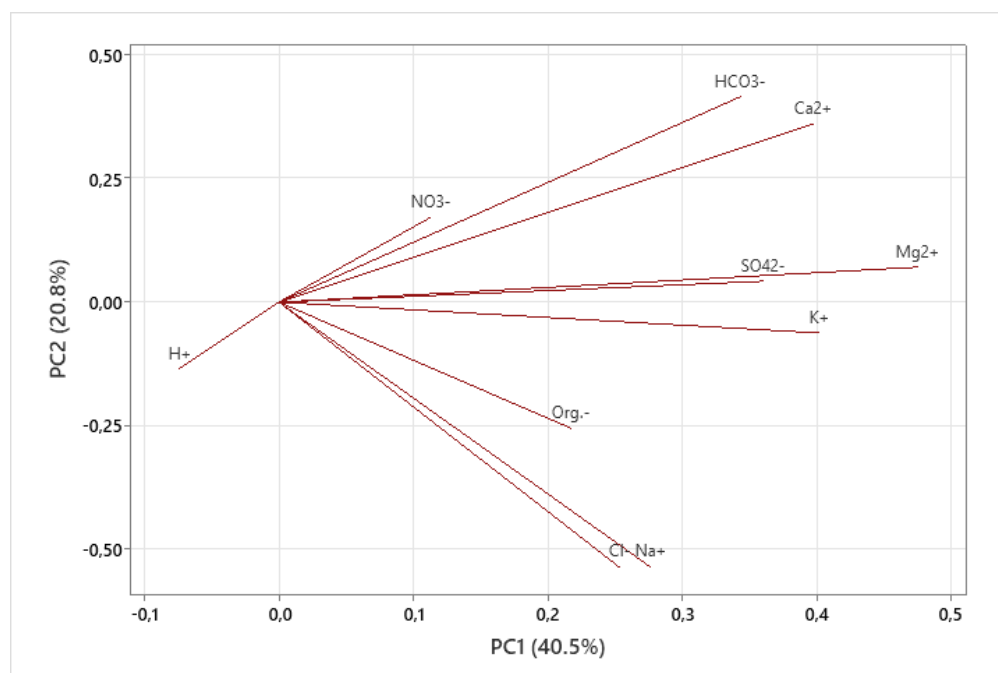
*Figure A*1. PCA parameter loading plot of the major descriptive parameter's loadings along the two main principal components assessing the variation in space.
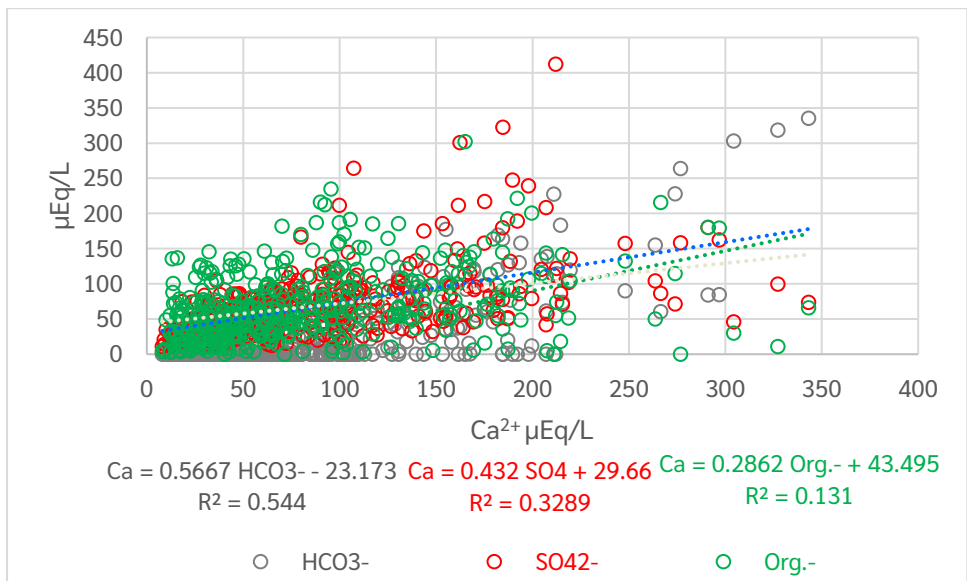
Figure A2. Correlation between median annual concentrations of Ca²⁺, at the 430 sites with data from 1990 to 2020, and the bicarbonate, sulphate, and Org.-, as deduced by the coefficient of determination (R2) in simple trendline analysis.

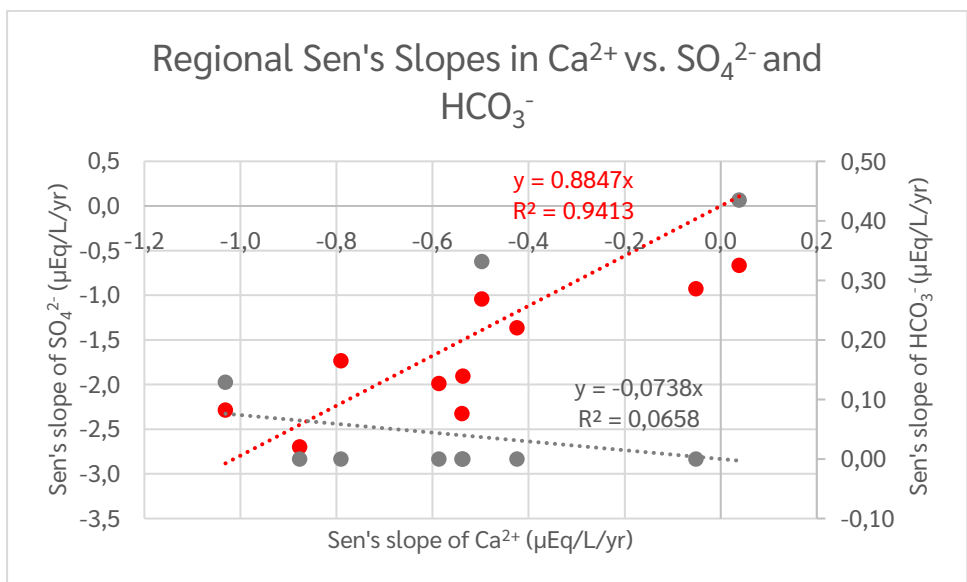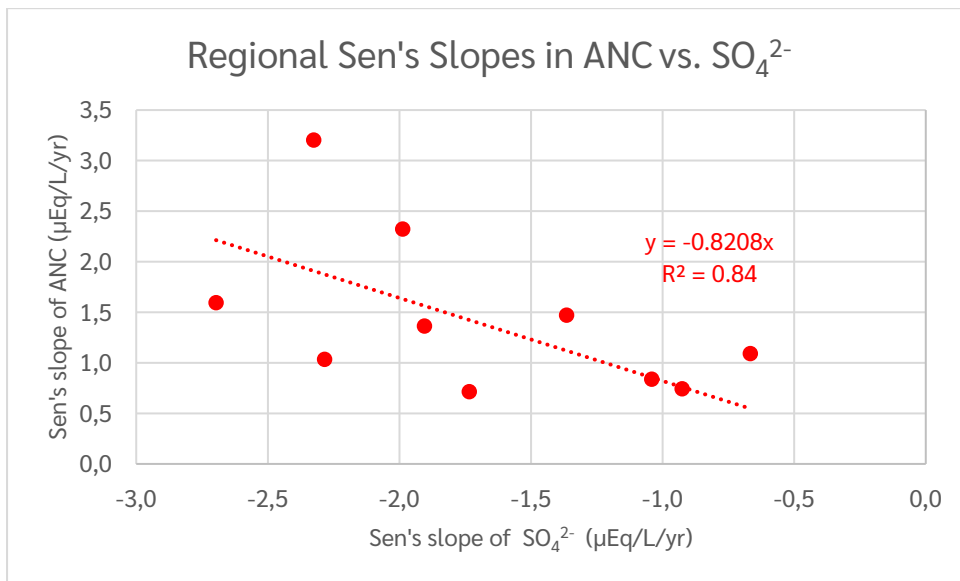*Figure A3.* The regional Sen's slopes of *Ca²⁺* correlated to regional slopes for *SO₄²⁻ and HCO₃⁻*.

Figure A4. The regional Sen's slopes in ANC correlated to regional Sen's slopes in SO_4^{2-}.
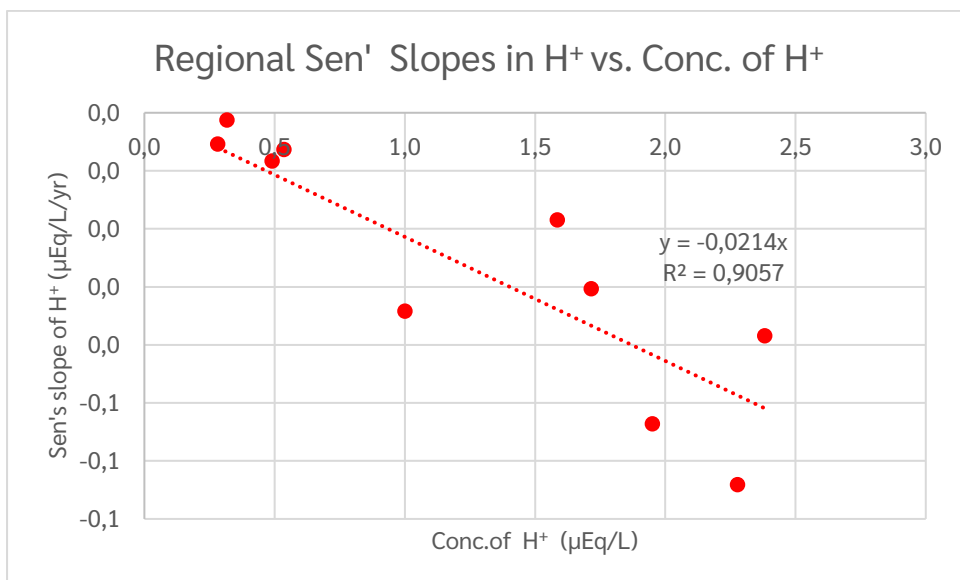
Figure A5. Regional Sen Slopes in H^+ vs. Conc. of H^+.
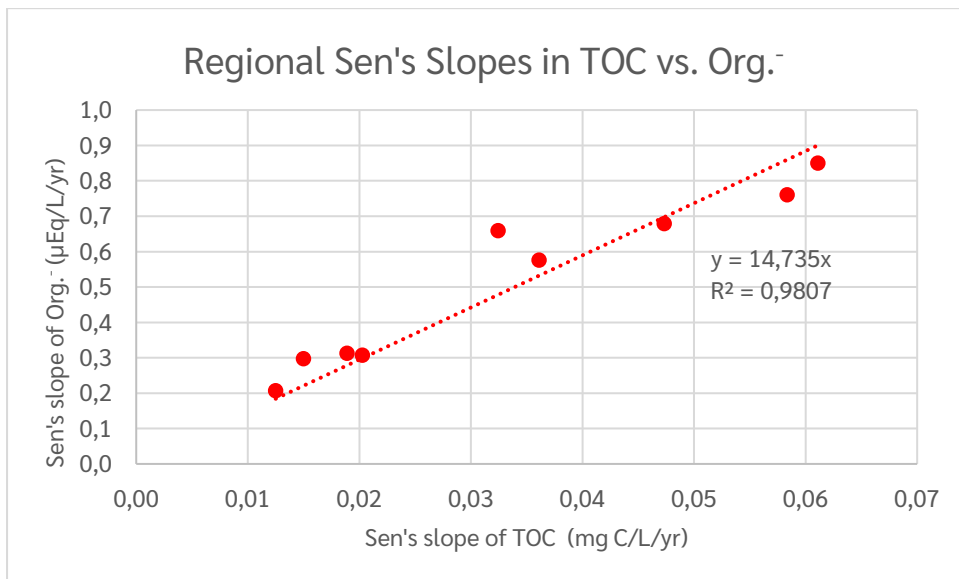
Figure A6. Regional Sen's Slopes in TOC vs. Sen's slope of Org.⁻.

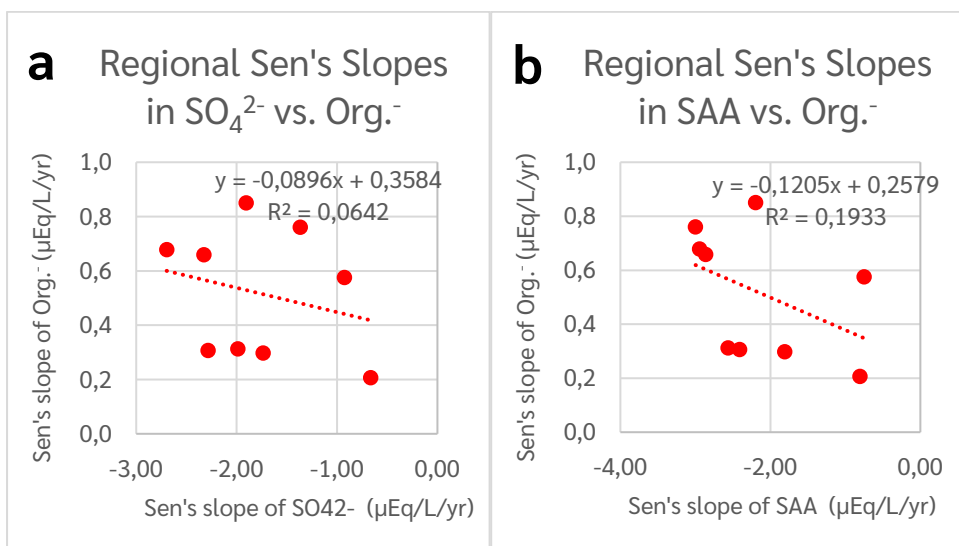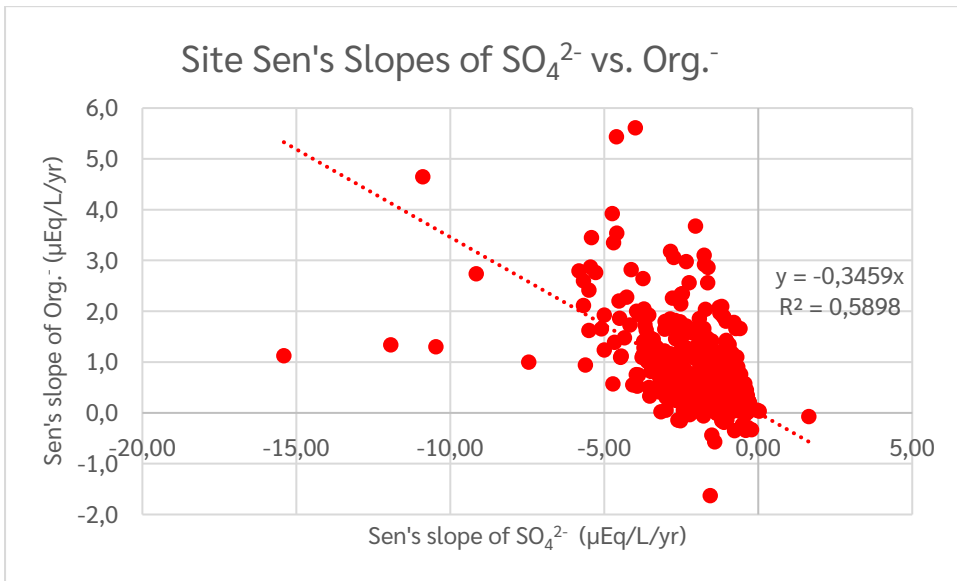*Figure A7. Regional Sen's Slopes in SO_4^{2-} vs. Org.⁻ (a) and SAA vs. Org.⁻(b)*
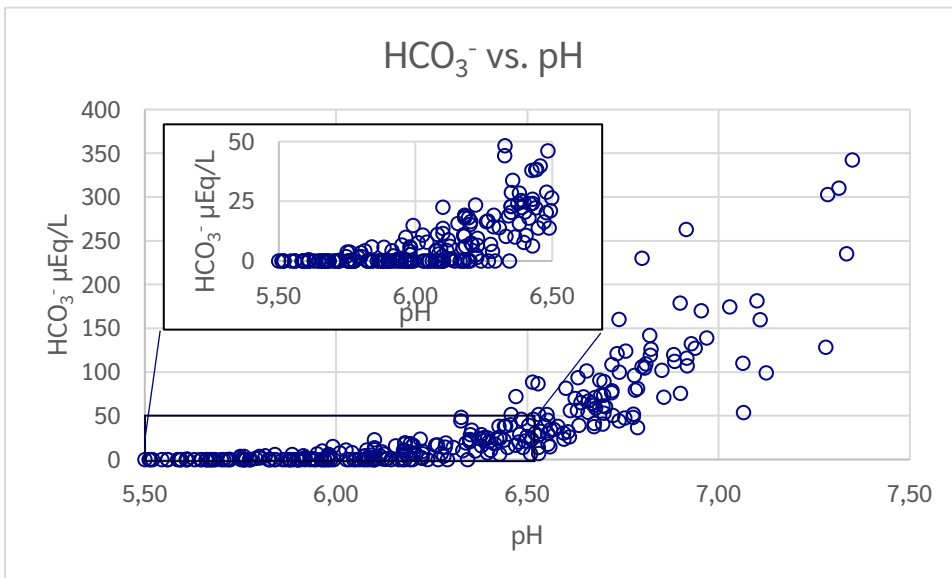
Figure A8. Site Sen's Slopes of SO_4^{2-} vs. $Org.^-$.
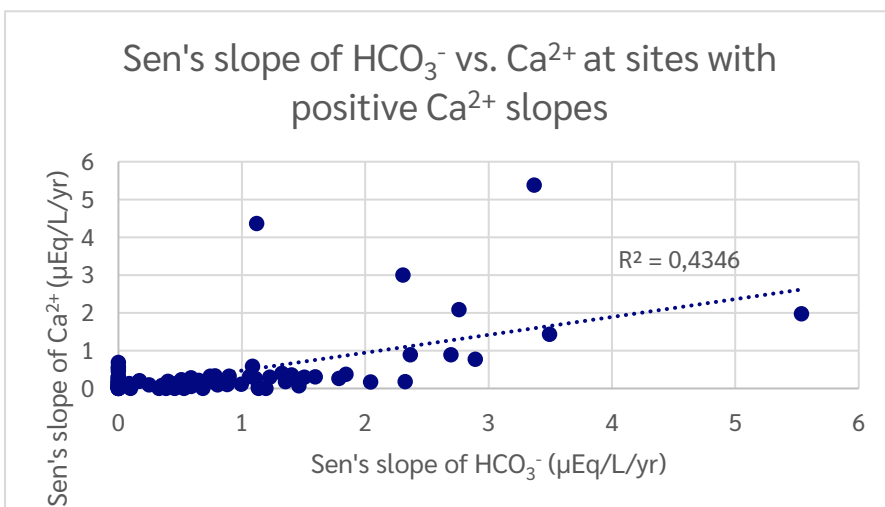

Figure A9. Relationship between bicarbonate levels and pH

Figure A10. Sen's slope of HCO_3^- vs. Ca^{2+} at sites with positive Ca^{2+} slopes.

Thematic reports from the ICP Waters programme

Since its establishment in 1985, the ICP Waters programme has prepared numerous assessments, reports and publications that address the effects of long-range transported air pollution, including thematic reports, chemical intercalibrations, biological intercalibrations, proceedings of Task Force meetings, and peer-reviewed articles. Reports and publications are available at the ICP Waters website; http://www.icp-waters.no/

Thematic reports from the ICP Waters programme from 2000 up to present are listed below.

Velle, G.; Bodin, C.L.; Arle, J.; Austnes, K.; Boggero, A.; Bojkova, J.; Fornaroli, R.; Fölster, J.; Goedkoop, W.; Jones, I.; Juggins, S.; Lau, D.C.P.; Monteith, D.; Murphy, J.; Musazzi, S.; Shilland, E.; Steingruber, S.; Wiklund, M.-L.; de Wit, H. 2023. Responses of benthic invertebrates to chemical recovery from acidification. NIVA SNO 7881-2023. **ICP Waters report 153/2023**.

Austnes, K., Hjermann, D.Ø., Sample, J., Wright, R. F., Kaste, Ø., and de Wit, H. 2022. Nitrogen in surface waters: time trends and geographical patterns explained by deposition levels and catchment characteristics. NIVA SNO 7728-2022. **ICP Waters report 149/2022**.

Thrane, J.E., de Wit, H. and Austnes, K. 2021. Effects of nitrogen on nutrient-limitation in oligotrophic northern surface waters. NIVA report SNO 7680-2021. **ICP Waters report 146/2021.**

Garmo, Ø., Arle, J., Austnes, K. de Wit, H., Fölster, J., Houle, D., Hruška, J., Indriksone, I., Monteith, D., Rogora, M., Sample, J.E., Steingruber, S., Stoddard, J.L., Talkop, R., Trodd, W., Ulańczyk, R.P. and Vuorenmaa, J. 2020. Trends and patterns in surface water chemistry in Europe and North America between 1990 and 2016, with particular focus on changes in land use as a confounding factor for recovery. NIVA report SNO 7479-2020. **ICP Waters report 142/2020**

Austnes, K. Aherne, J., Arle, J., Čičendajeva, M., Couture, S., Fölster, J., Garmo, Ø., Hruška, J., Monteith, D., Posch, M., Rogora, M., Sample, J., Skjelkvåle, B.L., Steingruber, S., Stoddard, J.L., Ulańczyk, R., van Dam, H., Velasco, M.T., Vuorenmaa, J., Wright, R.F., de Wit, H. 2018. Regional assessment of the current extent of acidification of surface waters in Europe and North America. NIVA report SNO 7268-2018. **ICP Waters report 135/2018**

Braaten, H.F.V., Åkerblom, S., de Wit, H.A., Skotte, G., Rask, M., Vuorenmaa, J., Kahilainen, K.K., Malinen, T., Rognerud, S., Lydersen, E., Amundsen, P.A., Kashulin, N., Kashulina, T., Terentyev, P., Christensen, G., Jackson-Blake, L., Lund, E. and Rosseland, B.O. 2017. Spatial and temporal trends of mercury in freshwater fish in Fennoscandia (1965-2015). NIVA report SNO 7179-2017. **ICP Waters report 132/2017**.

Velle, G., Mahlum, S., Monteith, D.T., de Wit, H., Arle, J., Eriksson, L., Fjellheim, A., Frolova, M., Fölster, J., Grudule, N., Halvorsen, G.A., Hildrew, A., Hruška, J., Indriksone, I., Kamasová, L., Kopáček, J., Krám, P., Orton, S., Senoo, T., Shilland, E.M., Stuchlík, E., Telford, R.J., Ungermanová, L., Wiklund, M.-L. and Wright, R.F. 2016. Biodiversity of macro-invertebrates in acid-sensitive waters: trends and relations to water chemistry and climate. NIVA report SNO 7077-2016. NIVA report SNO 7077-2016. **ICP Waters report 127/2016**.

De Wit, H., Hettelingh, J.P. and Harmens, H. 2015. Trends in ecosystem and health responses to long-range transported atmospheric pollutants. NIVA report SNO 6946-2015. **ICP Waters report 125/2015**.

De Wit, H. A., Garmo Ø. A. and Fjellheim A. 2015. Chemical and biological recovery in acid-sensitive waters: trends and prognosis. **ICP Waters Report 119/2014**.

Holen, S., R.F. Wright and Seifert, I. 2013. Effects of long-range transported air pollution (LTRAP) on freshwater ecosystem services. NIVA report SNO 6561-2013. **ICP Waters Report 115/2013**.

Velle, G., Telford, R.J., Curtis, C., Eriksson, L., Fjellheim, A., Frolova, M., Fölster J., Grudule N., Halvorsen G.A., Hildrew A., Hoffmann A., Indriksone I., Kamasová L., Kopáček J., Orton S., Krám P., Monteith D.T., Senoo T., Shilland E.M., Stuchlík E., Wiklund M.L., de Wit, H. and Skjelkvaale B.L. 2013. Biodiversity in freshwaters. Temporal trends and response to water chemistry. NIVA report SNO 6580-2013. **ICP Waters Report 114/2013**.

Wright, R.F., Helliwell, R., Hruska, J., Larssen, T., Rogora, M., Rzychoń, D., Skjelkvåle, B.L. and Worsztynowicz, A. 2011. Impacts of Air Pollution on Freshwater Acidification under Future Emission Reduction Scenarios; ICP Waters contribution to WGE report. NIVA report SNO 6243-2011. **ICP Waters report 108/2011**.

Skjelkvåle B.L. and de Wit, H. (eds.) 2011. Trends in precipitation chemistry, surface water chemistry and aquatic biota in acidified areas in Europe and North America from 1990 to 2008. NIVA report SNO 6218-2011. **ICP Waters report 106/2011**.

ICP Waters Programme Centre 2010. ICP Waters Programme manual. NIVA SNO 6074-2010. **ICP Waters report 105/2010**.

De Wit, H.A. and Lindholm M. 2010. Nutrient enrichment effects of atmospheric N deposition on biology in oligotrophic surface waters – a review. NIVA report SNO 6007 - 2010. **ICP Waters report 101/2010**.

Ranneklev, S.B., De Wit, H., Jenssen, M.T.S. and Skjelkvåle, B.L. 2009. An assessment of Hg in the freshwater aquatic environment related to long-range transported air pollution in Europe and North America. NIVA report SNO 5844-2009. **ICP Waters report 97/2009**.

Skjelkvåle, B.L., and De Wit, H. (eds.) 2008. ICP Waters 20 year with monitoring effects of long-range transboundary air pollution on surface waters in Europe and North-America. NIVA report SNO 5684-2008. **ICP Waters report 94/2008**.

Wright, R.F., Posch, M., Cosby, B. J., Forsius, M., and Skjelkvåle, B. L. 2007. Review of the Gothenburg Protocol: Chemical and biological responses in surface waters and soils. NIVA report SNO 5475-2007. **ICP Waters report 89/2007**.

Skjelkvåle, B.L., Forsius, M., Wright, R.F., de Wit, H., Raddum, G.G., and Sjøeng, A.S.M. 2006. Joint Workshop on Confounding Factors in Recovery from Acid Deposition in Surface Waters, 9-10 October 2006, Bergen, Norway; Summary and Abstracts. NIVA report SNO 5310-2006. **ICP Waters report 88/2006**.

De Wit, H. and Skjelkvåle, B.L. (eds) 2007. Trends in surface water chemistry and biota; The importance of confounding factors. NIVA report SNO 5385-2007. **ICP Waters report 87/2007**.

Wright, R.F., Cosby, B.J., Høgåsen, T., Larssen, T. and Posch, M. 2005. Critical Loads, Target Load Functions and Dynamic Modelling for Surface Waters and ICP Waters Sites. NIVA report SNO 5166-2005. **ICP Waters report 83/2006**.

Fjeld, E., Le Gall, A.-C. and Skjelkvåle, B.L. 2005. An assessment of POPs related to long-range air pollution in the aquatic environment. NIVA report SNO 5107-2005. **ICP Waters report 79/2005**.

Raddum, G.G, et al. 2004. Recovery from acidification of invertebrate fauna in ICP Water sites in Europe and North America. NIVA report SNO 4864-2004. **ICP Waters report 75/2004.**

Skjelkvåle, B.L. (ed) 2003. The 15-year report: Assessment and monitoring of surface waters in Europe and North America; acidification and recovery, dynamic modelling and heavy metals. NIVA report SNO 4716-2003. **ICP Waters report 73/2003.**

Wright, R.F. and Lie, M.C. 2002.Workshop on models for Biological Recovery from Acidification in a Changing Climate. 9-11 september 2002 in Grimstad, Norway. Workshop report. NIVA report 4589-2002.

Jenkins, A. Larssen, Th., Moldan, F., Posch, M. and Wrigth, R.F. 2002. Dynamic Modelling of Surface Waters: Impact of emission reduction - possibilities and limitations. NIVA report SNO 4598-2002. **ICP Waters report 70/2002**.

Halvorsen, G.A, Heergaard, E. and Raddum, G.G. 2002. Tracing recovery from acidification - a multivariate approach. NIVA report SNO 4564-2002. **ICP Waters report 69/2002**.

Wright, R.F. 2001. Note on: Effect of year-to-year variations in climate on trends in acidification. NIVA report SNO 4328-2001. **ICP Waters report 57/2001**.

Hovind, H. 2000. Trends in intercomparisons 8701-9812: pH, K_{25}, $NO_3 + NO_2$, Cl, SO_4, Ca, Mg, Na, K and aluminium - reactive and nonlabile, TOC, COD-Mn. NIVA report SNO 4281-2000, **ICP Waters Report 56/2000**.

Skjelkvåle, B.L., Olendrzynski, K., Stoddard, J., Traaen, T.S, Tarrason, L., Tørseth, K., Windjusveen, S. and Wright, R.F. 2001. Assessment of trends and leaching in Nitrogen at ICP Waters Sites (Europe And North America). NIVA report SNO 4383-2001. **ICP Waters report 54/2001.**

Skjelkvåle, B. L., Andersen, T., Halvorsen, G. A., Raddum, G.G., Heegaard, E., Stoddard, J. L., and Wright, R. F. 2000. The 12-year report; Acidification of Surface Water in Europe and North America; Trends, biological recovery and heavy metals. NIVA report SNO 4208/2000. **ICP Waters report 52/2000**.

NIVA